Solid-state NMR studies of polymer adsorption onto metal oxide surfaces

by

Michael McAlduff

A thesis submitted to McGill University in partial fulfillment of the requirements for the degree of

Doctor of Philosophy

Department of Chemistry
McGill University
Montreal, Quebec
Canada

January 2009

Library and Archives
Canada

Published Heritage
Branch

395 Wellington Street
Ottawa ON K1A 0N4
Canada

Bibliothèque et
Archives Canada

Direction du
Patrimoine de l'édition

395, rue Wellington
Ottawa ON K1A 0N4
Canada

Your file Votre référence
ISBN: 978-0-494-66319-6
Our file Notre référence
ISBN: 978-0-494-66319-6

NOTICE:

The author has granted a non-exclusive license allowing Library and Archives Canada to reproduce, publish, archive, preserve, conserve, communicate to the public by telecommunication or on the Internet, loan, distribute and sell theses worldwide, for commercial or non-commercial purposes, in microform, paper, electronic and/or any other formats.

The author retains copyright ownership and moral rights in this thesis. Neither the thesis nor substantial extracts from it may be printed or otherwise reproduced without the author's permission.

AVIS:

L'auteur a accordé une licence non exclusive permettant à la Bibliothèque et Archives Canada de reproduire, publier, archiver, sauvegarder, conserver, transmettre au public par télécommunication ou par l'Internet, prêter, distribuer et vendre des thèses partout dans le monde, à des fins commerciales ou autres, sur support microforme, papier, électronique et/ou autres formats.

L'auteur conserve la propriété du droit d'auteur et des droits moraux qui protège cette thèse. Ni la thèse ni des extraits substantiels de celle-ci ne doivent être imprimés ou autrement reproduits sans son autorisation.

In compliance with the Canadian Privacy Act some supporting forms may have been removed from this thesis.

While these forms may be included in the document page count, their removal does not represent any loss of content from the thesis.

Conformément à la loi canadienne sur la protection de la vie privée, quelques formulaires secondaires ont été enlevés de cette thèse.

Bien que ces formulaires aient inclus dans la pagination, il n'y aura aucun contenu manquant.

Canada

Abstract

This dissertation presents solid-state NMR studies that probe the dynamic and conformational properties of polymers adsorbed on solid surfaces in the dry state. The systems studied include a series of ethylene based random copolymers where the binding group is modified, and two diblock copolymer systems where the blocks have different intrinsic mobilities and surface interactions. The thesis begins by looking at the structures formed by the adsorption of poly (ethylene-*co*-acrylic acid) (PEA), poly (ethylene-*co*-vinyl alcohol) (EVOH), poly (ethylene-*co*-vinyl acetate) (EVA), and polyethylene (PE) on metal oxide powders (zirconia and alumina). NMR spectroscopy, FTIR-PAS, and TGA were used to characterize the surface behaviour of the systems with comparisons made between the bulk and adsorbed copolymers. ^{13}C CPMAS, ^{1}H and T_1 relaxation measurements were all recorded with the aim of correlating the microscopic structure of the surface with changes in NMR data. The chain conformation of adsorbed ethylene copolymers was found to strongly depend on the binding strength of the polar sticker groups with the substrates.

The chain dynamics of adsorbed diblock copolymers in the dry state are reported for the first time. Poly (styrene)-*b*-poly (*t*-butyl acrylate) (PS-PtButA) and poly (styrene)-*b*-poly (acrylic acid) (PS-PAA) were selected to vary both the block size and the binding strength. Once again the primary surface characterization methods are NMR spectroscopy, FTIR-PAS, and TGA. ^{13}C CPMAS, ^{1}H, T_1, and $T_{1\rho}$ relaxation measurements were all recorded with the aim of correlating the surface structures with changes in NMR data. For the most part, the observed trends in the chain mobilities of the anchor (PAA) and buoy (PS) blocks with block size can be correlated with the

predicted mushroom, intermediate and extended brush structures which collapse upon removal of the solvent. However, the chain mobility of the PS buoys decreases with increasing anchor block size. Although the chain mobility of the PS buoys are moderately enhanced relative to the bulk state, the mobility is sufficiently restricted to confirm the picture of a thin glassy layer with adhesive properties similar to the surface of bulk polystyrene.

The diblock copolymers poly (2-vinylpyridine), poly (isoprene)-*b*-poly (2-vinylpyridine), (PI-P2VP) and poly (isoprene)-*b*-poly (4-vinylpyridine) (PI-P4VP) were selected to complement the PS-PAA system as both systems have been studied by surface force microscopy. The large contrast in chain mobilities of the PI and PVP blocks allowed spectral editing through variation of the ^{13}C cross polarization parameters. The trends in mobility with block size differ from that of PS-PAA in that the segmental mobility of the buoys increases with anchor block size as expected. The chain mobility of the collapsed PI brushes is significantly enhanced as compared to the bulk state, again supporting the interpretation of surface microscopy studies which require an entropically unfavorable flattened, yet rubbery, surface structure.

Abstrait

Cette dissertation présente des études par RMN à l'état solide sondant les propriétés dynamiques et conformationelles de polymères adsorbés sur une surface solide à l'état sec. Les systèmes étudiés incluent des séries de copolymères aléatoires faits à base d'éthylène où le groupe liant est modifié et deux systèmes de copolymères diblocs dont les blocs possèdent une mobilité et une surface d'interaction intrinsèquement différentes. Cette thèse commence par l'examinassions des structures formées par l'adsorption de poly (éthylène-co-acrylique acide), poly (éthylène-co-vinyle alcool), poly (éthylène-co-vinyle acétate) et polyéthylène sur de la poudre de métal oxydée, soit la zircone et l'alumine. La spectroscopie par résonance magnétique nucléaire, infrarouge photoacoustique à transformée de Fourier et l'analyse thermique différentielle ont été utilisés afin de caractériser le comportement de ces systèmes en contrastant les polymères libres avec ceux étant adsorbés. Des mesures de relaxation du ^{13}C CPMAS, ^{1}H et T_1 ont été effectuées afin de corréler la structure microscopique de surface avec le changement des données RMN. Il y a été découvert que la conformation des chaînes des copolymères d'éthylènes adsorbés dépend grandement de la force de liaison entre les groupes polaires de liaisons et les substrats.

Un compte-rendu de la dynamique des chaînes pour les copolymères diblocs adsorbés à l'état sec est présenté pour la première fois. Le poly (styrène)-bloc-poly (*t*-butyle acrylate) (PS-PtButA) et le poly (styrène)-bloc-poly (acrylique acide) (PS-PAA) ont été sélectionnés afin de varier la longueur du bloc et la force de liaison. Les méthodes de caractérisation de base sont de nouveau la spectroscopie par RMN, FTIR-PAS et l'ATD. Des mesures de relaxation du ^{13}C CPMAS, ^{1}H et T_1 ont été de plus

effectuées dans le but de corréler la structure de surface avec le changement des données RMN. Pour la majorité des expérimentations, la tendance observée au niveau de la mobilité des chaînes en fonction de la longueur des blocs ancrés (PAA) et bouées (PS) peut être corrélée avec les structures prédites — soit champignon, intermédiaire et brossée — qui s'effondrent lorsque le solvant est soustrait du system. Cependant, la mobilité des chaînes des bouées PS diminue avec la longueur du bloc ancré. Bien que la mobilité de ces chaînes soit modérément accrue relativement à celles étant à l'état libre, la mobilité est suffisamment limitée pour confirmer le concept d'une mince couche vitreuse ayant des propriétés adhésives semblables à celles retrouvées à la surface de polystyrène à l'état libre.

Les copolymères diblocs poly (pyridine 2-vinyle), poly (isoprène)-bloc-poly (pyridine 2-vinyle) et poly (isoprène)-bloc-poly (pyridine 4-vinyle) ont été choisis pour compléter le système PS-PAA car ces deux systèmes ont été étudiés par la microscopie à force de surface. Le contraste prononcé de la mobilité des chaînes faites de blocs PI et PVP a permis la mise au point spectrale faite par la variation des paramètres de la polarisation croisée du ^{13}C. Les tendances de la mobilité en fonction de la longueur des blocs diffèrent de celles de PS-PAA parce que, comme prévu, la mobilité segmentaire des bouées augmente avec la longueur du bloc ancré. La mobilité des chaînes des brosses PI effondrées est sensiblement amplifiée par rapport aux chaînes étant à l'état libre. Ceci soutient encore une fois l'interprétation des études microscopiques de surface qui exigent une structure de surface aplatie, qui est entropiquement défavorable, et malgré tout caoutchouteuse.

Acknowledgements

I would like to begin by thanking Dr. Linda Reven for her help and guidance over the time while I've worked on my Ph.D. I would also like to thank Dr. Fred Morin for his help over the years in coaxing as much as possible out of the NMR spectrometers. A special thanks to all of my labmates over the years Shane, Victor, Andrew, Petr, Andrew, Blythe, Jon, and Violetta for all their help and support. To all the people who I've played intramural hockey, ball hockey, and soccer with over the years; thanks for making my time at McGill more enjoyable. Thanks to the Montreal Irish Rugby football club for giving me something to do for the last five summers. It never hurts to run into/or get run into someone at the end of the day to get rid of any work frustration. Thanks to the TFTC, especially Maggie, Emily, Tiffany, and Dr.Gray for a half an hour break every day. Also, thanks to Adil for years of Sunday football/feeding me. Thanks to all the people on my drinking team for helping me destroy my liver, especially Oleh, Adil, Hassler, and Jeff who were always ready to go grab a quick beer at 4. Thanks to my roommates over the last year, for giving me a place to stay. I would like to especially thank Dr. A. Kassam, Dr. E. McAlduff, and Mrs. K. McAlduff for help with editing of the following thesis, any mistakes will be blamed on you. Finally, I would like to thank friends and family for their support over the last six years.

Forward

In compliance with the "Thesis Preparation and Submission Guidelines" for the Faculty of Graduate Studies and Research at McGill University, the work herein is presented in a manuscript-based format. The guidelines are cited as follows.

"As an alternative to the traditional thesis format, the thesis can consist of a collection of papers of which the student is an author or co-author. These papers must have a cohesive, unitary character making them a report of a single program of research. The structure for the manuscript-based thesis must conform to the following:

1. Candidates have the option of including, as part of the thesis, the text of one or more papers submitted, or to be submitted, for publication, or the clearly-duplicated text (not the reprints) of one or more published papers. These texts must conform to the "Guidelines for Thesis Preparation" with respect to font size, line spacing and margin sizes and must be bound together as an integral part of the thesis. (Reprints of published papers can be included in the appendices at the end of the thesis.)

2. The thesis must be more than a collection of manuscripts. All components must be integrated into a cohesive unit with a logical progression from one chapter to the next. In order to ensure that the thesis has continuity, connecting texts that provide logical bridges preceeding and following each manuscript are mandatory.

3. The thesis must conform to all other requirements of the "Guidelines for Thesis Preparation" in addition to the manuscripts.

The thesis must include the following:

1. a table of contents;
2. a brief abstract in both English and French;
3. an introduction which clearly states the rational and objectives of the research;
4. a comprehensive review of the literature (in addition to that covered in the introduction to each paper);
5. a final conclusion and summary;
6. a thorough bibliography;
7. Appendix containing an ethics certificate in the case of research involving human or animal subjects, microorganisms, living cells, other biohazards and/or radioactive material.

4. As manuscripts for publication are frequently very concise documents, where appropriate, additional material must be provided (e.g., in appendices) in sufficient detail to allow a clear and precise judgement to be made of the importance and originality of the research reported in the thesis.

5. In general, when co-authored papers are included in a thesis the candidate must have made a substantial contribution to all papers included in the thesis. In addition, the candidate is required to make an explicit statement in the thesis as to who contributed to such work and to what extent. This statement should appear in a single section entitled "Contributions of Authors" as a preface to the thesis. The supervisor must attest to the accuracy of this statement at the doctoral oral defense. Since the task of the examiners is

made more difficult in these cases, it is in the candidate's interest to clearly specify the responsibilities of all the authors of the co-authored papers.

6. When previously published copyright material is presented in a thesis, the candidate must include signed waivers from the publishers and submit these to the Graduate and Postdoctoral Studies Office with the final deposition, if not submitted previously. The candidate must also include signed waivers from any co-authors of unpublished manuscripts.

7. Irrespective of the Internal and External Examiners reports, if the oral defense committee feels that the thesis has major omissions with regard to the above guidelines, the candidate may be required to resubmit an amended version of the thesis. See the "Guidelines for Doctoral Oral Examinations," which can be obtained from the web (http://www.mcgill.ca/gps), Graduate Secretaries of departments or from the Graduate and Postdoctoral Studies Office, James Administration Building, Room 400, 398-3990, ext. 00711 or 094220.

8. In no case can a co-author of any component of such a thesis serve as an External Examiner for that thesis."

This dissertation is written in the form of three papers, each presented as one chapter. A comprehensive background in addition to an introduction to the work conducted by the author is presented in chapter 1. Chapters 2-4 have been published. Conclusions are given in chapter 5.

Contributions of the author

The author performed and initiated the work in this thesis, unless otherwise stated, under the supervision of Professor Linda Reven.

Table of contents

List of Figures

List of Tables

List of Abbreviations

Acronym	Abbreviation
NMR	Nuclear Magnetic Resonance
FTIR-PAS	Fourier Transform Infrared-Photoacoustic Spectroscopy
TGA	Thermogravimetric Analysis
CP-MAS	Cross Polarization-Magic Angle Spinning
H	Hamiltonian
CS	Chemical Shift Anisotropy
D	dipole-dipole
Z	Zeeman
γ	magnetogyric ratio
μ_I	nuclear magnetic moment
$\mathbf{H}_0$	static magnetic field
ω	Larmor frequency
σ	chemical shielding tensor
T_1, T_2	Spin-lattice, spin-spin relaxation times
$T_{1\rho}$	Spin-lattice relaxation in rotating frame
T_{CH}	initial ^{13}C magnetization build-up
t_{CP}	cross polarization time
τ_c	correlation time
M	magnetization
δ_{iso}	isotropic shift
TOSS	total suppression of spinning sidebands

PS	polystyrene
PAA	poly (acrylic acid)
PtBuA	poly (*t*-butyl acrylate)
PI	polyisoprene
PP	polypropylene
PB	polybutadiene
PVP	poly (vinyl pyridine)
PE	polyethylene
PEA	poly (ethylene-co-acrylic acid)
EVA	poly (ethylene-co-vinyl acetate)
EVOH	poly (ethylene-co-vinyl alcohol)
PMDETA	N,N,N',N',N''-pentamethyl diethylene triamine
ATRP	Atom Transfer Radical Polymerization
ZrO_2	zirconia
Al_2O_3	alumina
wt%	weight percent
M_w	weight average molecular weight
M_n	number average molecular weight
BET	Brunauer, Emmett, Teller
T_g	glass transition temperature
DP	degree of polymerization
PI	polydispersity index
THF	tetrahydrofuran

Γ	surface excess
c	concentration
p	bound fraction
ΔH	change in enthalpy
ΔS	change in entropy
G_A, G_C	adhesive strength, cohesive strength
N_B, N_A	buoy block size, anchor block size
β	asymmetry parameter
R_g	radius of gyration
CMC	critical micelle concentration
θ	adsorbed amount
σ	surface density

Chapter 1: Introduction

1.1 Preface

This chapter is a general introduction and consists of five main sections. The first is a brief introduction to polymers at the solid-air interface. The next section provides an introduction to solid-state NMR spectroscopy. Subsequent sections focus on solid-state NMR experiments, and FTIR-PAS, as characterization methods of surface behaviour. Finally, the last section gives an outline of the material in subsequent chapters.

1.2 Polymers at the Solid-Air Interface

Polymers are an important class of materials whose properties and applications can be modified by changing their structure and chemical composition. Over the last few decades there has been a great deal of interest in polymers and in particular polymer films and coatings. These materials play a significant role in the fields of colloids, surface chemistry, protective coatings, adhesion, gas permeability, and microelectronics.[1]

1.2.1 Homopolymer Adsorption

The overall polymer concentration determines how a polymer adsorbs onto a solid surface from a solution containing chains of different sizes. When the polymer has a broad molecular weight distribution, the shorter chains adsorb at low concentrations. At low concentration the surface is not fully saturated and it can accommodate chains of different sizes. However, at higher concentrations the surface becomes completely saturated and the shorter chains are displaced by the longer chains. Therefore, there will be a larger number of longer chains on a completely saturated surface. This is because for higher molecular weight chains the total loss of translational entropy is lower then for shorter chains, while the change in the enthalpy is the same. For longer chains upon adsorption, the change in total free energy is lower than it is for shorter ones.[2]

As seen in Figure 1.1, the structure of the adsorbed chain can be described in terms of loops, tails, and trains. The relative fractions of loops, tails, and trains in an adsorbed chain depend upon the strength of interactions, polymer concentration, and molecular weight. Unfortunately, it is not possible to make a distinction between the loops and tails experimentally. The Scheutjens–Fleer theory [1] provides information about the structure of the adsorbed chains. According to this theory, the structure of low molecular weight polymers is primarily determined by the train segments. As the molecular weight increases there is an increase in the population of loops and tails and a subsequent decrease in trains. As the chain size increases, the fraction of the chain forming loops increases; while the fraction of the chain forming tails remains constant after an initial increase.[2]

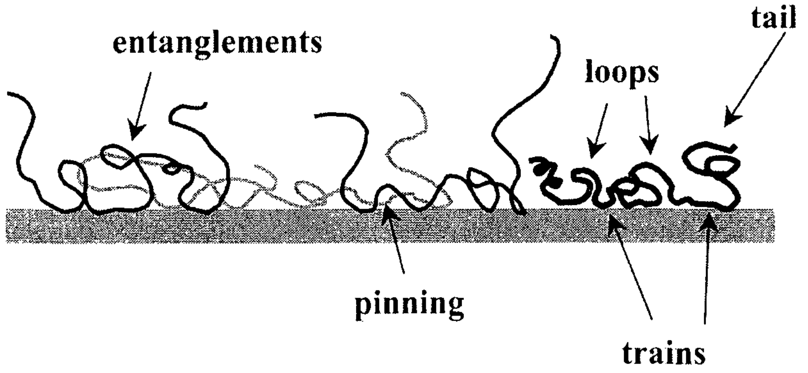

Figure 1.1: Adsorbed layer of tails, loops, and trains. The highlighted chain is both pinned and tangled with neighbours. (Pinning is defined to be trapping of a train by loops or other trains. Entanglements are trappings of loops by other loops.)[3]

Takahashi and Kawaguchi [4] reviewed a large number of polymer adsorption studies, mostly focused on the adsorption from organic solvents onto silica; they found that the bound fraction is molecular weight dependent. The adsorbed amount depends on the solvent, the polymer–surface interaction, and the surface coverage. In a good solvent the bound fraction is constant when the surface is not fully saturated, corresponding to adsorption from a dilute solution. The surface becomes fully saturated at higher concentrations and the bound fraction starts to decrease. This decrease suggests that chains initially lie flat on the surface but as the surface becomes more populated the chains begin to form loops and tails [5]. When the polymer-surface interaction increases or when the solvent quality decreases the bound fraction increases. For homopolymers the average density decays with the distance from the surface.[2]

In solution, conformational changes in a polymer chain occur very quickly, in approximately microseconds. At a surface, conformational changes can take hours because of adsorption of train segments. Exchange kinetics of adsorbed polystyrene molecules have been used to study this non-equilibrium adsorption [6, 7]. The duration of time that the adsorbed chains are allowed to stay on the surface before being displaced is given by the exchange time constants. The adsorbed chains continuously relax toward an equilibrium state by increasing the bound fraction. The direct IR measurements of bound fraction in poly (methyl methacrylate) and poly (dimethyl siloxane) adsorbed from a dilute carbon tetrachloride solution onto a silicon oxide substrate suggests that the bound fraction increases with time [8, 9].

In a good solvent, the adsorbed polymers do not desorb from the surface. This irreversibility of adsorption is because the activation energy required to remove a chain from a surface can be extremely high. However, studies have been performed where an adsorbed molecule is displaced by a molecule that has a higher affinity for the surface [10]. Figure 1.2 shows the adsorption isotherm for a polymer in a good solvent as the polymer concentration increases. The average molecular weight and the molecular weight distribution of the adsorbing polymer both influence the shape of the isotherm. For polymers having a low molecular weight and a broad molecular weight distribution, the isotherm has a rounded profile, while a polymer with a large molecular weight and a narrow molecular weight distribution has a sharper profile.

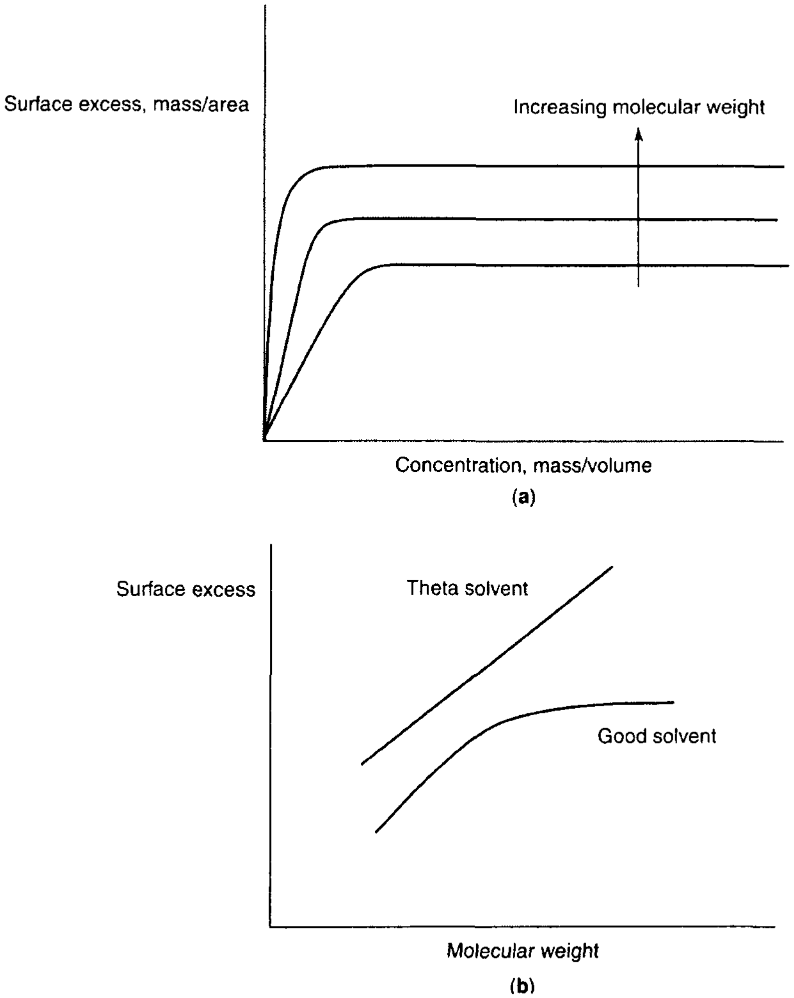

Figure 1.2: (a) High affinity adsorption isotherm, and (b) molecular weight dependence of surface excess. Adapted from figure 3 of ref [2]

1.2.2 Random Copolymer Adsorption

Random copolymers are used in commercial applications as adhesives, dispersion stabilizers, and flocculating agents. A random copolymer usually contains two different segment types. An example of a random copolymer is poly (ethylene-co-vinyl acetate) (EVA) where the acetate groups break up the crystalline ethylene segments, making it easier for the polymer to dissolve. In random copolymers, the different segments have different surface affinities, and the thermodynamic and structural properties are intermediate between the two corresponding homopolymers. This is different from block copolymers, where the blocks maintain their individual properties.[1]

The adhesion of polymers to surfaces can be improved by using random copolymers with functional groups that form surface bonds. Polymers can adhere to surfaces by weak non-covalent interactions or by stronger covalent bonds that are of importance in many composite materials. This thesis focuses on the use of non-covalent bonds to modify surfaces with copolymers. The adhesive and cohesive strengths of a random copolymer coating on a solid surface are determined by the combination of the chain configuration, and the type and number of surface linkages. The enthalpy of the polymer-surface interaction is the driving force for adsorption, and it depends on the type of surface interaction: hydrogen bonding, interfacial tension, van der Waals attraction, polar interactions, and electrostatic attractions. The change in enthalpy is offset by the loss in entropy due to localization of the polymer chains at the interface, and a balance of these two effects controls the polymer adsorption. A chain cannot easily desorb from the surface because that would require synchronized detachment of all the sticker groups, and therefore adsorption is often irreversible.[2]

The change in enthalpy upon adsorption of the polymer chain can be connected to the increase of the intrinsic adhesive strength, G_A, between an adsorbed chain and a surface. The entropy loss of an adsorbed chain collapsing to the surface can be connected to the decrease in the intrinsic cohesive failure, G_C, between an adsorbed chain and neighboring chains. As shown in Figure 1.3 G_A and G_C are not independent of each other, but move in opposite directions as *r* increases, where *r* is the distance from the surface. The choice of polymer sticker group and substrate both play a role in the enthalpy and entropy of adsorption that results in the G_{IC} effect seen in Figure 1.4. [11]

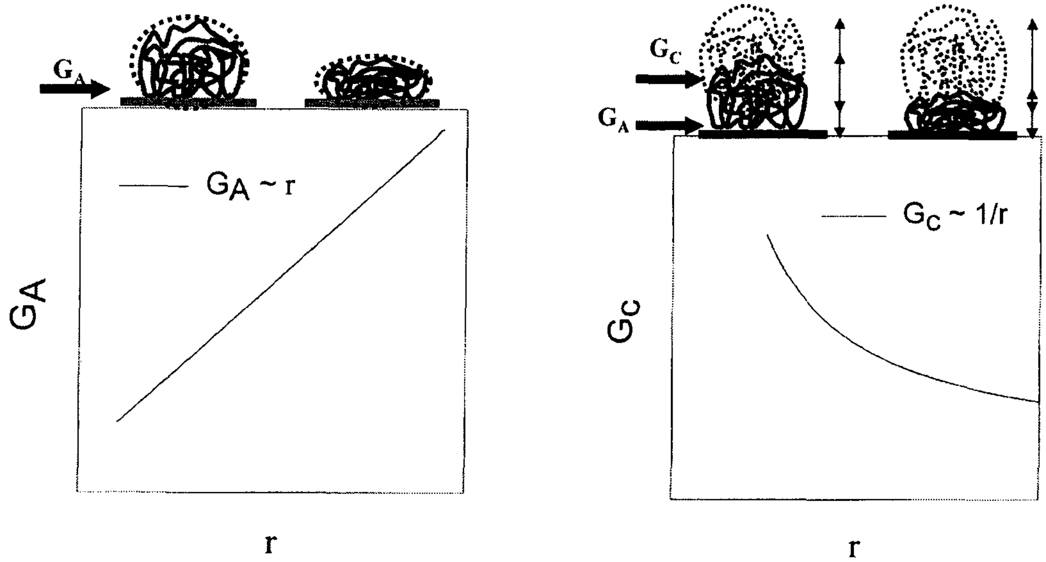

Figure 1.3: Schematic representation of the conformational dimension of an adsorbed chain on a solid surface and the two adhesion potentials, the adhesive potential between an adsorbed chain and a solid surface (G_A) and the cohesive potential between an adsorbed chain and neighboring free chains (G_C). They move in opposite directions as r increases at the interface. [11]

In the case of random copolymers, there is an optimal sticker group density due to competition between cohesive failure of the polymer–polymer interface and adhesive failure of the adsorbed polymer-solid interface (Figure 1.4). The decreasing fracture energy after the optimum concentration is caused by the entanglement of the interfacial chains with themselves rather than with the chains in the bulk [11]. As the sticker group density increases, there is a decrease in cohesion since the chain conformation flattens out leading to fewer chain entanglements between directly adsorbed chains and neighbouring chains. This balance between the adsorption of sticker groups onto the solid substrate and good chain connectivity may be achieved through correct selection of the type and the concentration of sticker groups. The overall goal of our study of adsorbed random copolymers was to see how the sticker group density and binding strength variables effect the chain conformation as observed by solid-state NMR.

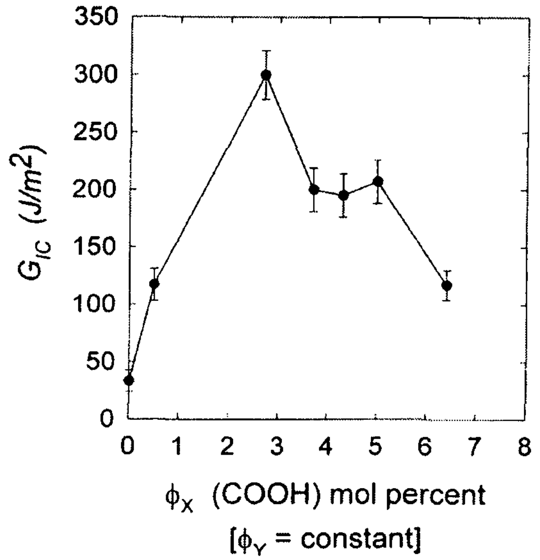

Figure 1.4: Polymer sticker concentration effect on the fracture energy of cPBD-Al interfaces at 1000 minutes annealing time in which the receptor concentration were the same (100 mole% -OH) and the peeling rate was 30 mm/min.[11]

1.2.3. Block Copolymer Adsorption

In block copolymers, the properties of two homopolymers are combined, with each block preserving many of the properties of the homopolymer. Block copolymers are interesting to study because the polymer-surface interaction, the relative block lengths, and the choice of solvent all play a role in the possible surface structures.[1] In comparison to homopolymers where adsorption is a competition between sticking and solvation, the adsorption of block copolymers can combine strong binding with good solvation. Although considerable research has been carried out on block copolymer adsorption over the last two decades, experimental confirmation of the surface morphologies is still far from reliable. Most theoretical and experimental work has concerned adsorbed copolymers in contact with solvent rather than in the dry state. These studies have focused on a few central themes which include dynamics[12-16], kinetics[17-20], solvent effects,[21, 22] and the effect of the block length.[23]

If both blocks are soluble the solvent is called non-selective; if one block is insoluble, so that micelles may form in solution, the solvent is selective. The adsorption of block copolymers from selective solvents is one way of sticking a polymer onto a surface it would not usually bind. In an adsorbed block copolymer layer the block that is adsorbed is called the "anchor" while the non-adsorbing block is called the "buoy". Adsorption from a non-selective solvent leads to a swollen anchor layer similar to an adsorbed layer of pure anchor in a good solvent. The adsorbed amount is determined by a competition between attractive interactions between the anchor and the surface and repulsive interactions between the buoys.[1]

Marques and Joanny [24] have developed a scaling description for adsorption from a non-selective solvent. They describe the adsorbed state as a swollen anchoring layer and a more dilute and extended buoy layer. The relative length of the blocks is important in determining the layer structure. When the block copolymer has a short anchor and a long buoy, the number of chains on the surface is determined by the repulsion between the buoy blocks. As the size of the anchor block is increased the adsorbed amount increases because of a higher adsorption energy, which is balanced by the repulsion between the buoys. This regime is called the buoy-dominated regime. When the anchor blocks are long the overlap and repulsion between the buoys is weak and the adsorption is limited by the saturation of the anchor layer. In the anchor-dominated regime the adsorbed mass of the anchor remains constant with increasing anchor content while the number of adsorbed chains and the number of buoy blocks decrease, as does the adsorbed amount. Marques and Joanny [24] introduced an asymmetry ratio β as the ratio between the areas occupied by the two blocks. In a non-selective solvent, β is defined as the ratio between the squares of the Flory radii of the buoy and anchor blocks:

$$\beta = \left(\frac{N_B}{N_A}\right)^{6/5} \tag{1.1}$$

Marques and Joanny found that there is a transition between buoy and anchor regimes at $\beta \approx N_A$. Above this value the adsorbed amount increases with increasing N_A (buoy regime), below it decreases (anchor regime). The two regimes are shown in Figure 1.5.

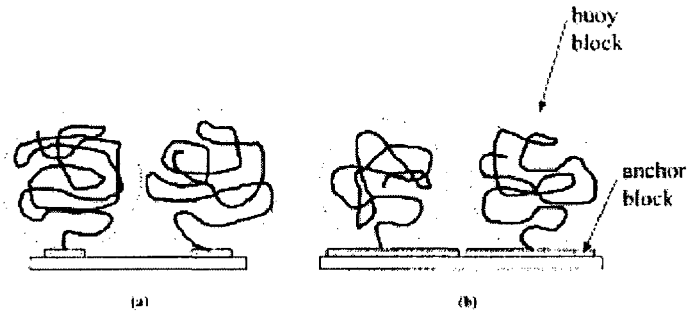

Figure 1.5: Two extremes of asymmetry of block copolymers and the resulting structures. The buoy-dominated (a) and anchor-dominated (b) regimes.[23]

A scaling picture for adsorption from a selective solvent has been developed by Marques, Joanny, and Liebler.[25] They assumed the anchor layer forms a melt at the surface that fully wets the surface due to the van der Waals attraction. The effective area of the anchor block will scale as N_A. The buoy segments are still in a good solvent environment and form a fully solvated layer with an effective size that varies as $N_B^{6/5}$, as with the non-selective case. The asymmetry parameter for a selective solvent is:

$$\beta = \frac{N_B^{6/5}}{N_A} \qquad (1.2)$$

The van der Waals brush regime is only one of a number of possible regimes for the selective solvent case. Other possibilities include the Rollin regime, the buoy dominated regime, and the anchor dominated regime. Tirrell and coworkers [26] used the asymmetry parameter β to express the asymmetry of a selectively solvated block copolymer chain in a quantitative way. They found that the adsorbed amount is a function of the asymmetry parameter (β). For the PS block, in good solvent conditions, the projected area scales as $(N_{PS}^{3/5})^2$ while for the PVP block, in bad solvent conditions, the projected area scales as $(N_{PVP}^{1/3})^2$.

$$\beta = \frac{R_{G,PS}^2}{R_{G,P2VP}^2} = \frac{N_{PS}^{6/5}}{N_{P2VP}^{2/3}} \qquad (1.3)$$

The adsorption of block copolymers can lead to a wide variety of structures when carried out above the critical micelle concentration (cmc). If the surface has no affinity for the buoy block, micelles do not adsorb and the initial adsorption rate is determined by the critical micelle concentration or the concentration of free chains in solution. As the polymer concentration is increased more micelles form, but there is no change in the adsorption rates. If the cmc is low, adsorption may not occur, Dewalt et al. [27] studied block copolymers of poly (styrene-*b*-ethylene oxide). They found that the PS-*b*-PEO in aqueous solution did not adsorb onto polystyrene particles, only by adding THF (a good solvent for PS) did PS-*b*-PEO adsorb. This suggested that micelle formation ties up most of the free chains and hinders adsorption. Studies have also shown that micelles cause an increase in the rate of adsorption when compared to free chains alone. Bijsterbosch et al.[28] reported the adsorption of poly (dimethylsiloxane-*b*-2-ethyl-2-oxazoline) onto titanium dioxide, even though the cmc was very small and the buoy had no real affinity for the surface. Munch et al.[19] found that the rate of adsorption of poly (ethylene oxide-*b*-styrene) micelles onto sapphire in cyclopentane depended on the overall micelle concentration even though the buoy block (PS) did not adsorb onto the surface. Johner and Joanny [18] explained the behaviour of the adsorption rates on micelle relaxation near the surface. Initially, the region next to the surface is exhausted of free chains breaking the equilibrium between free chains and micelles. In order to re-establish the equilibrium, micelles relax and release chains, which adsorb onto the surface.

If the buoy block is attracted to the surface then micelle adsorption is a possibility. Hong et al.[29] studied the adsorption of poly (styrene-*b*-2-vinylpyridine) from toluene onto silver, and they found evidence of micelle adsorption. While Webber et al.[30] showed that poly (2-(dimethylamino)ethyl methacrylate-*b*-methyl methacrylate) micelles formed in aqueous solution adsorbed onto mica. Both of these studies also looked at the buoy homopolymer adsorption, and gave this adsorption as the reason for the micelle adsorption. Despite the attraction of the buoy block to the surface, it is still expected that the buoy must deform upon adsorption, which is unlikely due to the energetics involved.[31] Therefore, micelle adsorption is expected to follow different behavior than that of individual chains.

1.2.4. Block Copolymer Films: Pattern Surfaces

Block copolymer films with patterned surfaces can be prepared from ultrathin films where the thickness is smaller than the equilibrium structure in the bulk [32-38].

Ultrathin films have been prepared by the adsorption of poly (styrene)-*block*-poly(4-vinylpyridine) (PS-PVP) from a dilute solution onto mica.[33-36, 38] The buoys aggregate into clusters to decrease the number of unfavorable contacts between the buoy block and the environment (Figure 1.6a). Depending on the relative block lengths of the copolymer, mushroom-like micelles ordered with the symmetry of a hexagonal lattice, stripe-like micelles, and a double layer (planar brush) are all possible structures (Figure 1.6a) [32, 33]. The PVP-PS diblock on mica surface structure can be attributed to a copolymer with "sticky" (PVP) and "nonsticky" (PS) blocks. Examples of diblock copolymers where both blocks are sticky, include poly (ethylene oxide)-*block*-poly (2-vinylpyridine) (PEO-P2VP) and poly (butyl acrylate)-*block*-poly (2-vinylpyridine) (PBA-P2VP) on mica.[39] The stickiness of the blocks can be varied by changes in temperature and pressure. In Figure 1.6b, both blocks were considered to be in contact with the substrate: one of the blocks is completely adsorbed, and the conformation of the second block varies from completely adsorbed to partially desorbed. Various nanostructures including flat, prominent disks and stripes were observed. What Potemkin [34] noted was that changes in the degree of adsorption of one of the blocks can result in morphological changes. For the case of a single molecule adsorbed on the patterned solid surface, changes of the stickiness of one of the blocks can result in directional motion (reptation) of the copolymer.

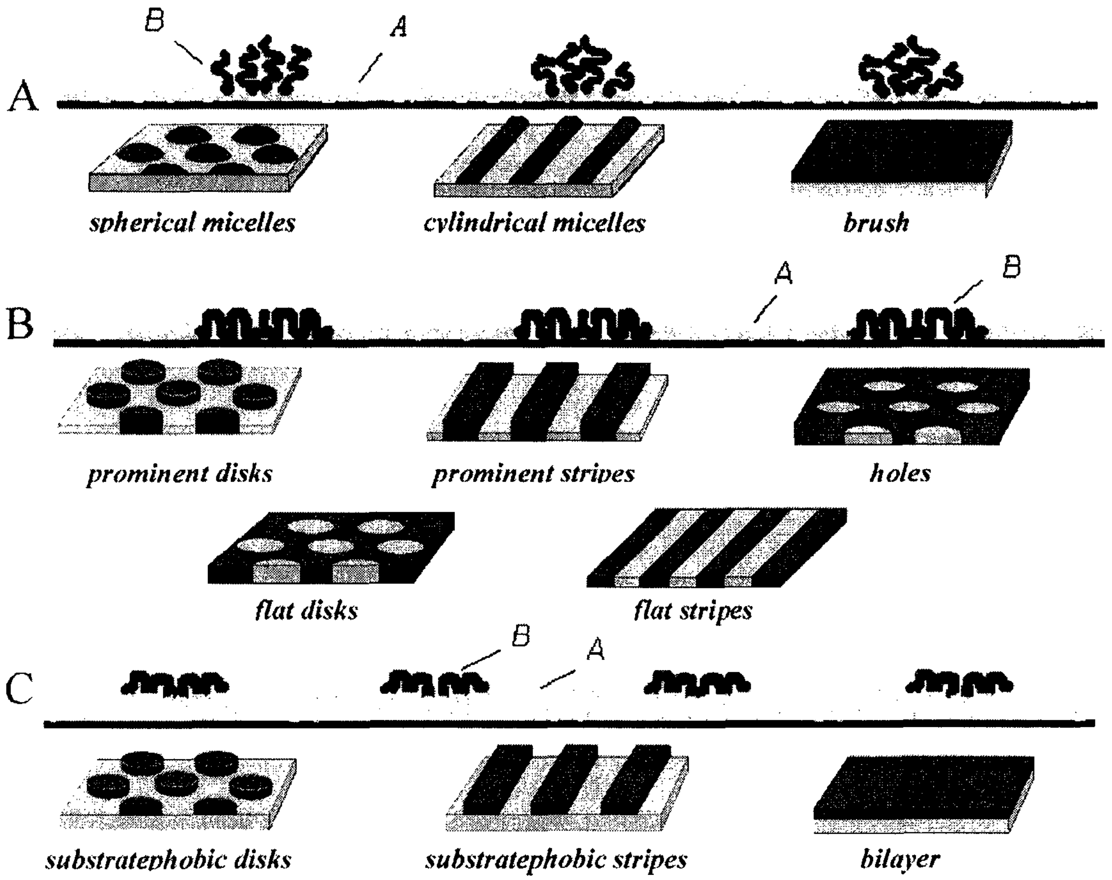

Figure 1.6: Schematic representation of three kinds of ultrathin diblock copolymer films: (A) anchor blocks are strongly adsorbed on the substrate, whereas buoy blocks are not compatible with either the substrate or the layer of anchor blocks. Structured films with spherical and cylindrical micelles or planar brushes were predicted. (B) Both blocks are adsorbed on the substrate. Possible morphologies of the film are calculated in [34]. (C) Anchor blocks are adsorbed on the substrate (variable degree of adsorption). Buoy blocks are incompatible with the substrate, but they can spread atop the layer of anchor blocks.[39]

Patyukova et al.[39] have developed a theory of nanostructures in ultrathin diblock copolymer films in the case where one of the blocks (A) is attracted to the substrate and the other block (B) is repelled from the substrate but spreads atop the A layer. It has been shown that the morphology of the film is controlled by the composition of the diblock copolymer and by the strength of attraction of the A blocks to the substrate and the B blocks to the A layer.(Figure 1.7) The structures of the film calculated include disk-like, stripe-like, and bilayer.

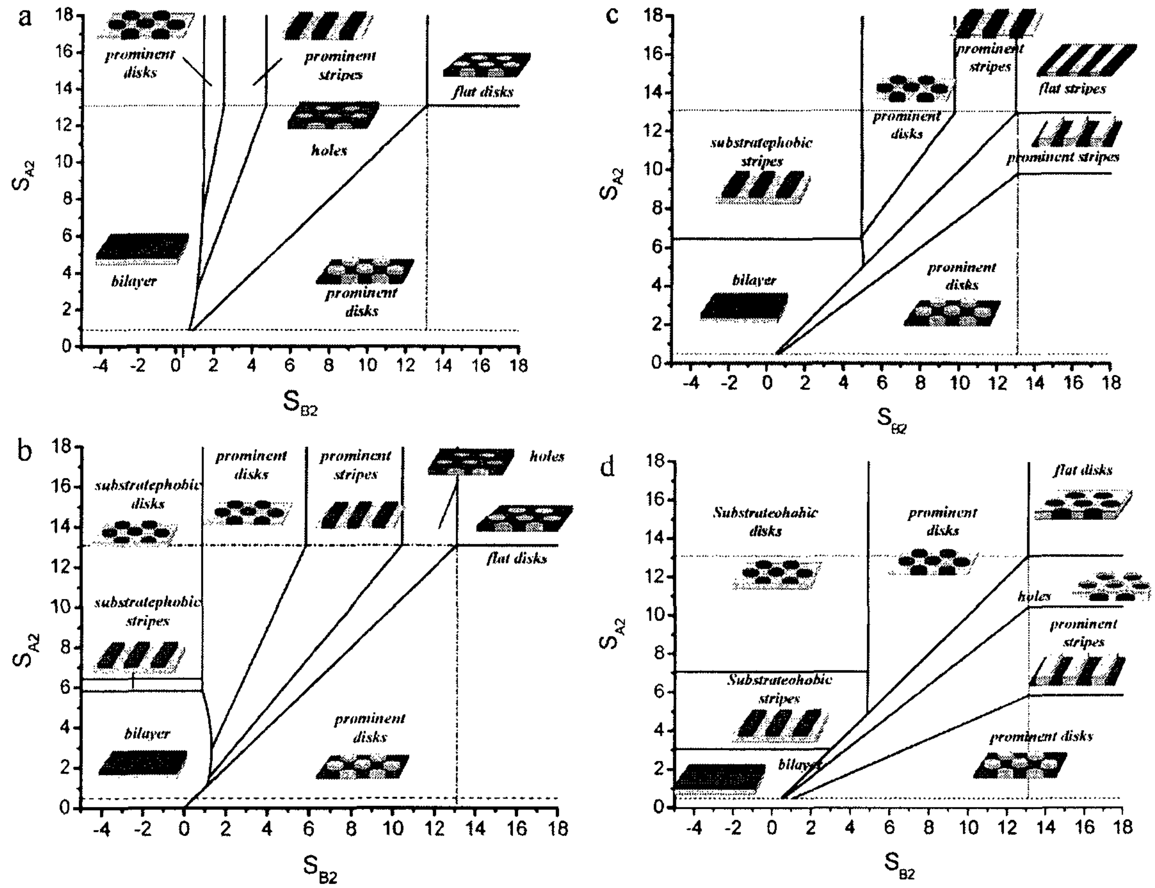

Figure 1.7: S_{A2} – S_{B2} phase diagram of the film for (a) strongly asymmetric copolymer; (b) A block copolymer similar to (a), but with smaller N_B, (c) stronger A and B interaction than (a); and (d) stronger A and B interaction, but smaller buoy block; The anchor and buoy blocks are depicted in blue and cyan, respectively. S_{A2} is the spreading of anchor blocks on the substrate, and S_{B2} is the spreading of buoy blocks on the substrate.[39]

The NMR characterization of adsorbed PVP-PS copolymers in the presence of solvents was carried out by Blum[15, 40, 41]. This work employed deuterium NMR relaxation measurements to study the segmental mobility of a selectively labeled block copolymer, (deuterostyrene-*b*-2-vinylpyridine) (DSVP), adsorbed on silica and alumina. The dynamics of low molecular weight PVP-PS copolymers on silica and alumina, swollen with toluene, appear to be between that of highly extended brushes and homopolymers. The dynamics were successfully modeled based on rigid, intermediate, and mobile components, though a more continuous distribution of species with different mobilities were thought to exist. In general, the surface had a restricting effect on the motion of the adsorbed molecules above its NMR Tg. A small amount of material, assigned to that near the polymer-air interface had a greater mobility than bulk. In general, the mobility of the backbone decreased as the surface adsorbed amount decreased. The partial collapse of the deuterium NMR quadrupole splitting pattern provides a sensitive means of probing surface mobilities as a function of temperature.

Most of the literature on PS-PAA diblocks has focused on the possible morphologies available when these block copolymers are in solution. Poly (styrene-*b*-acrylic acid) chains can form several supermolecular structures, such as rods, micelles, tubules, onions, spindles, and vesicles in solution. The assemblies can be controlled by different factors, such as the absolute and relative block lengths, the presence of additives (ions, homopolymers, and surfactants), the nature and composition of the solvent, the temperature, and the polydispersity of the hydrophilic block. This amphiphilic block copolymer is usually synthesized by the anionic block polymerization of styrene and butyl acrylate, followed by the hydrolysis of poly(*t*-butyl acrylate) blocks into poly(acrylic acid) (PAA).[42, 43] The effects of varying the block length, concentration of copolymer, and solvent have been extensively explored.[44, 45] To a lesser extent, morphology studies have been carried out on spin-coated thin films of PS-PAA.[46-50]

1.3 Introduction to Solid-state NMR

NMR spectroscopy is one of the most important techniques used to investigate the structure, dynamics, and morphology of polymers. The NMR spectra of solid polymers are different from polymers in solution because local interactions such as the chemical shift anisotropy (CSA) and dipolar couplings are not averaged to zero by molecular motion. However, bond rotations and other motions in the chain backbone and side groups may average these interactions. For solids, the extent and nature of the averaging of these broadening interactions determines the techniques used to obtain high-resolution spectra.

The interpretation of solid-state NMR spectra requires the consideration of the nuclear spin Hamiltonian of the system in order to understand how nuclear spins interact with each other and with their surroundings. For spin ½ nuclei the spin Hamiltonian is composed of a number of possible interactions; the dominant ones are the Zeeman, the dipolar and the chemical shift anisotropy.[51]

$$H = H_Z + H_D + H_{CS} \tag{1.4}$$

The Zeeman term, H_z, is the interaction of the nuclear magnetic moment, μ_I, with the static magnetic field, $\mathbf{H}_0$, which is assumed to lie along the z-axis:

$$H_z = -\gamma\hbar H_0 \bar{I}_z \tag{1.5}$$

where γ is the magnetogyric ratio. The Zeeman interaction is linear with applied field, i.e., at higher fields there is a corresponding increase in the population difference between energy levels. The Zeeman interaction allows the experimenter to probe molecular motions on the order of MHz via the measurement of the spin lattice relaxation time [51] (see below).

The dipole-dipole term in a system of two types of spins, H_D, is the interaction due to the magnetic dipoles of nuclear magnetic moments of like (homonuclear,) and unlike (heteronuclear) spins, and takes the form:

$$H_D = H_{II} + H_{SS} + H_{IS} \tag{1.6}$$

where, for example,

$$H_{IS} = \frac{\gamma_I \gamma_S}{r^3} \hbar^2 \bar{I} \cdot \hat{D} \cdot \bar{S} \qquad (1.7)$$

and D is the dipolar coupling tensor.[51] The equations for H_{SS} and H_{II} are analogous. The size of the interaction depends on (i) the magnetogyric ratios, and is therefore greatest for interactions between protons, and (ii) the internuclear distance. Dipolar interactions between ^{13}C nuclei can be ignored due to their low natural abundance (1.1%).

Finally, the chemical shift anisotropy, H_{CS}, is the shielding of the nucleus from the static applied field that occurs due to the surrounding electrons:

$$H_{CS} = \hbar \gamma \bar{I} \cdot \hat{\sigma} \cdot \overline{H} \qquad (1.8)$$

where σ is the chemical shielding tensor. Since the chemical shift anisotropy involves the surrounding electrons, it is the interaction most sensitive to the identity and geometry of other atoms surrounding a given nucleus. The latter two interactions have a dependence on the orientation of the molecule with respect to the external applied field, and are described by 3x3 matrices or tensors, D, and σ respectively, which describe the three dimensional nature of the interactions. [51]

1.4 Solid-State NMR Techniques

1.4.1 Carbon-13 Cross Polarization with Magic Angle Spinning (^{13}C CP-MAS)

Nuclei of one species, for example ^{1}H, exchange energy with each other to develop an equilibrium magnetization because they precess at the same frequency (i.e. have the same Larmor frequencies). However, due to the wide difference in precession frequencies at the magnetic fields employed for NMR, each type of nucleus can be thought of as a closed system. In 1962, Hartman and Hahn found a way to create a connection between spin systems. They realized that by simultaneously applying continuous wave radiofrequency power (rf) at the Larmor frequencies, ν_A and ν_X, two rotating frames are defined, and the rotation of A and X in their respective rotating frames are [52]

$$\omega_{1A} = \gamma_I B_{1A} \qquad (1.9)$$

$$\omega_{1X} = \gamma_S B_{1X} \qquad (1.10)$$

By choosing

$$\frac{B_{1X}}{B_{1A}} = \frac{\gamma_A}{\gamma_B} \qquad (1.11)$$

the "Hartman-Hahn condition" is met and $\omega_{1A}=\omega_{1X}$. The precession frequencies in the rotating frame are identical, they behave as like spins and energy can be transferred between A and X spins.[52]

This principle is applied by using the cross polarization technique, which transfers some of the large magnetization of abundant, large γ like ^{1}H or ^{19}F to rare spin nuclei such as ^{13}C or ^{29}Si. The ^{1}H nucleus has a magnetic moment four times larger than that of ^{13}C, and protons are approximately 100% abundant. The pulse sequence for cross polarization is shown in Figure 1.8. The first step is a 90^{o} pulse applied to the protons followed by a $90\,^{o}$ phase shift to spin lock the proton magnetization in the transverse plane. A radio frequency field is simultaneously applied to ^{13}C under the condition of equation 1.11 until equilibrium is reached, typically between 1 and 5 ms, resulting in a theoretical maximum enhancement of the ^{13}C magnetization by a factor of 4. The ^{13}C rf is turned off, and a ^{13}C FID is observed with proton decoupling. An acquisition delay on the order of the proton T_1 required to allow recovery of the proton longitude magnetization. In solids the proton T_1 is usually much less than the ^{13}C T_1 so that the entire process produces a ^{13}C signal many times larger than would be obtained by applying single pulses to the ^{13}C nuclei directly.

In this sequence the rate of proton transverse relaxation, which is normally determined by the ^{1}H T_2, is determined by the longer time, $T_{1\rho}$, the spin-lattice relaxation time in the rotating frame due to the presence of the continuous ^{1}H rf field. This field spin locks the magnetization and prevents the proton magnetization from decaying by the proton T_2. The ^{13}C magnetization builds up initially with a time constant, T_{CH}, which is characteristic of the strength of the dipolar coupling between protons and carbons. For rigid systems methine and methylene carbons will normally have the shortest T_{CH} values while nonprotonated carbons cross polarize more slowly because of the inverse dependence of the dipolar coupling on the internuclear distance (equation 1.7). Methyl carbons will typically have an intermediate value of T_{CH} as the methyl group rotational motion partially averages the ^{1}H-^{13}C dipolar interaction on which the cross polarization depends. The presence of molecular motion reduces the efficiency of the cross polarization process. As the cross-polarization time, t_{CP}, increases the magnetization passes through a maximum and then diminishes due to the influence of the spin relaxation processes in the rotating frame ($T_{1\rho H}$ and $T_{1\rho C}$). The behaviour of the ^{13}C magnetization as a function of t_{CP} follows the expression:

$$M(t_{CP}) = M_0\left(1 - e^{-\frac{t_{CP}}{T_{CH}}}\right)e^{\left(\frac{-t_{CP}}{T_{1\rho}^{H}}\right)} \qquad (1.12)$$

where $T_{1\rho C}$ is assumed to be long enough to be ignored. Multiple homonuclear dipole-dipole couplings among ^{1}H usually result in one $T_{1\rho H}$ for the proton spins that are dipolar coupled to each other. T_{CH} values are different for different carbons of the molecule and an estimate of their values is needed for a quantitative analysis of CP signals.[51]

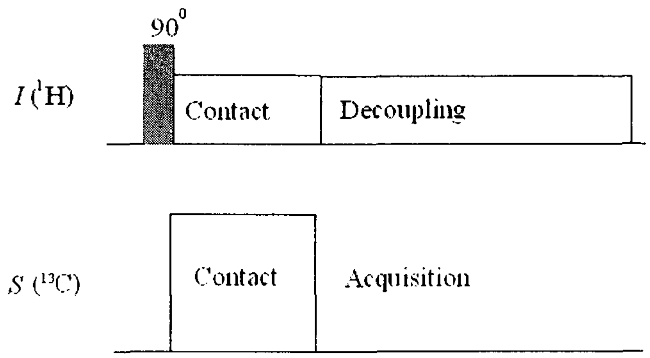

Figure 1.8: Pulse sequence for cross polarization. After a 90° pulse the I spins transfer polarization to S spins during the contact time. The S signal is the detected while the I spins are decoupled.[52]

In 1958, before dipolar and multiple pulse methods were developed, a different approach was introduced to narrow magnetic dipolar broadened NMR lines in solids.[52] In a static sample the chemical shift of a spin ½ nucleus in a single given orientation in a magnetic field is written as a sum of two terms: $\delta_{obs} = \delta_{iso} + \delta(\theta,\phi)$ where δ_{iso} is the isotropic shift and $\delta(\theta,\phi)$ is a contribution that is dependent on the orientation of the molecule in the magnetic field. If the sample is spun about an angle to the magnetic field, β, the equation becomes $\delta_{obs} = \delta_{iso} + \delta(\theta,\phi) \times (3\cos^2\beta - 1)$. The second term disappears if β is averaged over all space by isotropic molecular motion, but it also disappears if $\cos^2\beta = 1/3$, which occurs when $\beta = 54.7°$. Thus rapid rotation of the sample at an angle of 54.7° to B_0 eliminates the orientation dependence, and therefore dipolar interactions and CSA effects, leaving only the isotropic chemical shift. Magic angle spinning (MAS) can be combined with proton decoupling to eliminate the effects of CSA and provide high resolution NMR spectra in the solid phase. When magic angle spinning is combined with cross polarization, the method is referred to as CP-MAS.

When the spinning speed is much less than the magnitude of the CSA, spinning sidebands are generated at multiples of the spinning rate. These spinning sidebands can be removed by the application of pulse sequences such as TOSS (TOtal Suppression of Spinning sidebands).[52]

1.4.2 Relaxation Measurements Via the Methods of Inversion Recovery and Torchia

Spin-lattice relaxation or longitudinal relaxation (T_1) corresponds to the process in which the spins, excited by radiofrequency irradiation, give up energy to their surroundings, the lattice, to return to the equilibrium population distribution of the spin states. As described above, the dipolar interaction operates through space and depends on the orientation of the internuclear vector relative to the magnetic field as well as on the distance between the dipoles. As the I-S internuclear vector undergoes motion, a magnetic dipole provides a fluctuating magnetic field and a mechanism for relaxation for other nearby nuclei. For isotropic motion, the relaxation rate $R_1 = 1/T_1$ where T_1 is the spin-lattice relaxation time, has the following expression for two unlike spins [52]:

$$R_1 = \frac{\gamma_I^2 \gamma_S^2 \hbar^2}{10 r_{IS}^6} \left[\frac{\tau_C}{1 + (\omega_I - \omega_S)^2 \tau_C^2} + \frac{3\tau_C}{1 + \omega_I^2 \tau_C^2} + \frac{6\tau_C}{1 + (\omega_I + \omega_S)^2 \tau_C^2} \right] \tag{1.13}$$

where ω_I and ω_S are the Larmor frequencies of the two spins and τ_c is the correlation time. For nonisotropic motion the parameter τ_c can be replaced by an "effective" correlation time τ_{eff}.

The variation of T_1 with the correlation time, τ_c (or equivalently τ_{eff}), and temperature gives information about the dynamics of the system. In the fast motional regime or extreme narrowing condition, T_1 decreases as temperature decreases and τ_c increases, and then passes through a minimum at which the Larmor frequency equals the reciprocal of τ_c. The more restricted the mobility of the sample the higher the temperature at which the T_1 minimum occurs. Above the minimum, T_1 once again increases as temperature decreases and τ_c increases. This is called the slow motional regime.

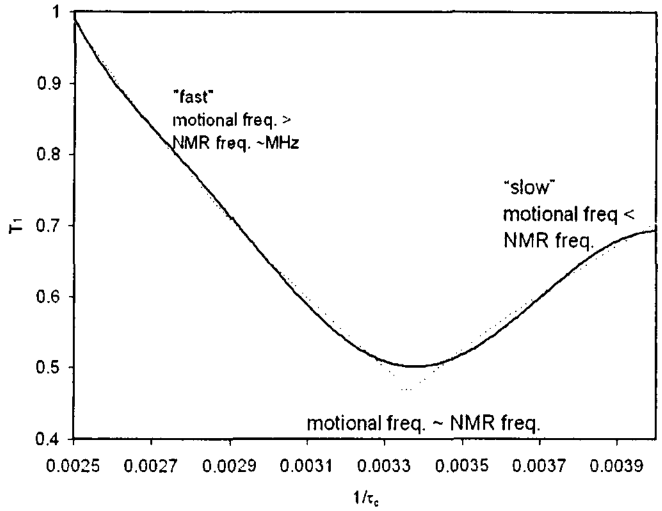

Figure 1.9: Correlation curve showing the relation between T_1 and the correlation time.[52]

There are several ways to measure T_1. In the inversion recovery experiment, the system is initially at equilibrium with the spins occupying levels according to the Boltzmann distribution resulting in a net magnetization vector, M_0, along the z-axis (B_0 direction). After applying a 180° pulse, the magnetization is inverted. The magnetization relaxes back along the z-axis during a relaxation period, τ, and a second pulse (90°) is applied. M_Z varies according to equation 1.14 [51]:

$$M_Z = M_0(1-2e^{(-\tau/T_1)}) \qquad (1.14)$$

The inversion-recovery pulse sequence 180°-τ-90° is shown in Figure 1.10. Plotting the variation of the population difference (M_z) as a function of time τ gives an exponential curve starting at -M_0 and increasing towards the Boltzmann equilibrium value, +M_0, with a time constant T_1, the spin-lattice relaxation time.

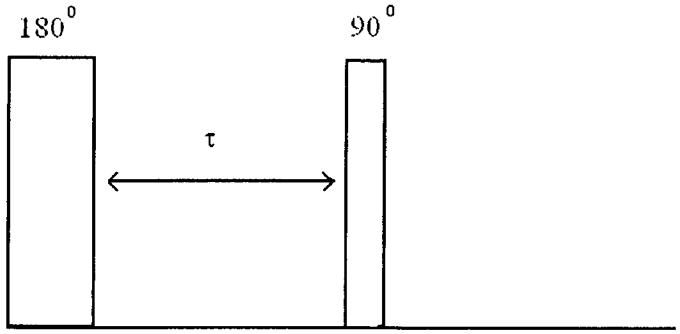

Figure 1.10: The inversion-recovery pulse sequence.[52]

While the inversion-recovery method is useful for measuring short T_1's typical of mobile solids, another technique is used to measure the longer T_1 values typical of organic solids and semi-crystalline polymers. For example, for polyethylene, T_{1c} is 2000s in the crystalline regions, and T_{1a} is 0.5s in amorphous regions where significant molecular motion occurs.[50] This large difference in T_1 can be used to separate the crystalline signal from the amorphous signal in solid-state ^{13}C NMR. The pulse sequence, described by Torchia [52] is a modified cross-polarization (CP) pulse sequence (Figure 1.8) and allows the determination of T_1 of rigid polymers whose spectra are usually acquired under CP conditions. The Torchia pulse sequence is shown in Figure 1.11. A variable delay τ is inserted between the spin locking and decoupling of the proton spins and then the pulse is repeated, but this time using a 90° proton pulse of opposite phase in the second sequence. When the signal from the second sequence is subtracted from the first sequence, the net signal does not depend on: M_0 (the equilibrium longitudinal magnetization), the residual carbon magnetization due to spin-lattice processes at the beginning of the sequence or during a long delay τ, and artifact transients. The sequence keeps the signal increase of a CP experiment, and the signal I after N scans (N is even) is proportional to:

$$I \propto NM_{CP}(0)e^{(-t/T_1)} \qquad (1.15)$$

where $M_{CP}(0)$ is the initial proton-enhanced longitudinal magnetization. Depending on the delay time t_D (Figure 1.11) one can focus on the amorphous or crystalline region of a polymer. The pulse sequence involves a pulse (D_2) chosen to rotate the magnetic moments by 90° in either the positive or the negative direction about the y-axis. The magnetization of the amorphous carbons (M_a) relaxes to the equilibrium value, M_a^0, in a delay time of t_D because t_D was chosen to be longer than T_{1a}. The magnetization, M_c, of crystalline carbons stays does not relax to an equilibrium value after t_D because T_{1c} is longer than t_D. Therefore M_{1c}, is parallel to the z-axis after the +90° pulse, but antiparallel after the -90° pulse; M_c, and M_a are aligned parallel by the +90° pulse but antiparallel by the -90° pulse. The phases of the observed signals from crystalline and amorphous regions are opposite depending on the sign of the 90° pulse.[50] If the spectra, A and B, obtained from the two pulses are added, the spectrum of the amorphous regions is observed selectively. If spectrum A is subtracted from spectrum B, the crystalline spectrum is observed selectively.

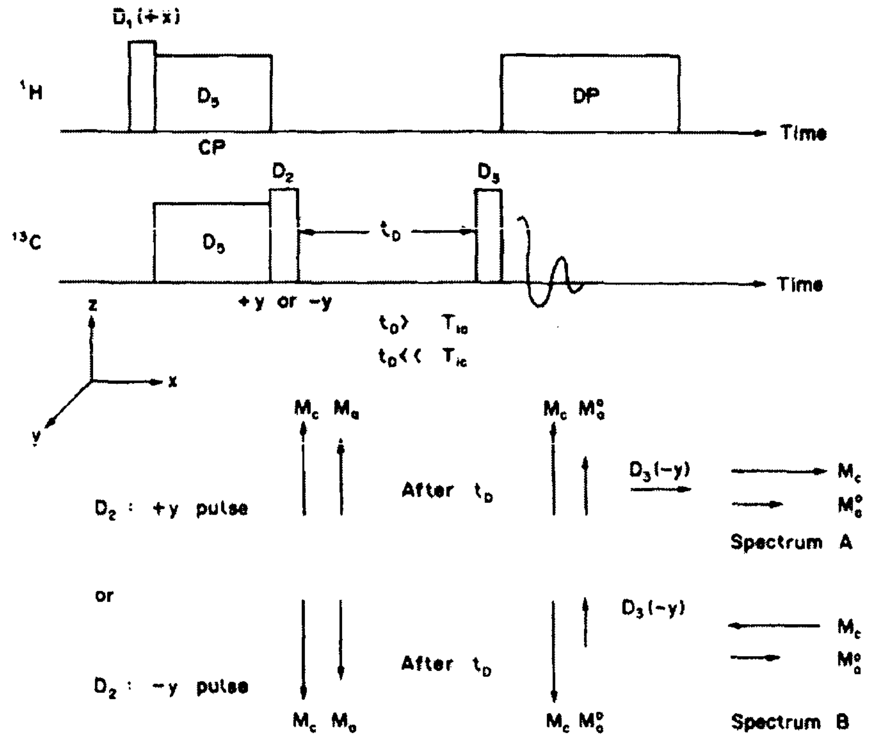

Figure 1.11: The Torchia pulse sequence and behaviour of the magnetic moments M_c and M_a. Figure 1.11 is derived from Sohma et al.[50]

Spin-lattice relaxation can also be measured in the rotating frame. The pulse sequence for proton spin-lattice relaxation in the rotating frame ($T_{1\rho H}$) includes the initial 90^o proton pulse but leaves the ^1H rf field on for a time delay, τ, before the cross polarization contact time. The proton magnetization decays exponentially with $T_{1\rho}$ as

$$M(\tau) = M_0 e^{(-\tau / T_{1\rho})} \qquad (1.16)$$

and is monitored by cross polarizing the proton magnetization to ^{13}C and subsequent measurement of the ^{13}C signal. The ^{13}C $T_{1\rho}$ is similar to that of the ^1H $T_{1\rho}$, except the carbon spin lock time is varied instead of the proton spin lock. $T_{1\rho}$ measurements probe motions in the kHz region, which are sometimes associated with cooperative polymer backbone rearrangements that involve a large number of monomer units. It should also be noted that $T_{1\rho}$ measurements are less reliable than T_1 measurements as they can be complicated by contributions from T_2 if the spinlock field is not strong relative to the proton dipolar coupling.[53, 54]

1.5 Fourier Transform Infrared Spectroscopy with Photoacoustic Detection (FTIR-PAS)

The main sample handling problem in FTIR analysis of solid and semi-solid materials is that most materials are not transparent for direct transmission analysis in the mid-infrared spectral region. This problem can be overcome by grazing angle geometries or by using various methods of sample preparation where the optical density of the sample is reduced.[55] Unfortunately this leads to other problems, the risk of changes to the sample, increased time, labor, preparation errors, and the destructive nature of the process. A variety of approaches have been tried to avoid or to minimize sample preparation.

The photoacoustic effect was observed for the first time by Alexander Graham Bell in 1880 [56]. Photoacoustic spectroscopy, PAS, has proven to be a mid-infrared solution to the transparency problem. If a sample adsorbs energy from radiation, which is modulated at acoustic frequencies, some of that adsorbed energy will eventually be emitted as acoustic waves. If the sample is a gas in a sealed vessel, the periodic absorption of radiation will cause a periodic fluctuation in temperature, and pressure, with the period determined by the modulation frequency of the incoming radiation. The pressure modulations can then be detected as sound with a microphone. If acoustic energy is to be emitted then electromagnetic energy must be adsorbed, and therefore the photoacoustic signal reflects the adsorption spectrum of the sample. Due to its basic characteristics, the PAS/FTIR technique is used to study the surfaces of materials and coatings, and is widely used in the study and characterization of pigments, opaque samples and dark (black) samples, which it would be very difficult to study using other IR absorption techniques. One example of importance to the study of polymer blends and composites is the study by Vidrine [57] that shows that the PAS spectrum is independent of the physical state of the sample. PAS has proven useful in polymer spectroscopy because samples may be examined in any physical form and without the inconvenience and destructive nature of alternative techniques such as dispersion in a KBr pellet. The dependence of PAS signal intensity on the physical state reflects the efficiency of the energy transfer between the sample surface and the surrounding gas. The efficiency depends on the surface area of the sample and is highest for powdered samples. When comparing PAS with other IR spectroscopic techniques, the most useful comparison is with DRIFT spectroscopy, since both techniques are used on samples with irregular geometries, which make them unsuitable for transmission analysis. Yang [56] recently compared PAS and DRIFT in a study of the particle size and distribution of sucrose powder. Both techniques exhibited some degree of surface specificity, but PAS was found to be better in this application for the detection of surface modification of the fibers. PAS is an interesting technique as it is able to characterize samples inaccessible to other techniques while providing surface information. Unfortunately, the signal-to-noise is usually less than for conventional absorption or reflection techniques, and the spectra can show signs of saturation effects and other problems of quantification.

1.6 Scope of Thesis

Overall scope of the thesis

The research in the following thesis is composed of two related parts. The first part focuses on the adsorption of a series of random copolymers onto different substrates. This work is motivated by the role that the chain conformation plays in the adhesion of polymer films to solid surfaces. At the interface, the chain conformation and mobility will vary with the chain length, the density of binding groups on the polymer chain, the density of the surface binding groups and the strength of the polymer-substrate interactions. In our study we varied the sticker group density as well as the binding strength through different polar sticker groups and substrates. Chain conformation at the interface determines the cohesive strength. There is a balance between the adsorption of sticker groups onto the solid substrate and good chain connectivity, which may be achieved through correct selection of the type and the concentration of sticker groups. The goal of our study was thus to study, using NMR techniques, how these two variables affect the chain conformation and mobility.

The second part of the thesis is a solid-state NMR study of the dynamics of adsorption of block copolymers onto zirconia. In contrast to the adsorbed random copolymers where the chain configuration was not known, the surface structures of block copolymers in the presence of solvent have been predicted theoretically and verified to some extent experimentally. Little is known however about the chain dynamics of these structures, especially in the absence of solvent. Such information is relevant to the use of these copolymers as surface modifiers in composites.

Chapter 1, as per the foregoing gives an introduction to the theory and applicability of solid-state NMR. A review of relevant literature concerning the adsorption of block and random copolymers onto a solid substrate is presented. In addition, other relevant techniques are described.

Chapter 2 is a study of the effect of sticker group density and binding strength on chain conformation and dynamics of adsorbed ethylene copolymers for a number of random copolymers with different monomer ratios. The polymers used for this study were polyethylene (PE), poly (ethylene-*co*-vinyl acetate) (EVA), poly (ethylene-*co*-vinyl alcohol) (EVOH), and poly (ethylene-*co*-acrylic acid) (PEA). The effect of the substrate was observed by varying the surface area, and the basicity of the metal oxide substrates.

Chapter 3 is a study of the effect of block length and binding strength on chain conformation and dynamics of adsorbed block copolymers. The block copolymers employed in this study were poly (styrene)-*b*-poly (acrylic acid), and poly (styrene)-*b*-poly (*t*-butyl acrylate). Copolymers of various block length were adsorbed on zirconia. Solid-state NMR spectroscopy, FTIR-PAS, and thermogravimetric analysis (TGA) were used to characterize the surface behaviour of the systems, with comparisons made between the bulk and adsorbed block copolymers.

Chapter 4 presents research that focuses on block copolymer adsorption on metal oxide surfaces. The block copolymers employed in this study were poly (isoprene)-*b*-poly (2-vinylpyridine), and poly (isoprene)-*b*-poly (4-vinylpyridine)). Copolymers of various block length were adsorbed on zirconia. Solid-state NMR spectroscopy, FTIR-PAS, and thermogravimetric analysis (TGA) were used to characterize the surface behaviour of the systems. ^{13}C CP-MAS, ^{1}H and T_1 relaxation measurements were all recorded with the aim of correlating the microscopic structure of the surface with changes in NMR data.

Chapter 5 provides general conclusions obtained from the body of work presented, and also describes some suggestions for future work.

1.7 References

1. Fleer, G.J., et al., *Polymers at Interfaces.* 1993, London: Chapman and Hall.
2. Silberberg, A., *Encyclopedia of Polymer Science and Technology.* 2nd ed. Vol. 1: John Wiley and Sons, Inc. 577-594.
3. Santore, M.M., *Dynamics in adsorbed homopolymer layers: Understanding complexity from simple starting points.* Current Opinion in Colloid and Interface Science, 2005. **10**: p. 176-183.
4. Takahashi, A. and Kawaguchi, M., *The Structure of Macromolecules Adsorbed on Interfaces.* Advances in Polymer Science, 1982. **46**: p. 1-65.
5. Fu, Z. and Santore, M.M., *Evolution of Layer Density and Thickness during Poly(ethylene oxide) Adsorption onto Silica.* Langmuir, 1997. **13**: p. 5779-5784.
6. Frantz, P. and Granick, S., *Kinetics of Polymer Adsorption and Desorption.* Physical Review Letters, 1991. **66**: p. 899-902.
7. Frantz, P. and Granick, S., *Exchange Kinetics of Adsorbed Polymer and the Achievement of Conformational Equilibrium.* Macromolecules, 1994. **27**: p. 2553-2558.
8. Johnson, H.E. and Granick, S., *Exchange kinetics between the adsorbed state and free solution: poly(methyl methacrylate) in carbon tetrachloride.* Macromolecules, 1990. **23**: p. 3367-3374.
9. Soga, I. and Granick, S., *Infrared Dichroism and Surface Conformational Dynamics of Adsorbed Poly(dimethylsiloxane).* Macromolecules, 1998. **31**: p. 5450-5455.
10. Stuart, M.A.C., Fleer, G.J., and Scheutjens, J.M.H.M., *Displacement of polymers. II. Experiment. Determination of segmental adsorption energy of poly(vinylpyrrolidone) on silica.* Journal of Colloid and Interface Science, 1984. **97**: p. 526-535.
11. Lee, I. and Wool, R.P., *Optimum Polymer-Solid Interface Design for Adhesion Strength: Carboxylation of Polybutadiene and Mixed Silanes Surface Modification of Aluminum Oxide.* Journal of Adhesion, 2001. **75**: p. 299-324.
12. Lin, W.-Y. and Blum, F.D., *Segmental Dynamics of Bulk and Adsorbed Poly(methylacrylate)-d_3 by Deuterium NMR: Effect of Adsorbed Amount.* Macromolecules, 1997. **30**: p. 5331-5338.
13. Nagashima, K. and Blum, F.D., *Adsorption and dynamics of sodium alkylbenzenesulfonates on alumina.* Colloids and Surfaces A: Physicochemical and Engineering Aspects, 2001. **176**: p. 17-24.

14. Oslanec, R., et al., *Crossover of a block copolymer brush in a polymer melt from a stretched to collapsed conformation.* Physical Review E, 1997. **56**(3): p. 2383-2386.
15. Sinhat, B.R., Blum, F.D., and Schwab, F.C., *Dynamics of Adsorbed, Swollen Block Copolymers.* Macromolecules, 1993. **26**: p. 7053-7057.
16. Xie, M. and Blum, F.D., *Adsorption and Dynamics of Low Molecular Weight Poly(styrene-b-2-vinylpyridine) on Silica and Alumina in Toluene.* Langmuir, 1996. **12**: p. 5669-5673.
17. Huguenard, C. and Pefferkorn, E., *Rate of Adsorption of Diblock Copolymers from Micellar Solutions on Solid-Liquid Interfaces.* Macromolecules, 1994. **27**: p. 5271-5276.
18. Johner, A. and Joanny, J.F., *Block Copolymer Adsorption in a Selective Solvent: A Kinetic Study.* Macromolecules, 1990. **23**: p. 5299-5311.
19. Munch, M.R. and Gast, A.P., *Kinetics of block copolymer adsorption on dielectric surfaces from a selective solvent.* Macromolecules, 1990. **23**: p. 2313-2320.
20. Tassin, J.F., et al., *Kinetics of Adsorption of Block Copolymers Revealed by Surface Plasmons.* Journal of Physical Chemistry, 1989. **93**: p. 2106-2111.
21. Bijsterbosch, H.D., Stuart, M.A.C., and Fleer, G.J., *Nonselective Adsorption of Block Copolymers and the Effect of Block Incompatibility.* Macromolecules, 1998. **31**: p. 7436-7444.
22. Boss, F., Schreiberf, H.P., and Eisenberg, A., *Specific Adsorption of Some Styrene/Vinylpyridine Diblocks from Selective Solvents onto Solid Substrates-An NMR Study.* Macromolecules, 1993. **26**: p. 6447-6454.
23. Belder, G.F., ten Brinke, G., and Hadziioannou, G., *Influence of Anchor Block Size on the Thickness of Adsorbed Block Copolymer Layers.* Langmuir, 1997. **13**: p. 4102-4105.
24. Marques, C. and Joanny, J.F., *Block Copolymer Adsorption in a Nonselective Solvent.* Macromolecules, 1989. **22**: p. 1454-1458.
25. Marques, C., Joanny, J.F., and Leibler, l., *Adsorption of Block Copolymers in Selective Solvents.* Macromolecules, 1988. **21**: p. 1051-1059.
26. Parsonage, E., et al., *Adsorption of Poly(2-vinylpyridine)-Poly(styrene) Block Copolymers from Toluene Solutions.* Macromolecules, 1991. **24**: p. 1987-1995.
27. Dewalt, L.E., Ouyang, H.D., and Dimonie, V.L., *Competition Between Micellization and Adsorption of Diblock Copolymers in a Colloidal System.* Journal of Applied Polymer Science, 1995. **58**: p. 265-269.
28. Bijsterbosch, H.D., Stuart, M.A.C., and Fleer, G.J., *Adsorption Kinetics of Diblock Copolymers from a Micellar Solution on Silica and Titania.* Macromolecules, 1998. **31**: p. 9281-9294.
29. Hong, P.P., et al., *An investigation of the adsorption of polystyrene/poly(2-vinylpyridine) diblock copolymers onto silver substrates using surface-enhanced Raman scattering.* Macromolecules, 1993. **26**: p. 3953-3959.
30. Webber, G.B., et al., *Adsorption of Amphiphilic Diblock Copolymer Micelles at the Mica/Solution Interface.* Langmuir, 2001. **17**: p. 5551-5561.
31. Halperin, A. and Joanny, J.F., *Adsorption of Star Polymers.* Journal de Physique II France, 1991. **1**: p. 623-636.
32. Eibeck, P., et al., Polymer Preprint, 1999. **40**: p. 990.

33. Potemkin, I.I., et al., *Nanopattern of Diblock Copolymers Selectively Adsorbed on a Plane Surface.* Langmuir, 1999. **15**: p. 7290-7298.
34. Potemkin, I.I. and Moller, M., *Microphase Separation in Ultrathin Films of Diblock Copolymers with Variable Stickiness of One of the Blocks to the Surface.* Macromolecules, 2005. **38**: p. 2999-3006.
35. Spatz, J.P., et al., *Ultrathin Diblock Copolymer/Titanium Laminates - A Tool for Nanolithography.* Advanced Materials, 1998. **10**: p. 849-852.
36. Spatz, J.P., et al., *Order-Disorder Transition in Surface-Induced Nanopattern of Diblock Copolymer Films.* Macromolecules, 2000. **33**: p. 150-157.
37. Spatz, J.P., et al., *Nanomosaic Surfaces by Lateral Phase Separation of a Diblock Copolymer.* Macromolecules, 1997. **30**: p. 3874-3880.
38. Spatz, J.P., Sheiko, S., and Moller, M., *Substrate-induced lateral micro-phase separation of a diblock copolymer.* Advanced Materials, 1996. **8**: p. 513-517.
39. Patyukova, E.S. and Potemkin, I.I., *Nanostructured Ultrathin Films Obtained by the Spreading of Diblock Copolymers on a Surface.* Langmuir, 2007. **23**: p. 12356-12365.
40. Xie, M. and Blum, F.D., Langmuir, 1996. **12**: p. 5669.
41. Blum, F.D., Sinhat, B.R., and Schwab, F.C., *Density Profile of Terminally Adsorbed Polymers.* Macromolecules, 1990. **23**: p. 3592-3598.
42. Yu, T., Zhang, L., and Eisenberg, A., *Morphogenic Effect of Solvent on Crew-Cut Aggregates of Amphiphilic Diblock Copolymers.* Macromolecules, 1998. **31**: p. 1144-1154.
43. Zhang, L. and Eisenberg, A., *Morphogenic Effect of Added Ions on Crew-Cut Aggregates of Polystyrene-b-poly(acrylic acid) Block Copolymers in Solutions.* Macromolecules, 1996. **29**: p. 8805-8815.
44. Bendejacq, D., et al., *Well-Ordered Microdomain Structures in Polydisperse Poly(styrene)-Poly(acrylic acid) Diblock Copolymers from Controlled Radical Polymerization.* Macromolecules, 2002. **35**: p. 6645-6649.
45. Terreau, O., Bartels, C., and Eisenberg, A., *Effect of Poly(acrylic acid) Block Length Distribution on Polystyrene-b-poly(acrylic acid) Block Copolymer Aggregates in Solution. 2. A Partial Phase Diagram.* Langmuir, 2004. **20**: p. 637-645.
46. Feng, C.L., Vancso, G.L., and Schonherr, H., *Interfacial Reactions in Confinement: Kinetics and Temperature Dependence of the Surface Hydrolysis of Polystyrene-block-poly(tert-butyl acrylate) Thin Films.* Langmuir, 2005. **21**: p. 2356-2363.
47. La, Y.-H., et al., *Directed Assembly of Cylinder-Forming Block Copolymer Films and Thermochemically Induced Cylinder to Sphere Transition: A Hierarchical Route to Linear Arrays of Nanodots.* Nano Letters, 2005. **5**: p. 1379-1384.
48. Miao, S., *Investigation on NIR, coating mechanism of PS-b-PAA coated calcium carbonate particulate.* Applied Surface Science, 2003. **220**: p. 298-303.
49. Perelstein, O.E., et al., Macromolecules Rapid Communication, 2007. **28**: p. 977.
50. Sohma, J., et al., *Solid-state high resolution ^{13}C-NMR study of crosslinks in heavily gamma-irradiated polyethylene.* Radiation Physical Chemistry, 1991. **37**: p. 47-51.

51. Fyfe, C.A., *Solid-State NMR For Chemists*. 1983, Guelph, Ontario, Canada: CFC Press.
52. Becker, E.D., *High Resolution NMR: Theory and Chemical Applications*. third ed. 2000, London: Academic Press.
53. Koenig, J.L., *Spectroscopy of Polymers*. 1992, USA: American Chemical Society.
54. Spatz, J.P., Sheiko, S., and Moller, M., Advanced Materials, 1996. **8**: p. 513.
55. Garton, A., *Infrared Spectroscopy of Polymer Blends, Composites and Surfaces*. 1992, Barcelona: Hanser.
56. Yang, H. and Irudayaraj, J., *Estimation of Particle Size by DRIFTS and FTIR-PAS*. Particulate Science and Technology, 1999. **14**: p. 269-282.
57. Vidrine, D.W. and Lowry, S.R., *Photoacoustic Fourier transform IR spectroscopy and its application to polymer analysis*. Advances in Chemistry Series, 1983. **203**: p. 595-613.

Chapter 2: Chain Conformation of Ethylene Random Copolymers

2.1 Preface

Chapter 2 is a study of the effect of sticker group density and binding strength on chain conformation and dynamics of adsorbed ethylene copolymers by using a number of random copolymers at various weight percents. The polymer-surface interaction can be studied by solid-state NMR and FTIR-PAS allowing one to gain dynamic, conformation, and morphology information. This chapter was a continuation of work begun by Dr. Victor Nasreddine where he was able to see a definite correlation between the loading and the binding strength when studying poly (ethylene-co-acrylic acid) adsorbed on zirconia.

2.2 Abstract

The structures formed by the adsorption of poly (ethylene-*co*-acrylic acid) (PEA), poly (ethylene-*co*-vinyl alcohol) (EVOH), poly (ethylene-*co*-vinyl acetate) (EVA), and polyethylene (PE) on metal oxide powders were characterized by solid-state NMR spectroscopy and FTIR-PAS. The effect of the copolymer loading and the polar group density on the chain conformation and mobility were examined. In the case of the strongest polar group-substrate interactions, the chain conformation is determined by the sticker group density rather than the coverage until all the binding sites have been occupied. As the binding strength decreases, this trend diminishes, and there is a corresponding increase in the chain order as reflected by the ^{13}C chemical shifts of the ethylene segments. The chain conformation of the most weakly bound copolymer (EVA on alumina) shows no dependence on either the sticker group content or the coverage,

similar to the homopolymer, PE. Some surface hydrolysis of EVA and of the residual ester groups of EVOH is also detected.

2.3 Introduction

Copolymers of polyethylene-containing polar groups are commonly used as adhesion promoters between metal surfaces and polyethylene coatings. In previous work, Nasreddine et al.[1] studied poly (ethylene-*co*-acrylic acid) (PEA) random copolymers adsorbed onto zirconia by solid-state NMR and FTIR. The PEA/zirconia system was chosen because it is a convenient system that displays strong polymer adsorption. A connection between the chain conformation of polyethylene segments as determined by ^{13}C chemical shifts and the interaction of the acrylic acid with the surface as determined by FTIR was established. Solid-state 2D wide-line separation (WISE) and ^{1}H spin diffusion NMR experiments were used to determine chain motion and morphology of bulk and adsorbed copolymers. Results showed that the polymer conformation depended on sticker density and not on coverage. Also, the adsorbed copolymers with a low density of sticker groups had an ordered, less mobile component that was attributed to partially folded loops and not trains.[1]

In other relevant studies, Hjertberg et al.[2] showed that the adhesion between alumina and polyethylene increased with the content of butyl acrylate and vinyl acetate as comonomers. Ulrén et al.[3] looked at the effect of carboxylic acid, ester, and silane functional groups in ethylene copolymers on the adhesion with aluminum. The interface was studied by FTIR, and the adhesion mechanism for each functional group was evaluated. They were able to determine that the strength of the interfacial interactions depended on acidity/basicity and the concentration of the functional group. Cosgrove et al.[4] studied the adsorption of random copolymers of poly (ethylene-*co*-vinyl acetate) on modified silica surfaces by NMR, SANS, and MC. The solution-state NMR measurements showed that there was a direct correlation between the adsorbed amount and the bound fraction. Finally, Brogly and co-workers published a series of papers using surface IR methods to study the interaction of random copolymers of EVA with alumina and determined that the polymer interacted via a Lewis acid-base interaction. [5-11]

The goals of the present paper are to study the effect of sticker group density and binding strength on chain conformation and dynamics of adsorbed ethylene copolymers by using a number of random copolymers at various weight percents. Since the key parameter is interfacial sticker group density rather than bulk polymer sticker group density, the extent of binding was monitored by vibrational spectroscopy. In order of increasing binding strength, the polymers used were polyethylene (PE), poly (ethylene-*co*-vinyl acetate) (EVA), poly (ethylene-*co*-vinyl alcohol) (EVOH), and poly (ethylene-*co*-acrylic acid) (PEA).[2] The effect of the substrate was observed by varying the surface area, and the basicity of the metal oxide substrates. FTIR-PAS and TGA were used to characterize the polymer-substrate interactions and the surface coverage, respectively. Solid-state ^{13}C CP-MAS NMR was employed to obtain the conformation of adsorbed polymers from the transoid and gauchoid components of the polyethylene segments. Finally, variable temperature and NMR relaxation measurements were also carried out to obtain dynamic information; the presence of loops, trains, and tails was assigned on the basis of the chain mobility.

2.4 Experimental Section

2.4.1 Materials

Random copolymers of poly (ethylene-*co*-acrylic acid) (PEA) were obtained from Scientific Polymer Products Inc. Two copolymers were used that had 5 and 15 wt % acrylic acid and are denoted PEA 5% and PEA 15% throughout this article. Random copolymers of poly (ethylene-*co*-vinyl alcohol) (EVOH) were obtained from Scientific Polymer Products Inc. The two copolymers that were used had 15 and 25 wt % vinyl alcohol and are denoted EVOH 15% and EVOH 25%. Two poly (ethylene-*co*-vinyl acetate) (EVA) random copolymers were obtained from Aldrich Chemical Co. Inc. having vinyl acetate contents of 12 and 25 wt %, respectively. These two polymers are denoted EVA 12% and EVA 25% herein. Polyethylene (PE) was also obtained from Aldrich Chemical Co. Inc. M_n, M_w, crystallinity, and polydispersity values for the copolymers are listed in Table 2.1. The metal oxide surfaces, powdered aluminum oxide C (Al_2O_3) and zirconia (ZrO_2), were supplied by Degussa. Alumina had a reported average particle size of 13 nm and a BET surface area of 100 ± 15 m^2/g, while zirconia had a reported average particle size of 30 nm and a BET surface area of 40 ± 10 m^2/g. All chemicals were used as received.

As can be seen in Table 2.1, EVA is approximately 10 times the molecular weight of PEA. For both EVA and PEA the crystallinity is higher for the lower weight percent polymer. An average number of carbons between binding groups were estimated to see if loops could be formed, with PEA 5% having approximately 100 methylenes between binding groups and 15% EVOH having approximately 12 methylenes between binding groups.

Table 2.1 Information on PEA, EVA, and EVOH

	PEA 5%	PEA 15%	EVA 25%	EVA 12%	EVOH 15%
M_n or M_w	7900[1] M_w	1300[1] M_w	16000[12] M_n	37000[12] M_n	
crystallinity (%)	24	8	8	19	14
polydispersity	1.8	1.1	2.5	6	
Carbons between binding groups	~100	~30	~15	~37	~12

2.4.2 Sample Preparation

For each copolymer, 10 solutions were prepared by dissolving 30, 60, 90, 120, 180, 240, 300, 600, 900, and 1200 mg of copolymer in 50 ml of warm xylene. A second solution was prepared by dispersing 2 g of alumina in 250 ml of xylene with 15 min of sonication. The alumina and copolymer solutions were added and allowed to reflux for 24 h. The adsorbed copolymer was washed six times by redispersing in 40 ml of xylene under heating. After the final washing the adsorbed copolymer was filtered and dried under vacuum. Thermal gravimetric analysis (TGA) determined the weight percent of copolymer adsorbed on alumina. Samples were prepared in the same manner as stated above when zirconia was the substrate with the exception that zirconia was heated at 400 °C for 5 h before use.

2.4.3 Solid-State ^{13}C CP-MAS NMR

All solid-state ^{13}C NMR spectra (75.34 MHz) were recorded on a Chemagnetics CMX-300 NMR spectrometer with a 7.5 mm PENCIL probe. Samples were spun at a rate of 4 kHz. The ^{13}C CP-MAS spectra were obtained with a pulse delay of 1 s, 4000 scans, a pulse width of 4 μs, and a contact time of 1 ms. Two pulse sequences were used to determine the various T_1 values for the ethylene region of the ^{13}C spectra. The Torchia pulse sequence [13] was used for longer T_1 values, while the inversion recovery pulse sequence was used for shorter T_1 values. Torchia spectra were collected with the following parameters: a pulse delay of 1 s, 640 scans, a pulse width of 4.25 μs, and a contact time of 1 ms. The delay times were 1, 5, 8, 13, and 20 s. Inversion recovery spectra were obtained under the following conditions: a pulse delay of 4 s, 1600 scans, and a pulse width of 4.25 μs.

2.4.4 FTIR-PAS

A Fourier Transform IR spectrometer (Mattson Research Series 1 spectrometer) equipped with a photoacoustic cell (MTEC model 300) was used to collect all IR spectra. The spectra were collected with a 4.0 cm^{-1} nominal resolution.

2.4.5 Thermal Gravimetric Analysis (TGA)

All samples were heated to 600 °C in a nitrogen environment at a rate of 10 °C/min, and then they were held at 600 °C in an oxygen environment for 10 min. This process allowed the amount of organic material attached to the metal oxide surface to be determined. All samples were run on the TGA Q500 from TA Instruments.

2.5 Results and Discussion

2.5.1 Effect of Substrate: PEA on Alumina

Studies of the adsorption of carboxylic acids on metal oxides show that they bind much more strongly to zirconia as compared to alumina.[14] The adsorption of PEA on alumina was chosen as a starting point since previous work on PEA on zirconia showed distinctive trends as far as coverage and polar group density were concerned. Therefore, to see the effect of binding strength, the substrate was changed while using the same polymer. Alumina and zirconia contain both acid and base sites which are important for catalytic and adsorption processes. The isoelectric points, a rough measure of the basicity of the metal oxide, were reported to be 9 and 8.2 for alumina oxide C and VP zirconium oxide, respectively.[15] Strong Lewis acid sites can be exposed to the surface layer by oxygen and hydroxyl ion vacancies and Lewis base sites arise from surface hydroxyls and adsorbed molecular water.[16, 17] Characterization of the surface acid-base properties of γ-aluminum oxide C showed the presence of octahedrally and tetrahedrally coordinated Al^{3+} sites, Lewis base sites (OH^-), and H-bond donor sites (partially positively charged surface OH groups) which are either bridging or multicentered groups.[18] Infrared studies of zirconia have shown the presence of terminal and bridging hydroxyl groups. A surface study of the VP zirconium concluded that it is a weakly acidic oxide with Lewis acid sites (Zr^{4+}) but no Brönsted acid sites.[19] Weak Lewis base sites (OH^-) are also present as demonstrated by the formation of hydrogen carbonates from adsorbed CO_2. However, the exact densities of these acid/base surface sites have not been reported for either oxide.

For PEA 5% on alumina, samples were prepared with loadings from 1.6 to 23 wt % of copolymer adsorbed on the surface. The ^{13}C CP-MAS NMR spectra for PEA 5% on alumina, shown in Figure 2.1, have two distinct regions: one at low loadings (1.6-9 wt %) and the other at high loadings (10-23 wt %). The low loadings exhibit resonances in the methylene region at 33 and 31 ppm due to the backbone methylene carbons, which are of similar relative intensities. Above the 10 wt %, the peak at 33 ppm increases in intensity. In the bulk polymer these peaks were assigned to chains in the crystalline and amorphous regions, respectively. When considering the adsorbed copolymers, the resonance at 33 ppm is better described as originating from chain segments with a high trans content (transoid) and the 31 ppm resonance arises from conformationally disordered chain segments with a higher population of gauche defects (gauchoid). This distinction is important because long range order, crystallinity, does not occur in polymers adsorbed on heterogeneous surfaces. The ^{13}C NMR spectra were acquired using ^{1}H-^{13}C cross-polarization (CP) which is not a quantitative method since it is sensitive to differences in mobility and type of carbon (number of nearby protons). For the qualitative comparisons presented here, it is assumed that the CP relaxation parameters for the transoid and gauchoid peaks do not vary much with coverage.

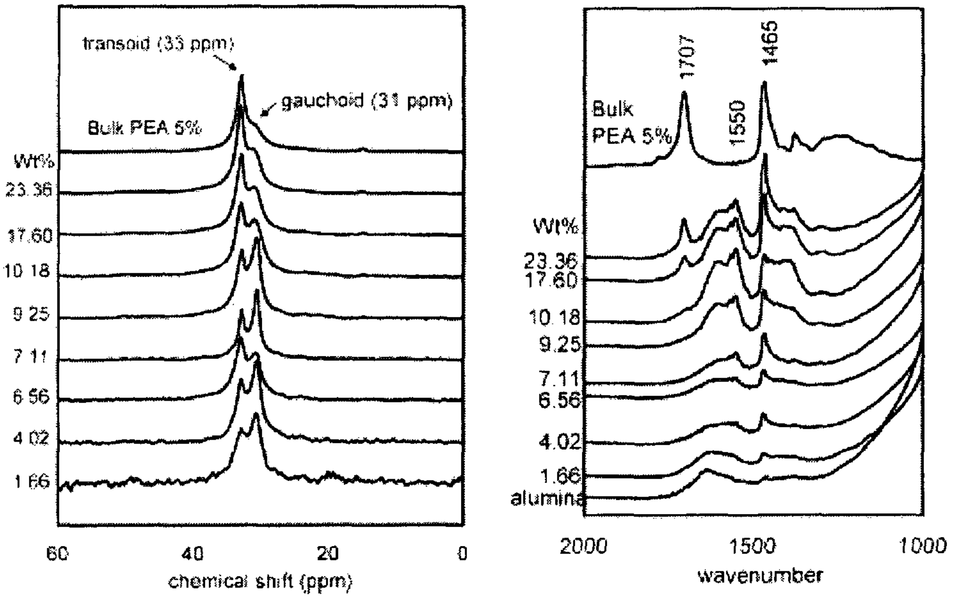

Figure 2.1: ^{13}C CP-MAS NMR spectra and FTIR-PAS spectra for PEA 5% on alumina.

For the lower loadings, all the carboxylic acid groups are bound to the surface as indicated by the lack of a free acid C=O band at ~1700 cm^{-1} in the FTIR-PAS spectra along with the appearance of new bands in the carboxylate region. The bands at 1550 and 1465 cm^{-1} are assigned to the asymmetric and symmetric -C-O stretches of surface-bound carboxylate groups. The band at 1465 cm^{-1} overlaps with the $-CH_2-$ stretch at 1460 cm^{-1}. A broad band at 1523 cm^{-1} was also reported for PEA spin-coated on hydrated aluminum. This band was assigned to carboxylate species, which form when the PEA comes into contact with the pseudoboehmite film produced by the hydration of the aluminum foil.[20] An earlier study of spin-coated and hot-pressed PEA films on oxidized aluminum surfaces suggested that PEA primarily interacts with the surface by Lewis acid/base interactions.[3] The IR spectra in Figure 2.1 all have a broad band at approximately 1610 cm^{-1} arising from the alumina. This band is also seen when the alumina was treated as described in the Experimental Section but without any polymer added. The FTIR methylene crystalline bands (i.e., CH_2 rocking modes) at 710-730 cm^{-1}, which are sensitive to chain conformation, were not detected because the metal oxide fingerprint region below 1100 cm^{-1} masks any polymer signal in this region. Likewise, no information was extracted from the very broad OH stretching modes of alumina at ~3500 cm^{-1}, which did not show any significant changes in the presence of adsorbed polymer.

At a loading of 17.60 wt %, a distinct peak at 1707 cm^{-1} appears in the FTIR-PAS spectrum due to unbound carboxylic acid groups. On zirconia powder, these bands for unbound acid groups appeared at much lower loadings due to the lower surface area of this substrate.[1] At the 10.18 wt % loading of PEA 5% on alumina, the transoid component becomes more intense than the gauchoid peak in the ^{13}C CP-MAS NMR spectra, indicating an increase in the chain order coinciding with the presence of unbound acid groups. However, this change in the chain conformation with the appearance of unbound acid groups was much more evident for PEA on zirconia.[1]

In the case of the adsorbed copolymer with a higher density of sticker groups, PEA 15%, the ^{13}C CP-MAS NMR also shows that there is very little change in the NMR spectra until most of the binding sites are occupied as signalled by the appearance of a

FTIR band for unbound acid groups (Figure 2.2a). Unlike the PEA 5% adsorbed on alumina, the ^{13}C CP-MAS NMR spectra of adsorbed PEA 15% contain only the 31 ppm component for low loadings (2.5-10 wt %). The 33 ppm transoid component does not appear until the 13.7 wt % loading, coinciding with the appearance of the 1705 cm^{-1} free acid peak in the FTIR spectra (Figure 2.3a). Unlike the PEA 5%, the PEA 15% ^{13}C CP-MAS NMR spectra do not approach the bulk copolymer spectrum at the highest loadings, and the chain order is still low (a small transoid component). Although there is a significant population of free acid groups at the highest loading, the band at 1554 cm^{-1} for surface-bound carboxylate groups is still intense relative to the free acid band at 1705 cm^{-1}. In the case of similar loadings of PEA 15% on zirconia powder, the NMR spectra did approach that of the bulk, but the amount of bound groups as compared to unbound groups was also smaller, indicating a larger proportion of the polymer is not in direct contact with the surface for this lower surface area substrate.[1] The relative proportion of bound and unbound groups is such that crystallization of PEA 15% is still hindered at the highest loading measured. The key finding is that despite the weaker binding of PEA on alumina as compared to zirconia, the same trend is seen as with the PEA/ZrO_2 system: the conformation depends on the sticker group content rather than the coverage. The only difference is that the bulk-like PEA 15% spectra are not seen at the highest loadings due to the much higher surface area of the alumina (100 m^2/g) as compared to the zirconia (40 m^2/g).

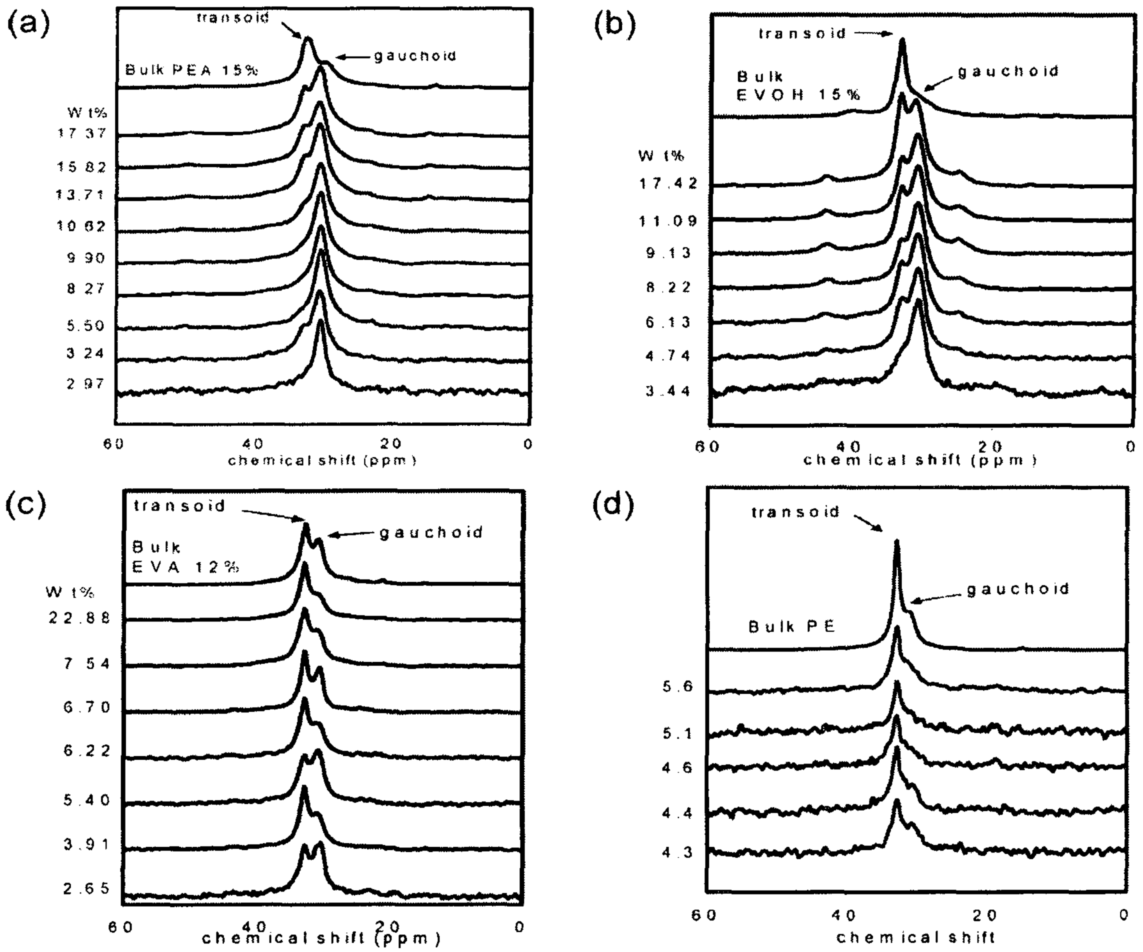

Figure 2.2: ^{13}C CP-MAS NMR spectra of (a) PEA 15%, (b) EVOH 15%, (c) EVA 12%, and (d) PE on alumina.

2.5.2 Effect of Weaker Binding Groups (EVOH, EVA, and PE on Alumina)

2.5.2.1 Chain Conformation: Solid-State ^{13}C NMR

Ethylene copolymers with other polar functional groups (OH, $OC{=}OCH_3$), as well as polyethylene, were examined next to see whether the trend in chain conformation with loading as noted above persists for much weaker polymer/substrate binding. Figure 2.2 compares the ^{13}C CP-MAS NMR spectra of PEA, EVOH, EVA, and PE adsorbed on alumina. The polar group contents of these copolymers are similar with relatively short ethylene segments of 30, 12, and 37 CH_2 groups between the CO_2H, OH, and $OC{=}OCH_3$

sticker groups of PEA 15%, EVOH 15%, and EVA 12% (Table 2.1). The trend in the trans/gauche populations of the ethylene segments of EVA 12% on alumina greatly differs from that observed for PEA 15% on the same substrate. The lowest loading of EVA 12% on alumina shows a strong transoid component at 33 ppm, whereas the ethylene segments of adsorbed PEA 15% are disordered with a single gauchoid peak at 31 ppm. Unlike PEA, the relative intensities of the 33 and 30 ppm components of adsorbed EVA 12% do not show a smooth trend with loading but are bulk-like at the highest loadings.

The ^{13}C CP-MAS spectra of EVOH 15% on alumina (Figure 2.2b) show a general trend that is intermediate between EVA 12% and PEA 15%. A transoid component at 33 ppm appears at much lower loadings as compared to PEA 15% but is not present at the lowest loadings, unlike EVA 12%. However, at the highest loading the transoid component dominates unlike the adsorbed PEA 15%. The ^{13}C CP-MAS spectra of PE on alumina (Figure 2.2d) display a dominant transoid component at 33 ppm for all loadings. Only a minimal amount of polyethylene actually adheres to the alumina substrate, which is expected due to the lack of polar sticker groups. Most of the PE was removed during the washing steps, and a maximum loading of only 5.6 wt % was obtained. Literature precedence gives an explanation for the observed trends. Hjertberg [2] did studies of copolymers adsorbed on thin films; the order of binding strength that he noted was carboxylic acid > hydroxyl > acetate. The main conclusion that can be obtained from Figure 2.2 is that there is more conformational order with weaker binding strength. The picture that comes to mind is that of PEA binding so strongly that it sticks randomly and irreversibly to the surface during the adsorption process, so that until all the sites are occupied, the ethylene segments will be conformationally disordered, whereas for EVA the binding is sufficiently weak that the polymer chain can partially detach from the surface during the adsorption process and thus reach a more ordered chain conformation even at low loadings.

The competition between adsorption and self-association/crystallization of EVA/EVOH as compared to PEA should also be considered. In general, these ethylene copolymers display low crystallinities, which decrease with increasing polar group content. However, the 8% crystallinity of bulk PEA 15% is significantly lower than that of EVA 12% (19% crystallinity). In both copolymers, the polar groups are excluded from the crystals formed by the ethylene chains. However, the disruptive effect on crystallization is greater in the case of PEA due to the hydrogen-bonding interactions among the carboxylic acid groups, which are extensively dimerized. A FTIR study of ethylene copolymers concluded that whereas the restrained effect of the vinyl acetate groups in EVA is not strong enough to affect the crystalline behaviour of the PE segments, the hydrogen bonds among the carboxylic acid groups of PEA play a cross-linking role which prevents the PE segments from adopting the stable orthorhombic form.[21] Studies of the phase structure of EVA found that not only the degree of crystallinity but also the relative contents of two crystalline phases (monoclinic and orthorhombic) vary with VA content.[22] The stronger tendency of PEA to adsorb plus the more favourable crystallization of EVA can both play a role in the higher degree of order observed for adsorbed EVA vs. PEA. However, surface IR and AFM studies of EVA thin films spin-coated on alumina detected very low crystallinity, attributed to the effect of the chain conformation at the interface.[23] To further investigate this, DSC scans were run on bulk and adsorbed EVA 12%. The *T*g of bulk EVA, a semicrystalline polymer, was difficult to detect; therefore, it was not surprising that the *T*g was not seen for adsorbed EVA. A melting transition was only detected for the highest loading, but it was very broad and it was not possible within experimental error to determine whether it was significantly shifted from the bulk value.

2.5.2.2 Surface Binding: FTIR-PAS

The FTIR-PAS spectra of adsorbed PEA 15% in Figure 2.3a correlates well with the NMR data in that the chain conformation changes with the appearance at ~13.7 wt % of a free acid peak at 1705 cm^{-1}. The FTIR-PAS spectra of the lowest loadings of EVA 12% (Figure 2.3c) are characterized by the lack of a free acetate C=O band at ~1740 cm^{-1} along with the appearance of new bands in the carboxylate region. These spectra differ from previous surface IR studies of EVA films deposited on planar alumina substrates.[6] Brogly reported a splitting of the acetate C=O stretch band due to a Lewis acid-base interaction of the acetate groups with the alumina hydroxyl groups. The splitting was as large as 16 cm^{-1} when the EVA was bound to a weakly hydroxylated aluminum substrate. The absence of this splitting in the FTIR-PAS spectra of EVA adsorbed on powdered alumina may be due to the limited resolution or the different selection rules for surface IR. The acetate peak at 1740 cm^{-1} was only present at coverages above 7 wt %. Instead, a strong broad carboxylate band at 1571 cm^{-1} appears which is assigned to partial hydrolysis of the EVA in the presence of alumina along with heating; the products of this reaction would be EVOH and acetic acid. This assumption is supported by studies of the adsorption of acetic acid on alumina, which show a FTIR band at 1570 cm^{-1}.[23]

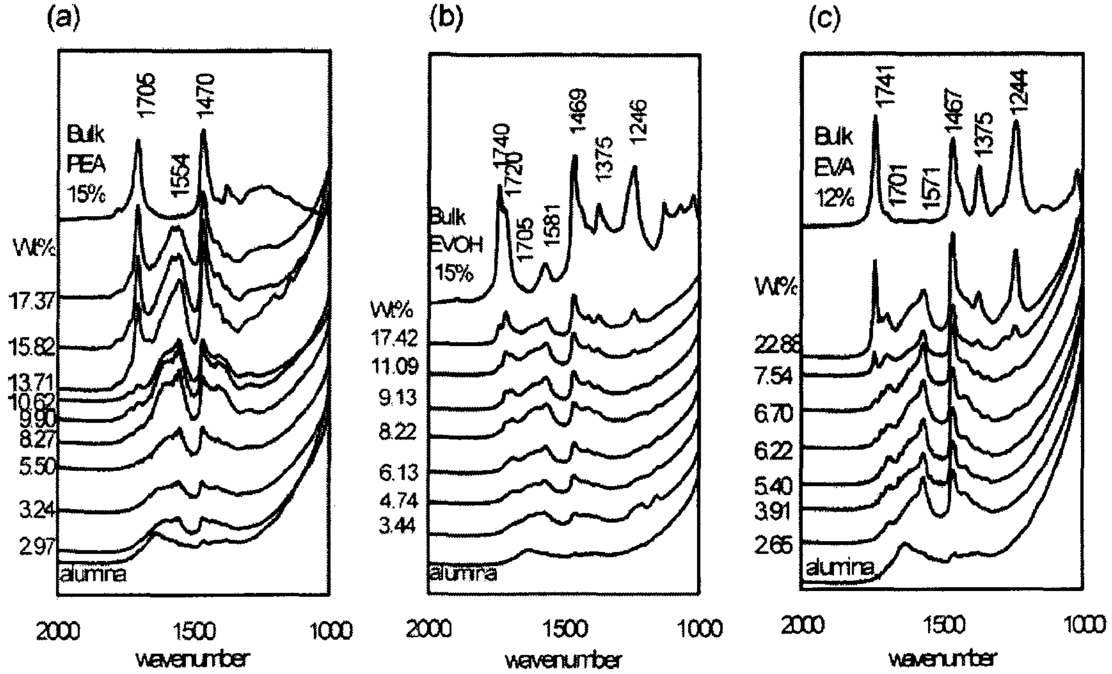

Figure 2.3: FTIR-PAS spectra of (a) PEA 15%, (b) EVOH 15%, and (c) EVA 12% on alumina.

The absence and occurrence of hydrolysis when EVA is deposited on aluminum by spin-coating vs. adsorption from solution was also reported for PMMA on the native metal oxide surfaces.[24] The lack of hydrolysis of the spincoated PMMA was attributed to the rapid removal of solvent and rapid vitrification of the polymer during the spin-coating process such that most of the PMMA segments are immobilized into positions where they cannot react with the surface. Presumably, a similar process occurs for EVA when it is spin-coated rather than adsorbed onto alumina.

The FTIR-PAS spectra of EVOH 15% on alumina, shown in Figure 2.3b, are complicated by incomplete hydrolysis of the initial polymer (which is commercially produced via hydrolysis of EVA) along with further hydrolysis occurring upon adsorption. The extent of hydrolysis of EVOH 15% was determined from solution ^{1}H NMR.[25] The ^{1}H NMR spectra showed that EVOH 15% contained approximately 22% unhydrolyzed starting material, while EVOH 25% was approximately 12%

unhydrolyzed. In the FTIR-PAS spectra of adsorbed EVOH 15%, the band at 1740 cm^{-1} is due to residual acetate groups, the band at 1720 cm^{-1} is due to the presence of ketones,[26] and the band at 1581 cm^{-1} is due to adsorbed acetic acid as in the case of EVA adsorbed on alumina. At low loadings, adsorbed EVOH has bands at 1705 and 1720 cm^{-1}, and the relative intensities of these two bands change as the loadings increase. At the highest loadings, there is no longer a band at 1705 cm^{-1}, assigned to acetic acid, but there are ketone and acetate bands at 1720 and 1740 cm^{-1}.

Apart from the complication of the IR spectra due to partial hydrolysis, it is not possible to correlate the occupation of the binding sites with the chain conformation for either EVA or EVOH. In the case of EVOH, the broad hydroxyl band cannot be used to determine binding and for EVA; no splitting of the acetate band was detected. However, the fact that the initial EVOH bulk polymer was incompletely hydrolyzed was useful for confirming that some hydrolysis of EVA as well as further hydrolysis of EVOH occurs upon adsorption. Although the extent of this hydrolysis cannot be easily measured from the IR bands, it appears that most of the EVA and EVOH are hydrolyzed at low coverages since no acetate bands are present.

Despite the FTIR evidence for extensive hydrolysis, which would convert EVA to EVOH, the trend in the chain conformation of EVA with loading is significantly different from EVOH. In the case of the hydrolysis and subsequent chemisorption of PMMA on metal oxides, Tannenbaum and co-workers argue that the adsorption process occurs via a two-step mechanism in which the first step of hydrolysis is a necessary but insufficient condition for anchoring the polymer to the surface.[24] The efficiency of the second step is dependent on the interfacial chemistry possible for a particular polymer/metal oxide pair as well as the conformation, flexibility, and molecular weight of the polymer.

2.5.3. Effect of Increasing Sticker Group Density.

The NMR and FTIR-PAS spectra of EVA 12% were compared to those of EVA 25% to study the effect of increasing the sticker group content for weak polymer/metal oxide binding. The ^{13}C CP-MAS NMR (Figure 2.4) shows that despite the high polar group content, there is still a significant transoid component. With the exception of the lowest loading, the chain conformation of the adsorbed polymer is not significantly perturbed from that of the bulk polymer as seen by the relative intensities of the transoid and gauchoid peaks. Figure 2.4 illustrates that there is little dependence on coverage, indicating that the weaker binding polymer can rearrange on the surface during the adsorption process. The IR spectra of EVA 25% on alumina are very similar to those of EVA 12%, with the appearance of the bands due to partial hydrolysis, and once again no splitting of the acetate band at 1740 cm^{-1} is seen. The ^{13}C CP-MAS NMR and FTIR-PAS spectra for EVOH 25% on alumina, not shown, show that the trans/gauche populations, as well as intensities of the FTIR bands with coverage, follow the same trends as for EVOH 15%.

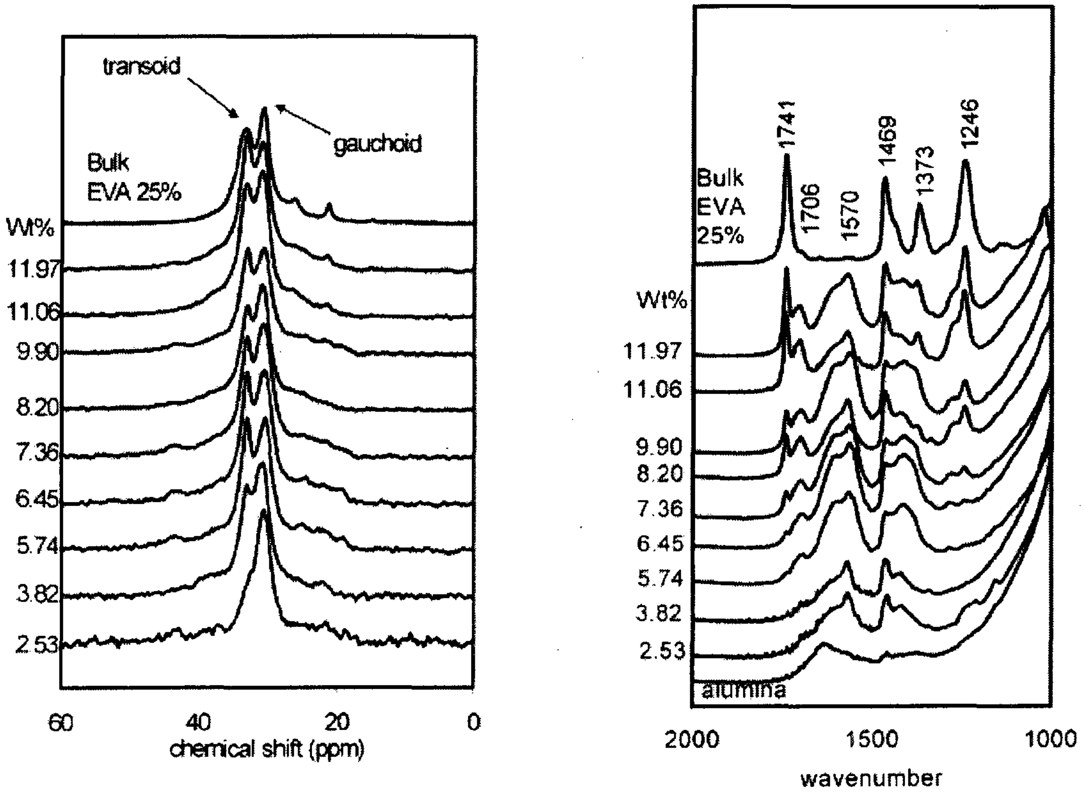

Figure 2.4: ^{13}C CP-MAS NMR spectra and FTIR-PAS spectra of EVA 25% adsorbed on alumina.

2.5.4. Effect of Increased Substrate Binding Strength (EVA/Zirconia and EVOH/Zirconia)

Samples where the ethylene copolymers were adsorbed onto a more basic metal oxide (ZrO_2) were examined next to see whether the trend in chain conformation persists. The ^{13}C CP-MAS NMR spectra for EVA 12% on zirconia (Figure 2.5) show the same trends as for EVA 12% on alumina. There is a transoid component for all loadings, which dominates over the gauchoid component.

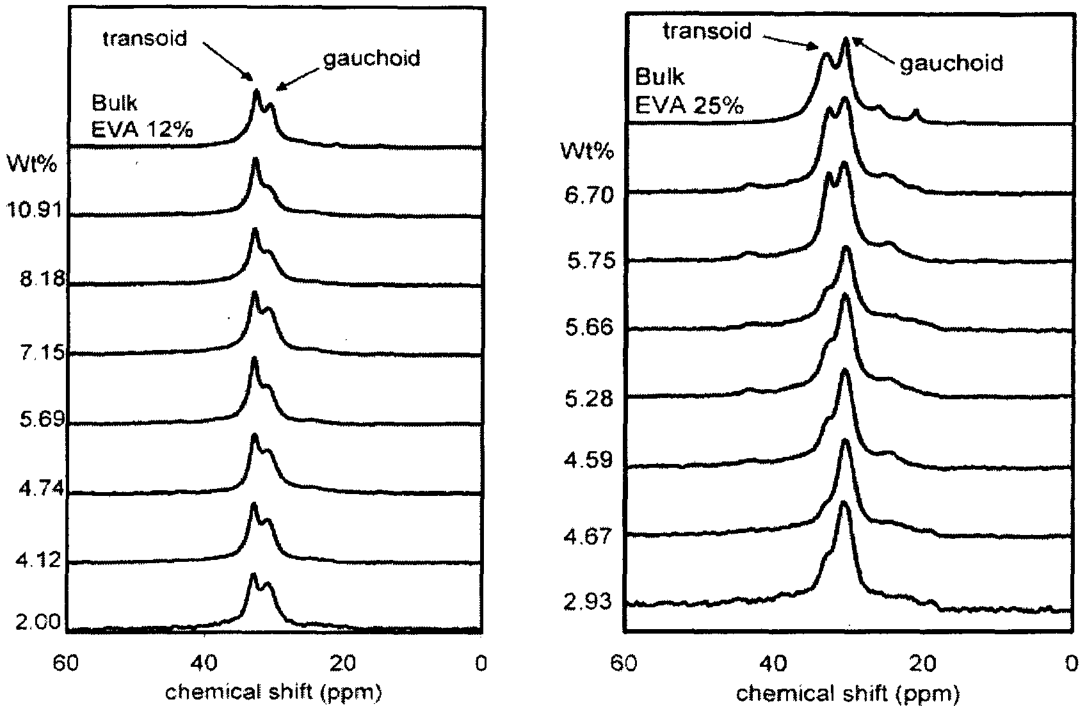

Figure 2.5: ^{13}C CP-MAS NMR spectra for 12% and 25% EVA on zirconia.

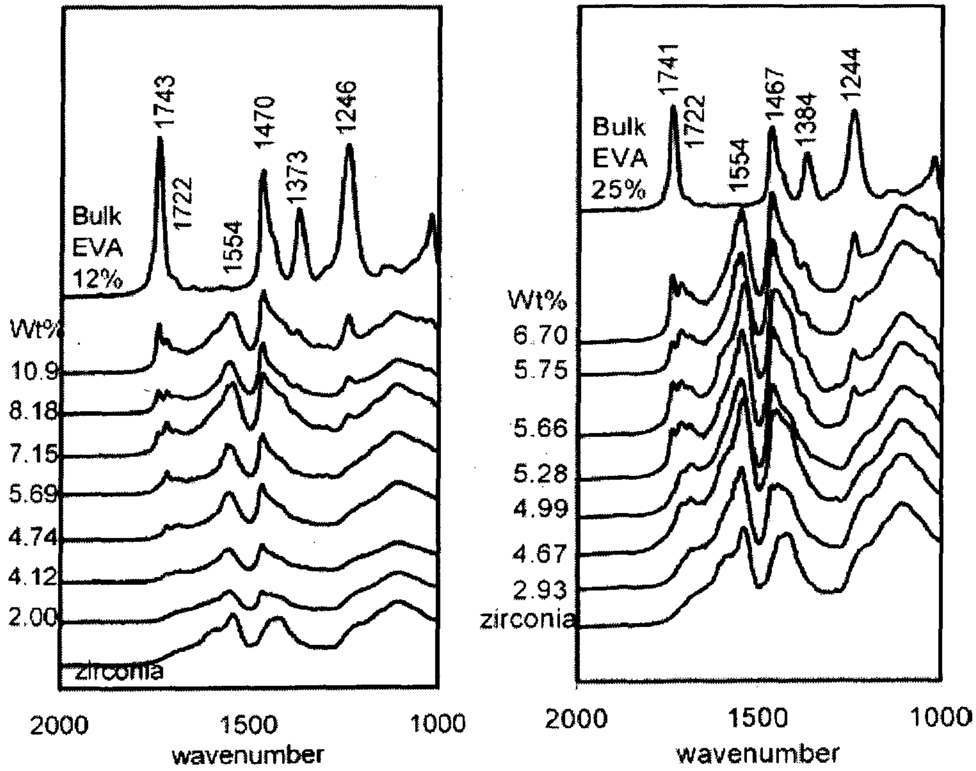

Figure 2.6: FTIR-PAS spectra for 12% and 25% EVA on zirconia.

The FTIR-PAS spectra (Figure 2.6) for EVA 12% adsorbed on zirconia show all the acetic acid groups are bound to the surface in the samples with the lowest copolymer loadings as indicated by the lack of a free acetate C=O band at ~1740 cm^{-1}. The bands in the carboxylate region are due to adsorbed CO_2, which overlap with the bands arising from the hydrolyzed EVA. The FTIR-PAS spectrum of zirconia contains a broad peak at 3500 cm^{-1} due to the surface hydroxyls, two weak peaks at 1630 and 1460 cm^{-1}, and a large fingerprint below 900 cm^{-1}.

EVA 12% was compared to EVA 25% to study the effect of increasing the sticker group content. The ^{13}C CP-MAS NMR of EVA 25% on zirconia (Figure 2.5) shows that there is a transoid component at all loadings, but it is minimal at low loadings as compared to the same copolymer on alumina. This difference may be due to the stronger binding strength of the zirconia substrate, which is usually viewed as being more basic than alumina.[27] The IR spectra of EVA 25% on zirconia in Figure 2.6 are very similar to that of EVA 12%, with the bands due to partial hydrolysis, and no splitting is seen at 1740 cm^{-1}. The ^{13}C CP-MAS and FTIR-PAS spectra of EVOH 15% on zirconia, not shown, showed the same trend as on alumina.

2.5.5 Relaxation and Variable Temperature Studies.

Variable temperature and relaxation studies were performed to explore the possible chain configurations that give rise to the high degree of conformational order seen for EVA on alumina. The ^{13}C CP-MAS NMR showed a transoid peak for all coverages for both EVA copolymers. This component could be the result of folded loops as proposed for the PEA/ZrO_2 system or the presence of trains lying flat on the surface. A folded loop is a loop that contains segments of an all-trans conformation of carbons atoms as shown schematically elsewhere.[1] ^{13}C NMR relaxation measurements were carried out using two pulse sequences. The Torchia pulse sequence was used to measure the longitudinal relaxation time (T_1) of the rigid component at 33 ppm, while the inversion recovery pulse sequence was used to examine the amorphous component at 31 ppm, which has a much shorter spin-lattice relaxation time. In previous work, Zhang et al.[22] used solid-state NMR to look at a series of ethylene-vinyl acetate copolymers. It was observed that the crystalline region of all samples had a biexponential ^{13}C NMR spin-lattice relaxation behaviour. The longer ^{13}C spin-lattice relaxation time was ascribed to the internal part of the crystalline region, whereas the component with shorter T_1 was accredited to the interfacial region between the amorphous and crystalline domains. The authors also noted that the crystallinity decreased with increasing vinyl acetate content.

Table 2.2: Carbon T_1 (s) for Bulk and Adsorbed EVA 12% and 25% on Alumina

sample	33 ppm	31 ppm
EVA 12%	3.35, 67.11	0.294
23 wt % EVA 12%	3.25, 59.22	0.396
4 wt % EVA 12%	2.74, 56.18	0.419
EVA 25%	1.47, 19.38	0.295
12 wt % EVA 25%	3.02, 52.35	0.401
6.5 wt % EVA 25%	4.38, 76.9	0.395

The relaxation results in Table 2.2 show that the T_1 values for the amorphous peak do not change from bulk to adsorbed polymer. The 33 ppm data was fit to a biexponential curve, yielding two T_1 values. For EVA 12% there was little change from bulk to adsorbed polymer. For EVA 25% there was an increase in T_1 from bulk to adsorbed polymer. Since variable temperature measurements showed that EVA 25% is on the slow side of the T_1 vs. correlation time curve, the ordered component of the adsorbed polymer is less mobile than the bulk state. This contrasts with previous relaxation studies of PEA adsorbed on ZrO_2, which showed an enhanced mobility of the 33 ppm component which arises from a folded loop structure.[1]

The possible sources for the ordered component of adsorbed EVA and EVOH can be considered. The 33 ppm transoid peak of the adsorbed polymer could arise from (i) a self-associated, crystallized polymer which is not interacting with the surfaces the 33 ppm component would arise from the crystalline regions in this case; (ii) a folded loop structure such as proposed for PEA 5% adsorbed on zirconia;[1] and (iii) flat, extended trains lying on the surface.

We suggest that the trans component of adsorbed EVA and EVOH arises from train configurations based on the following experimental data:

1. EVA and EVOH have a significant population of all-trans conformations of the polyethylene segments at low coverages where all the polymer chains are more likely to be in direct contact with the surface.
2. At low coverages, no free acetate groups are detected for adsorbed EVA, yet large carboxylate bands are present which are attributed to adsorbed acetic acid. The polymer has interacted sufficiently with the surface for significant hydrolysis to occur.
3. Adsorbed EVA showed reduced chain mobility for the transoid component, which is opposite to what was observed for PEA/ZrO_2 (folded loops).

In theory, the hydrolyzed polymer could only be self-associated and not interacting with the surface. However, most of the non-adsorbed polymer should have been removed by the extensive washing steps. Furthermore, studies of spin-coated EVA films by Brogly and coworkers strongly support the formation of train configurations.[5-10, 28] Their detailed surface IR studies of EVA films concluded that at the interface the EVA chains lie parallel to the alumina surface, which in turn hinders the crystallization of the polymer chains not in direct contact with the substrate.[10]

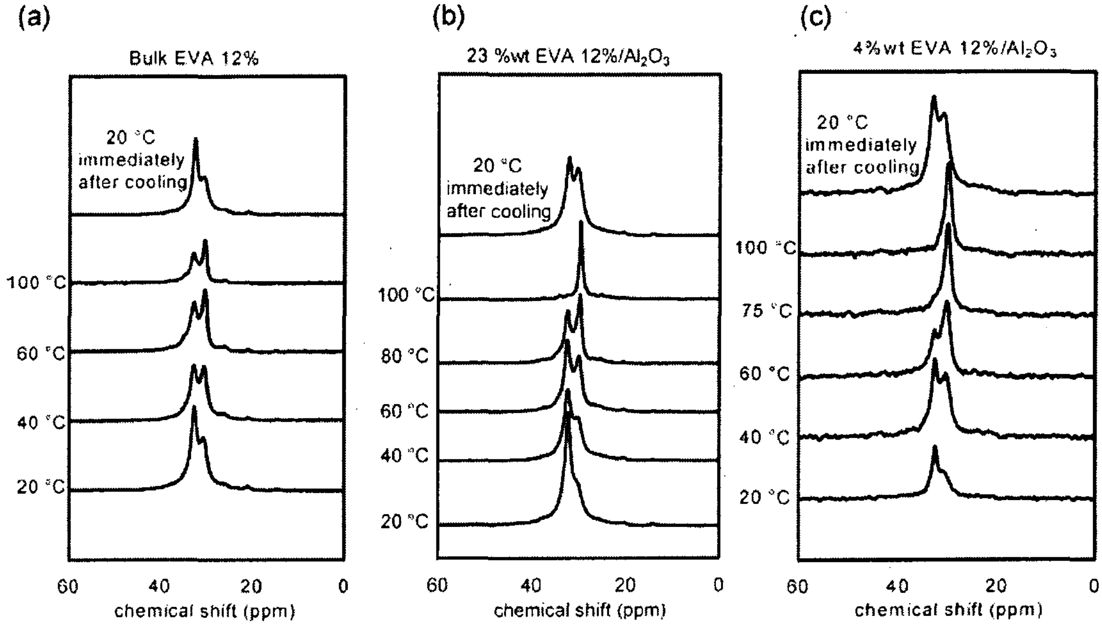

Figure 2.7: VT ^{13}C CP-MAS NMR spectra for (a) EVA 12%, (b) 23 wt % EVA 12%, and (c) 4 wt % EVA 12% on alumina.

Thermal stability studies (Figure 2.7) were also carried out in order to gain insight into the nature of the ordered component. When the bulk polymer was heated to 100 °C and then cooled to room temperature, it was slightly more ordered than the original polymer. At 100 °C there is still a transoid component at 33 ppm arising from the crystalline regions of the bulk copolymer. For both high and low loadings, the adsorbed copolymer is totally disordered at 100 °C, but given enough time, within a few days, the polymer returns to its initial configuration. The loss of the transoid component occurs at a lower temperature (below 75 °C) for the lower loading (4 wt %) as compared to the higher loading (23 wt %), which still has a transoid component at 80 °C. This behaviour was also observed for 5% PEA/ZrO_2; however, the chain conformation returned to the original state immediately upon cooling.[1] In this case the ordered component arises from folded loops which unfold with heating and then return to the original configuration since the loops are irreversibly pinned via strong zirconium carboxylate linkages. In the case of EVA, the ethylene segments between sticker groups are too short to form folded loops unless some of the acetate groups are not bound to the surface. However, the FTIR spectra show otherwise, and this along with the reduced mobility indicates that the 33 ppm component arises from train configurations. Thus, for complete disordering to occur, the polar groups must detach with heating. Unfortunately, there is no IR signature for polymer-surface interactions that would allow direct observation of detachment of EVA as heating occurs. In the case of PEA on ZrO_2, it was possible to show directly that the Zr-carboxylate surface bond remains completely immobile and intact during the chain disordering process through VT NMR studies of long chain fatty acids adsorbed on ZrO_2 which were ^{13}C-labeled at the C=O group. Presumably, the acetate groups of EVA interact via ionic or hydrogen bonds which are weak enough to be overcome by the thermal energy unlike the stronger Al or Zr carboxylate linkages of adsorbed PEA.

2.6. Conclusions

The chain conformation of adsorbed ethylene copolymers is strongly dependent on the binding strength of the polar sticker groups with the substrate. In the case of PEA on zirconia, the chain conformation was previously found to be strongly dictated by the polar group content rather than coverage. This behaviour persisted for PEA adsorbed on alumina, a more weakly binding substrate as compared to zirconia. The dependence of the conformation on sticker group density decreases with binding strength. A strong transoid component of the ethylene segments of EVA with a large acetate content was observed. This ordered component showed little dependence on coverage. Apparently, the chain conformation is not affected by irreversible binding during the adsorption process for this particular polymer/substrate pair. Instead, the binding is weak enough to allow detachment and the formation of an ordered component. Relaxation measurements, as well as the absence of an FTIR band for free acetate groups for low coverage samples, indicate that the trans component of EVA arises from chains lying flat on the surface. This trans component disappears completely with heating, which is only possible if the polar groups can detach. EVOH showed a trend intermediate between PEA and EVA, in agreement with the order of the binding strength, carboxylic acid > hydroxyl > acetate. The FTIR spectra reveal some hydrolysis of EVA occurs upon adsorption, but the extent of this surface reaction is insufficient to significantly perturb the distinct trend of an increasing chain order with decreasing binding strength.

2.7 Acknowledgments

The Natural Sciences and Engineering Research Council (NSERC) and the Centre for Self-Assembled Chemical Structures (CSACS) provided support for this research. The authors thank Professor Thomas Ellis and Mr. Craig Hyett of the Université de Montreal for access to the FTIR-PAS spectrometer. We thank also Dr. Fred Morin for valuable assistance.

2.8 References

1. Nasreddine, V., Halla, J., and Reven, L., *Conformation of Adsorbed Random Copolymers: A Solid-State NMR and FTIR-PAS Study.* Macromolecules, 2001. **34**: p. 7403-7410.
2. Hjertberg, T. and Lakso, J.E., *Functional group efficiency in adhesion between polyethylene and aluminum.* Journal of Applied Polymer Science, 1989. **37**(5): p. 1287-1297.
3. Ulren, L., Hjertberg, T., and Ishida, H., *An FT-IR study on interfacial interactions in ethylene copolymers/aluminum laminates in relation to adhesion properties.* Journal of Adhesion, 1990. **31**: p. 117-136.
4. Fleer, G.J., et al., *Polymers at Interfaces.* 1993, London: Chapman and Hall.
5. Brogly, M., *Adsorption induced ordering effects in thin polymer films.* Revue De Metallurgie-cahiers d'Informations Techniques, 2001. **98**: p. 175-184.
6. Brogly, M., Bistac, S., and Schultz, J., *Persistence of Molecular Orientation in Adsorbed Ethylene-Vinyl Acetate Copolymer Nanofilm Studied by Fourier Transform Infrared Reflectance Spectroscopy.* Macromolecules, 1998. **31**: p. 3967-3973.
7. Brogly, M., Bistac, S., and Schultz, J., *Infrared Reflectance as a Tool to Reveal Preferential Molecular Orientation of Polymers Adsorbed onto Flat Substrates.* Macromolecular Symposia, 1999. **141**: p. 129-143.
8. Brogly, M., Nardin, M., and Schultz, J., *Evidence of Acid-Base Interfacial Adducts in Various Polymer/Metal Systems by IRAS: Improvement of Adhesion.* Journal of Adhesion, 1996. **58**: p. 263-279.
9. Elzein, T., et al., *PM-IRRAS spectroscopy for the characterization of polymer nanofilms: Chains conformation, anisotropy and crystallinity.* Macromolecular Symposia, 2004. **205**: p. 181-190.
10. Elzein, T., Brogly, M., and Schultz, J., *Molecular orientation of EVA chains adsorbed on chemically controlled surfaces: Influence of specific interactions.* Surface and Interface analysis, 2003. **35**: p. 633-639.
11. Elzein, T., Brogly, M., and Schultz, J., *Crystallinity of adsorbed EVA nanofilms: Relevance to confinement and interfacial interactions.* Surface and Interface Analysis 2003. **35**: p. 785-792.
12. Yamaki, S.B., Prado, E.A., and Z.;, A.T.D., *Phase transitions and relaxation processes in ethylene-vinyl acetate copolymers probed by fluoescence spectroscopy.* European Polymer Journal, 2002. **38**: p. 1811-1826.
13. Torchia, D.A., *The Measurement of Proton-Enhanced Carbon-13 T_1 Values by a Method Which Suppresses Artifacts.* Journal of Magnetic Resonance, 1978. **30**: p. 613-616.
14. VanderKam, S.K., Bocarsly, A.B., and Schwartz, J., *Enhanced Bonding of Poly(ethylene-co-acrylic acid) to Oxides through Surface-Bound Alkoxyzirconium Complex Interfaces.* Chemical Materials, 1998. **10**: p. 685-687.
15. Xie, M. and Blum, F.D., *Adsorption and Dynamics of Low Molecular Weight Poly(styrene-b-2-vinylpyridine) on Silica and Alumina in Toluene.* Langmuir, 1996. **12**: p. 5669-5673.

16. Morterra, C. and Magnacca, G., *A case study: surface chemistry and surface structure of catalytic aluminas, as studied by vibrational spectroscopy of adsorbed species.* Catalysis Today, 1996. **27**: p. 497-532.
17. Thompson, W.R. and Pemberton, J.E., *Characterization of Octadecylsilane and Stearic Acid Layers on Al_2O_3 Surfaces by Raman Spectroscopy.* Langmuir, 1995. **11**: p. 1720-1725.
18. Zaki, M.I., Hasan, M.A., and Pasupulety, L., *Surface reactions of acetone on Al_2O_3, TiO_2, ZrO_2, and CeO_2: IR spectroscopic assessment of impacts of the surface acid-base properties.* Langmuir, 2001. **17**: p. 768-774.
19. Anderson, B.G., Dang, Z., and Morrow, B.A., *Silica-Supported Zirconia. 2. Effect of Sulfation on the Surface Acidity and Its Potential as a Catalyst for Methane-Olefin Coupling.* Physical Chemistry, 1995. **99**: p. 14444-14449.
20. Straalin, A. and Hjertberg, T., *FTIR study on interfacial interactions between hydrated aluminum and polar groups in ethylene copolymers.* Surface and Interface Analysis, 1993. **20**: p. 337-340.
21. Kang, N., et al., *The correlation between crystalline behavior of polyethylene segments and hydrogen bonds among carboxyl groups in ethylene-acrylic acid copolymers.* Physical Chemistry Chemical Physics, 2000. **2**: p. 3627-3630.
22. Zhang, Q., et al., *Studies on the Phase Structure of Ethylene-Vinyl Acetate Copolymers by Solid-State ^1H and ^{13}C NMR.* Journal of Polymer Science: Part B: Polymer Physics, 2002. **40**: p. 2199-2207.
23. Ferri, D., Burgi, T., and Baiker, A., *Probing Catalytic Solid-Liquid Interfaces by Attenuated Total Reflection Infrared Spectroscopy: Adsorption of Carboxylic Acids on Alumina and Titania.* Helvetica Chemica Acta, 2002. **85**: p. 3639-3656.
24. Tannenbaum, R., et al., *Infrared Study of the Kinetics and Mechanism of Adsorption of Acrylic Polymers on Alumina Surfaces.* Langmuir, 2004. **20**: p. 4507-4514.
25. Marie, E., et al., *The Controlled Solvolysis of Ethylene-Vinyl Acetate Copolymers.* Macromolecules, 2001. **34**: p. 5838-5847.
26. Rigny-Bourgeois, V., et al., *Photovieillissement d'un copolymere d'ethylene et d'acetate de vinyl en presence de sueur artificielle.* Die Angewandte Makromolekulare Chemie, 1995. **233**: p. 59-76.
27. Sahibed-Dine, A., et al., *Synthesis, acidic and basic properties of ZrO_2-TiO_2, Al_2O_3-ZrO_2 and Al_2O_3-TiO_2 mixed oxides.* Annales de Chimie (Paris), 1998. **23**: p. 139-142.
28. Elzein, T., Brogly, M., and Schultz, J., *Crystallinity of adsorbed EVA nanofilms: Relevance to confinement and interfacial interactions.* Surface and Interface analysis, 2003. **35**: p. 785-792.

Chapter 3: A solid-state NMR study of poly (styrene)-*b*-poly (acrylic acid) copolymer adsorption on a metal oxide surface

3.1 Preface

Chapter 3 is a study of the effect of block length and binding strength on the chain dynamics of adsorbed block copolymers in the dry state. The block copolymers employed are poly (styrene)-*b*-poly (acrylic acid), and poly (styrene)-*b*-poly (*t*-butyl acrylate). Solid-state ^{13}C and ^{1}H NMR measurements provide an assessment of the relative chain mobilities for comparison with the predicted brush, intermediate and mushroom surface structures.

3.2 Abstract

Building on previous work [1, 2] the goals of this project are to probe the dynamic properties of block copolymers at surfaces in the dry state through NMR relaxation measurements. The diblock copolymers, poly (styrene)-*b*-poly (*t*-butyl acrylate), PS-PtBuA, and poly (styrene)-*b*-poly (acrylic acid), PS-PAA, of various block lengths were adsorbed on zirconia powder. ^{13}C and ^{1}H chemical shift and spin lattice relaxation times were recorded to assess the effect of the surface coverage and block lengths on the chain mobility. For all copolymers studies, the segmental mobility of the PAA blocks is similar to or more restricted than the glassy bulk copolymers, reflecting the strong localization and binding at the surface. Asymmetric block copolymers with long PS blocks and short PAA blocks, which are predicted to form extended brush structures when in contact with a selective solvent, have PS segmental mobilities moderately enhanced over those of the bulk copolymers. The same diblocks at low coverages, where a mushroom conformation is expected, display a highly mobile component. The symmetric diblock and asymmetric

diblock with a short PS block, which are expected to form intermediate brush/mushroom and mushroom structures respectively, have restricted mobility similar to the glassy state of bulk PS. No significant dependence of the chain dynamics on the surface binding strength of the anchor blocks is observed.

3.3 Introduction

NMR spectroscopy is one of the most important methods to directly probe polymer dynamics at the chain level through line shape analysis and relaxation measurements. The NMR characterization of adsorbed PVP-PS block copolymers onto alumina and silica in the presence of solvents was carried out by Blum [3-5]. This work employed ^{2}H NMR relaxation measurements to study the segmental mobility of a selectively labeled block copolymer, (deuterostyrene-*b*-2-vinylpyridine) (DSVP), adsorbed on silica and alumina. The dynamics of low molecular weight PVP-PS block copolymers on silica and alumina, swollen with toluene, appear to be between that of highly extended brushes and homopolymers. The dynamics of these surface-bound species are similar to those of a corresponding solution of the same polymer. The enhanced dynamics observed for higher molecular weight PVP-PS block copolymers on silica does not occur. Comparison of the adsorption data with higher molecular weight copolymers suggests that these may not be brush-like. However, their dynamics are still enhanced relative to homopolymers with random attachments. They also found that the nature of the surface, alumina versus silica, had a minimal effect on surface mobility since both substrates adsorb similar amounts of copolymer.

NMR measurements of chain mobility of adsorbed diblock copolymers in the dry state have not been previously reported. Our earlier solid-state NMR studies focused on *random* copolymers of polyethylene containing polar groups, which are commonly used as adhesion promoters between metal surfaces and polyethylene coatings.[1,2] A connection between the chain conformation of polyethylene segments as determined by ^{13}C chemical shifts and the interaction of the acrylic acid with the surface as determined by FTIR was established. The goals of the present paper are to study the effect of block length and binding strength on the chain dynamics of block copolymers adsorbed on metal oxide surfaces. A series of poly (styrene)-*b*-poly (acrylic acid) block copolymers, PS-*b*-PAA, were selected because the ^{13}C and ^{1}H chemical shifts appear in distinct regions allowing the two blocks to be studied separately. Most of the literature on PS-PAA diblocks has focused on the possible morphologies available when these block copolymers are in solution. The effects of varying the block length, concentration of copolymer, and solvent have been extensively explored.[6, 7] To a lesser extent, morphology studies have been carried out on spin-coated thin films of PS-PAA.[8-12]

Zirconium oxide powder was chosen as the surface since the interaction of carboxylic acid functional groups with this metal oxide have been studied previously.[13-15] Solid-state NMR spectroscopy, FTIR-PAS, and thermogravimetric analysis (TGA) were combined to compare poly (styrene)-poly (acrylic acid) and poly (styrene)-poly (*t*-butyl acrylate) block copolymers in the bulk versus adsorbed states. ^{13}C and ^{1}H NMR relaxation measurements were carried out with the aim of correlating the changes in the chain dynamics with the microscopic surface structures.

3.4 Experimental Section

3.4.1 Materials.

Poly (styrene)-*b*-poly (*t*-butyl acrylate) and poly (styrene)-*b*-poly (acrylic acid) block copolymers were synthesized by *A*tom *T*ransfer *R*adical *P*olymerization (ATRP). The development of controlled/living radical polymerization arises from the interest in finding new methods which preserve the characteristics of the living processes and, in the same time, are less sensitive to the presence of impurities (water, traces of oxygen) and more tolerant towards different functional groups ($-NH_2$, -OH).

In order to achieve the desired compositions for the targeted block copolymers, in a first step, well defined poly (*t*-butyl acrylate) chains with high end-group functionality were synthesized as macroinitiators (Scheme 1)[16]. These were used, in a second step, to initiate the extension of the polymer chain by addition of the second monomer (styrene) (Scheme 2) in order to obtain the desired block copolymer. In the final step, hydrolysis of the *t*-butyl groups of the block copolymer gives the corresponding poly (styrene)-*b*-poly (acrylic acid). All the chemicals were used as received except where stated.

Synthesis of poly(t-butyl acrylate) macroinitators

In a typical procedure, CuBr (0.5eq) and $CuBr_2$ (0.025eq) were added to a 10ml round bottom flask (previously dried in the oven and cooled in a desiccator). The addition of $CuBr_2$ is necessary because the rate of addition of the *t*-butyl acrylate monomer to the active species is too high and therefore for better control of the molecular weight the equilibrium must be balanced towards the formation of the inactive species (see Scheme 1). Then the flask was sealed with a rubber septum, degassed and back-filled with argon three times, and left under argon. Deoxygenated acetone followed by *t*-butyl acrylate was added in a ¼ ratio (v/v).

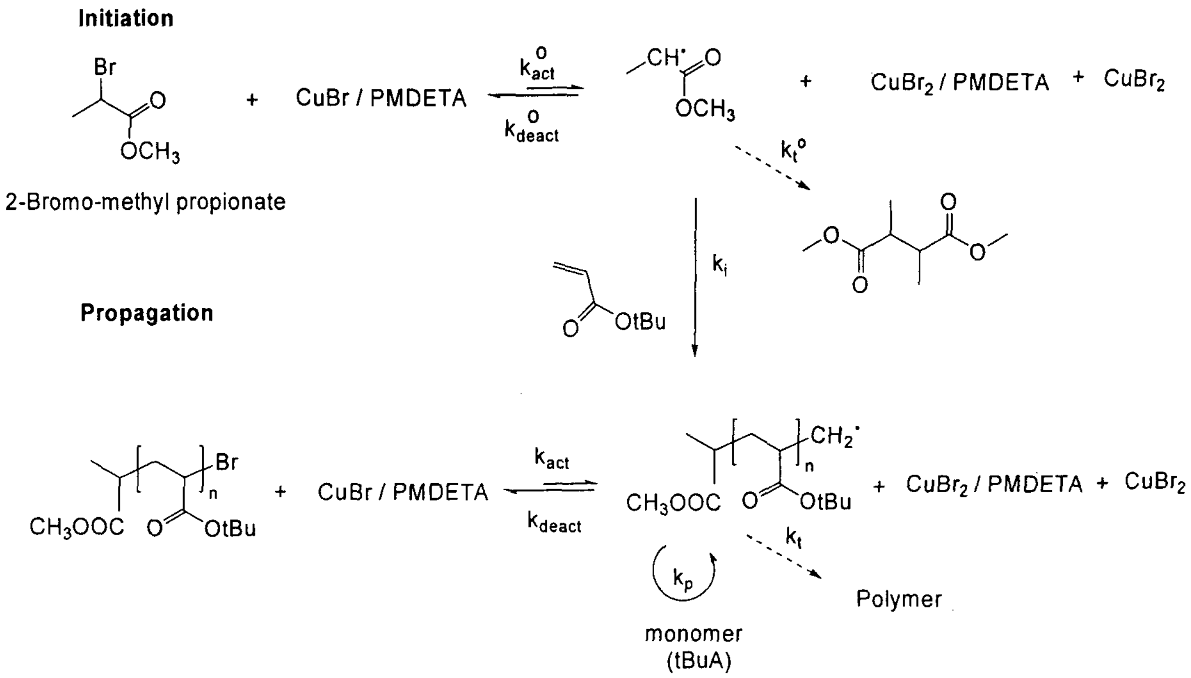

Scheme 1

The volume of the *t*-butyl acrylate monomer added to the reaction mixture was calculated depending on the targeted degree of polymerization (DP); for example 50eqs of *t*-butyl acrylate were used for a DP=50. The ligand (N,N,N',N',N"-pentamethyl diethylene triamine, PMDETA, 0.525 eq) was added and the solution was stirred until the copper complex was formed (the solution changed from cloudy and colorless to a clear light green). After the complex formation one freeze-pump-thaw cycle was performed. After the reaction mixture reached room temperature, the initiator (2-bromo-methyl propionate, 1eq, previously distilled) was added via a microsyringe and the flask was placed in an oil bath and heated at 60°C for 6.5h.

The resulting polymer was purified by dissolving the reaction mixture in acetone, washing with DOWEX MSC macroporous ion-exchange resin for about 1h, and filtering the solution through an alumina column. Both the resin and the alumina serve to remove the copper catalyst from the polymer. The acetone was removed under reduced pressure and the translucent material deposited on the flask wall was dissolved in a minimum amount of ethyl ether after which it was precipitated in a 10-fold excess of 50/50 (v/v) water/methanol. After decanting off the solvent, the poly (*t*-butyl acrylate) was dissolved in ethyl ether and the precipitation procedure was repeated two more times. Finally, the polymer was dried on a vacuum line.

The polymer was characterized by ^{1}H-NMR (300 MHz) and molar masses and mass distribution were measured by Gel Permeation Chromatography (GPC), performed on a Waters instrument (HR-1 and HR-4 columns), in THF eluent, interfaced to a PC running Millenium software with a Varian RI-4 refractive index detector, calibrated against polystyrene standards.

Four reactions were performed under the above conditions and are listed as entries 1-4 in Table 3.1.

Table 3.1. ATRP synthesis of poly (*t*-butyl acrylate).

Sample code	[M]/ [I]	[I]/ [CuBr]	[PMDETA]/ [CuBr]	Reaction time, h	T, °C	M_n (pred)	M_n (obs)	PI	DP (obs)
PB1	50/1	2/1	1.05	6.5	60	6575	6572	1.09	49
PB2	30/1	2/1	1.05	6.5	60	4012	4992	1.09	37
PB3	15/1	2/1	1.05	6.5	60	2090	2600	1.13	19
PB4	10/1	2/1	1.05	6.5	60	1449	1659	1.09	11
PB5	200/1	1/1	1/1	16	60	25632	21268	1.07	165
PB6	400/1	1/1	1/1	24	60	51431	42693	1.05	332

When a higher molecular weight was needed (see Table 3.1, entries 5 and 6) the reactions were performed with a 1/1 ratio [Initiator]/[CuBr], in the absence of the $CuBr_2$, and longer reaction times. Even so, the process stops at lower DP than those predicted most likely due to the increased viscosity of the system. The resulted polymer was dissolved in THF, washed with DOWEX MSC macroporous ion-exchange resin, passed through a short alumina column and purified by several precipitation from a high excess 70/30 (v/v) methanol/water mixture.

Synthesis of poly (t-butyl acrylate)-b-poly (styrene).

The extension of poly (*t*-butyl acylate) chain by ATRP of styrene (Scheme 2) was performed in the same manner as a typical one previously described for the macroinitiator synthesis. However, several changes regarding the order of addition of the reagents were made.

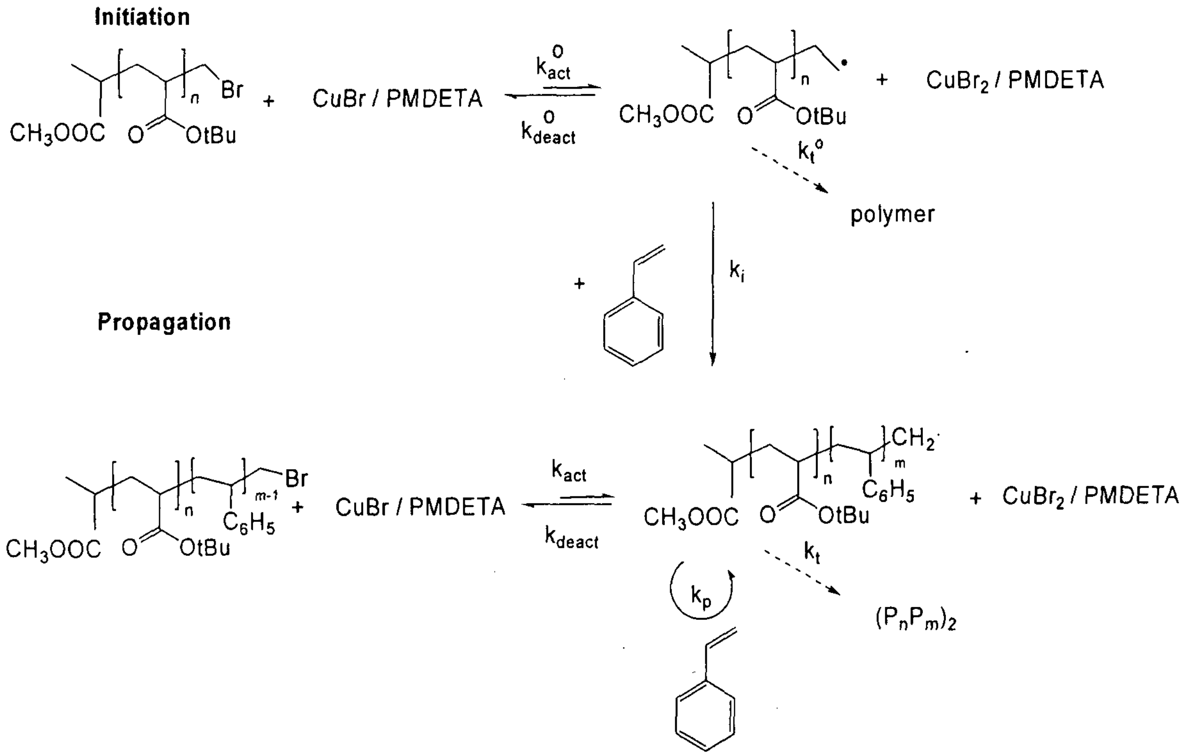

Scheme 2

Macroinitiator (PB2, PB4 and PB6) (1eq) and CuBr (1eq) were added to a 50ml round bottom flask (previously dried in the oven and cooled in a dessicator). Then, the flask was sealed with a rubber septum, degassed and back-filled with argon three times, and left under argon. Styrene was added via an argon purge syringe and the dissolution of the macroinitiator was observed resulting in a cloudy solution. The volume of styrene monomer was calculated taking into consideration the targeted degree of polymerization (DP) for the styrene block and the value of the average numeric molecular weight of the macroinitiator. For example 4.6405g of macroinitiator with a $M_n = 21268$ accounts for 0.2181 mmol. In order to achieve a styrene block of 100 residues, 21.81 mmol of styrene are necessary. The ligand (PMDETA, 1 eq) was added and the solution was stirred until the copper complex was formed (the solution changed from cloudy and colorless to a clear light green). After the complex formation three freeze-pump-thaw cycles were performed. After the reaction mixture reached room temperature, the flask was placed in an oil bath and heated at 100°C for a period of time given in Table 3.2.

The resulting block copolymer was purified by dissolving the reaction mixture in THF, washing with DOWEX MSC macroporous ion-exchange resin for about 1h and, filtering the solution through an alumina column in order to remove the copper catalyst from the block copolymer. The volume of THF was reduced under reduced pressure, and the block copolymer was separated by precipitation in a 10-fold excess of 25/75 (v/v) water/methanol. After decanting off the solvent, the precipitation procedure was repeated two more times. Finally, the product was dried on a vacuum line.

The block copolymers were characterized by ^{1}H-NMR (300 MHz) and the average molecular weights as well as the polydispersity indexes were determined by GPC analyses under the same conditions as those mentioned for the poly (*t*-butyl acrylate). The results are presented in Table 3.2.

Table 3.2. ATRP of poly (*t*-butyl acrylate)-b-poly (styrene). All the reactions were performed at 100°C and a ratio [Macronitiator]/[CuBr]/[PMDETA]=1/1/1

Sample code	[Styrene]/ [MacroI]	Reaction time, h	M_n (pred.)	M_n (obs)	PI	$DP_{Styrene}$/ DP_{tBuA}
COPM1	450/1(PB2)	20	51859	58094	1.12	509/37
COPM2	310/1(PB4)	16	33943	49851	1.15	462/11
COPM3	200/1(PB5)	16	42098	45349	1.11	231/165
COPM4	250/1(PB4)	16	27697	46506	1.16	430/11
COPM5	210/1(PB4)	17	23530	38259	1.09	351/11
COPM6	40/1(PB5)	2.5	-	23437	1.08	21/165

From Table 3.2, the obtained average numeric molecular weight is higher than the one predicted, and the polydispersity index increases compared to the polydispersity index of the macroinitiator. One explanation for this behaviour could be that some of the chains of the macroinitiator lost their functionality during the synthesis and therefore a smaller number of radicals were formed in the system during the second step. Both the presence of oxygen in the system as well as the increase of the viscosity might contribute to the observed higher molecular weight.

In the case of COPM6 due to the fact that the styrene volume is too small, a polymerization in solution was carried out using anisole as reaction media (80% of the total volume of reaction). With this exception the entire experimental procedure was performed in the same manner as reported above.

Among the synthesised block copolymers four were chosen to carry on the adsorption experiments on the solid support: COPM1, COPM3, COPM5 and COPM6. In order to transform these into the corresponding PS-PAA block copolymers ($PS_{509}PAA_{37}$,

$PS_{231}PAA_{165}$, $PS_{351}PAA_{11}$ and $PS_{21}PAA_{165}$ respectively) hydrolysis was performed applying two different procedures depending on the length of the PS block:

A. Hydrolysis of the block copolymers with long PS blocks (COPM1, COPM5):

The block copolymer was dissolved in toluene and to the homogenous solution p-toluene-sulfonic acid was added (the amount of which was calculated as 5-fold molar excess/mol ester group). The solution was refluxed for 4h and then stirred at room temperature overnight. The solvent was removed under reduced pressure, the residue was taken into a minimum amount of THF and the block copolymer was separated by precipitation from a mixture 9/1 (v/v) water/methanol.

B. Hydrolysis of the block copolymers with short polystyrene block (COPM3 and COPM6):

The block copolymer was dissolved in dry dichloromethane under an argon stream. Trifluoroacetic acid (in high excess) was added drop wise and the reaction mixture was stirred at room temperature for 48h. The precipitate formed (PAA is not soluble in dichloromethane) was separated by filtration, washed with an additional amount of dichloromethane and dried under vacuum.

Hydrolysis of the *t*-butyl acrylate group was monitored by the disappearance of the resonance at 1.41 ppm (protons of the t-butyl group). Furthermore, there was little or no evidence for residual ester carbonyls bands (~ 1730 cm^{-1}) in the recorded FTIR spectra (neat or KI pellets).

Table 3.3: Block length, M_w, polydispersity, a dimensionless asymmetry parameter (β), and radius of gyration for copolymers (provided by Dr. Adi Eisenberg* and Dr. Violetta Toader#) and homopolymers studied.

Block Copolymer	Block lengths	M_n (g/mol)	M_w/M_n	Asymmetry parameter (β)	R_g of PS blocks (nm)
$PS_{384}PAA_{10}$*	$N_{PS} = 384$ $N_{PAA} = 10$	40500	(S)=1.25, (AA)=1.10	272	8.9
$PS_{500}PAA_{30}$*	$N_{PS} = 500$ $N_{PAA} = 30$	54000	(S)=1.25, (AA)=1.10	179	10.4
$PS_{500}PtBuA_{10}$*	$N_{PS} = 500$ $N_{PtBuA} = 10$	53000	(S)=1.09, (tBuA)=1.11	373	10.4
$PS_{384}PtBuA_{30}$*	$N_{PS} = 384$ $N_{PtBuA} = 30$	43000	(S)=1.25, (tBuA)=1.10	130	8.9
PS_{400}	$N_{PS} = 400$	40000	(S)=1.05		9.1
$PS_{509}PAA_{37}$#	$N_{PS} = 509$ $N_{PAA} = 37$	58100	1.12	159	10.2
$PS_{351}PAA_{11}$#	$N_{PS} = 351$ $N_{PAA} = 11$	38250	1.09	229	8.4
$PS_{231}PAA_{165}$#	$N_{PS} = 231$ $N_{PAA} = 165$	45350	1.11	22.8	6.5
$PS_{21}PAA_{165}$#	$N_{PS} = 21$ $N_{PAA} = 165$	23440	1.08	1.28	1.6
PAA_{80}	$N_{PAA} = 80$	5700	(AA)=1.09		

Approximate block lengths, M_n, polydispersity and radius of gyration for the copolymers are listed in Table 3.3. The dimensionless asymmetry parameter is calculated using equation 1.3 provided in the introduction. The radius of gyration for the buoy block, polystyrene, is calculated in a manner similar to that found in Zhang and Eisenberg [17]. In a good solvent, a solvent that dissolves both blocks, the radius of gyration is given by, $Rg \approx aN_{PS}^{3/5}$, where "a" is the length of the repeat unit. Homopolymers were obtained from Polymer Source Inc. (Dorval, Canada) and were used as received. As can be seen in Table 3.3, a variety of block lengths were chosen, most have a large hydrophobic block and a short hydrophilic block, but there was one copolymer of approximately equal block lengths, and one with a small hydrophobic block and a large hydrophilic block.

3.4.2 Sample Preparation.

Solutions were prepared by dissolving each block copolymer in THF at initial concentrations of 1, 3, 5, 10, 40, 80, and 120 mg/ml. A second solution was prepared by dispersing 150 mg of zirconia in 5 ml of THF with 15 min of sonication. The zirconia and copolymer solutions were added and allowed to stir at room temperature for 24 h. The resultant solution was centrifuged at 4000 rpm for one hour, the supernatant was discarded, and the adsorbed block copolymer was dried under vacuum at 70°C overnight. Thermal gravimetric analysis (TGA) was used to determine the weight percent of copolymer adsorbed on alumina.

3.4.3 Solid-State ^{13}C and ^{1}H NMR

^{13}C CP-MAS NMR spectra (67.03 MHz) were recorded on a Chemagnetics CMX-270 NMR spectrometer with either a 9.5 mm HX MAS solids probe with low ^{13}C background or a 4.5 mm pencil probe. The probe used is indicated in the corresponding ^{13}C NMR figures. Spinning frequency, pulse delay, contact times, and number of scans are all reported in the appropriate figure captions. The inversion recovery pulse sequence was used to determine the various T_1 values, with spectra obtained under the following conditions: a pulse delay of 3 s, 2000 scans, τ values between 1 and 30 seconds, and a pulse width of 7.25 μs. ^{1}H $T_{1\rho}$ and ^{13}C $T_{1\rho}$ measurements were both collected with variations of the ^{13}C CP-MAS NMR pulse program. The ^{1}H $T_{1\rho}$ relaxation time was determined by varying the ^1H spin lock from 1 to 10 ms. The ^{13}C $T_{1\rho}$ relaxation time was determined by varying the ^{13}C spin lock from 0.001 to 5 ms.

^1H fast MAS NMR spectra were recorded on a Bruker Avance 600MHz wide bore NMR spectrometer with a Bruker bl2.5 probe. Spinning frequency, pulse delay, pulse width, and number of scans are all reported in the appropriate figure captions. The inversion recovery pulse sequence was used to determine the various T_1 values, with τ values between 0.01 and 10 seconds.

3.4.4 FTIR-PAS

A Fourier Transform IR spectrometer (Mattson Research Series 1 spectrometer) equipped with a photoacoustic cell (MTEC model 300) was used to collect all IR spectra. The spectra were collected with a 4.0 cm^{-1} nominal resolution.

3.4.5 Thermal Gravimetric Analysis (TGA)

All samples were heated to 600 °C in a nitrogen environment at a rate of 10 °C/min, and then held at 600 °C in an oxygen environment for 10 min. This process allowed the amount of organic material attached to the metal oxide surface to be determined. All samples were run on a TGA Q500 (Thermal Analysis Instruments).

3.4.6 Differential Scanning Calorimetry (DSC)

DSC experiments were performed on a Q1000 differential scanning calorimeter (Thermal Analysis Instruments) in a dry nitrogen atmosphere. Samples of ~ 8 mg were placed in an aluminum pan. All samples were first heated from 0 to 175 °C at a rate of 10 °C/min (first heating scan) and kept at that temperature for 5 min; subsequently, they were cooled to 0 °C at a rate of -10 °C/min and kept at that temperature for 5 min. Following the cooling scan, a second heating scan was conducted with the same heating rate as the first one. The midpoint of the slope change of the heat capacity plot was taken as the glass transition temperature (T_g).

3.5 Results and Discussion

3.5.1 FTIR-PAS

Figure 3.1a shows the FTIR-PAS spectra for the bulk copolymers. The six spectra in Figure 3.1a are all very similar in that they contain bands due to poly (acrylic acid) consisting of a broad OH band centered at approximately 3100 cm^{-1}, a broad carbonyl band at 1735 cm^{-1}, and two CH_2 bending bands at 1465 and 1440 cm^{-1}. The bands associated with the polystyrene block include a C-C stretching frequency in the plane of the ring at 1601 cm^{-1}, a C-H stretching vibration in the plane of the ring at 1493 cm^{-1}, and a CH_2 bend at 1453 cm^{-1}.[18]

Figure 3.1b shows the FTIR-PAS spectra for the adsorbed polymers. The initial concentration, 20 mg/ml, was chosen because it was believed that these solutions would lie on the plateau region (in terms of adsorption) for all of the block copolymers, Figure 3.4. However, when the adsorbed amounts in Figure 3.1b are compared to those in Figure 3.4, the adsorbed amounts are just on the onset of the plateau region for some of the copolymers, while for others the adsorbed amount is equivalent to the plateau quantity. Khougaz et al.[19] reported the CMC values for a series of PS-PAA block copolymers containing a long PS chain and a short PAA chain where the CMC's were in the range from 1×10^{-7} to 5×10^{-9} M. All of the solutions prepared are at least 2×10^{-5} M; therefore all solutions should be above the CMC. However it is assumed that free chains rather than micelles are adsorbed. Theoretical work by Johner and Joanny [20] showed that the potential barrier for direct adsorption of chains belonging to micelles is so high that only free chains adsorb on the wall. The adsorption of free chains creates a large region near the wall where the free chains are depleted and where the equilibrium between free chains and micelles is broken. The equilibrium is restored by micelle relaxation through the expulsion of chains one by one.[20]

A free acid C=O band at 1725 cm^{-1} in the FTIR-PAS spectra indicates that not all the carboxylic acid groups are bound to the surface, this peak is present for all spectra except for $PS_{351}PAA_{11}$ where due to the small block size the C=O band is very small. The bands at 1554 and 1465 cm^{-1} are assigned to the asymmetric and symmetric -C-O stretches of surface-bound carboxylate groups.[21] However, the band at 1554 cm^{-1} is the only band to indicate the formation of ionic surface bonds since the C-O symmetric band overlaps with the $-CH_2-$ stretch at 1460 cm^{-1}. Although the FTIR-PAS spectra show that not all of the carbonyl groups of the PAA blocks form ionic surface bonds, it is still possible for the remaining carboxylic acid groups to interact more weakly with the metal oxide surface through hydrogen bonds to the surface hydroxyl groups.

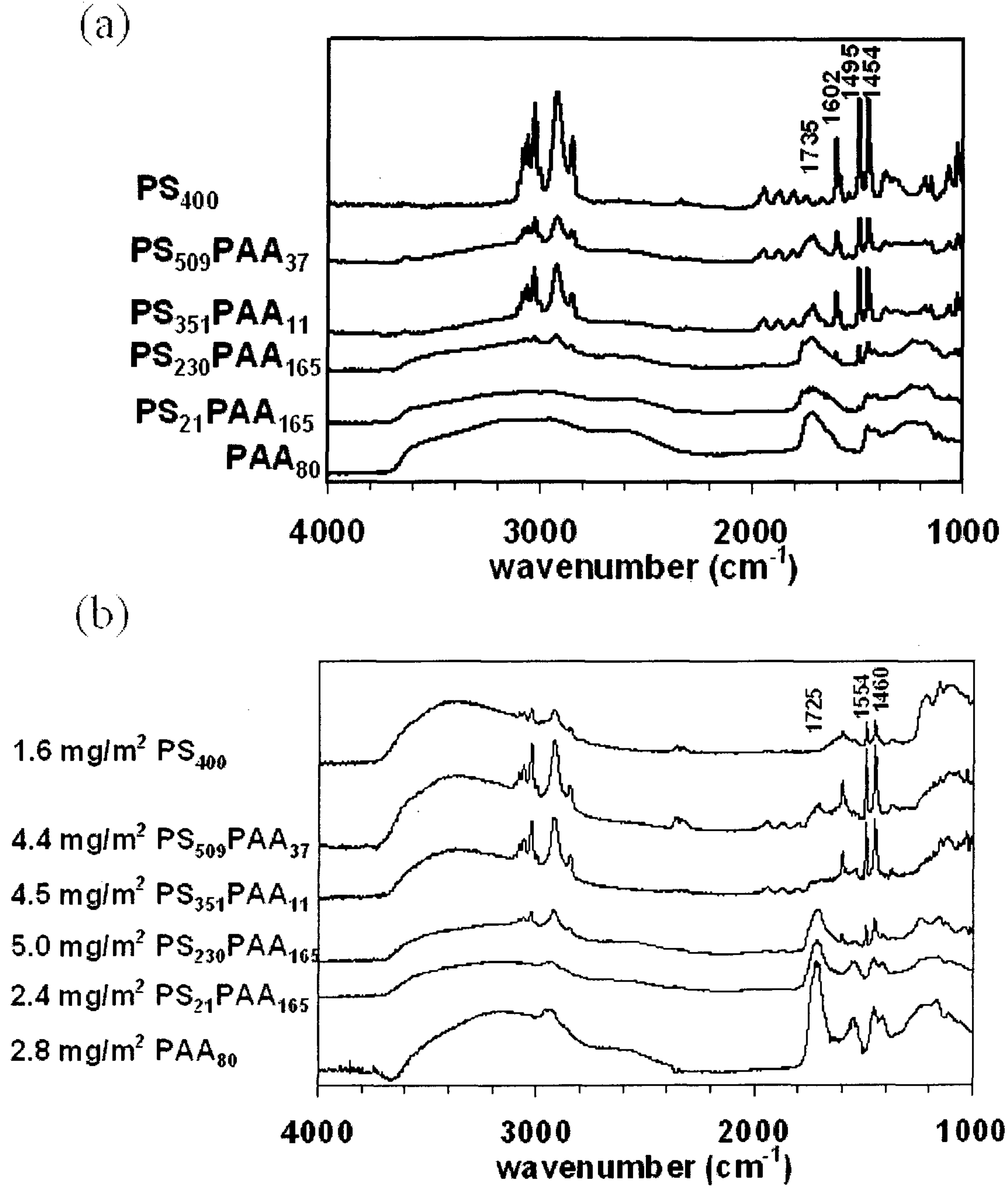

Figure 3.1: FTIR-PAS spectra for (a) bulk polymers, and (b) polymers adsorbed on zirconia. The initial concentration for all of the adsorbed copolymers was 20 mg/ml. (number of scans = 32 for bulk, and 64 for adsorbed, resolution = 4 cm^{-1})

3.5.2 Solid-State NMR of the Bulk PS-PAA Block Copolymers

In order to distinguish the effect of the surface on the chain dynamics, the bulk copolymers as well as the constituent homopolymers were first characterized by solid-state ^{13}C and ^{1}H NMR spectroscopies. Figure 3.2a shows the ^{13}C CP-MAS NMR spectra for a series of block copolymers along with the homopolymers. The ^{13}C CP-MAS NMR spectrum for bulk PS, Figure 3.2a, has three peaks: the peak at 41 ppm is a broad peak that is due to the methylene backbone carbons attached to the styrene block, the peak at 127 ppm is due to the protonated aromatic carbons, and the peak at 145 ppm is due to the non-protonated aromatic carbons. Spinning side bands appear due to the slow spinning frequency relative to the large ^{13}C chemical shift anisotropy of the carboxylic and aromatic carbon groups. The ^{13}C CP-MAS NMR spectrum for bulk PAA, Figure 3.2a, has two peaks: the broad peak at 41 ppm is due to the methylene backbone carbons attached to the acrylic acid block, and the carboxylic acid carbon signal appears at 178 ppm.

A pulse sequence (Total Suppression of Spinning Sidebands, TOSS) was initially applied to suppress the large array of spinning sideband signals but was found to result in too great a signal loss in the case of the adsorbed copolymers due to the small quantity of polymer present in each sample. Given the prohibitively long acquisition times to collect a complete set of variable contact times, it is assumed that the cross relaxation parameters do not vary much with coverage for the qualitative comparisons presented here. The signal intensities of the aromatic and carbonyl carbons reflect the relative PS and PAA block sizes. As expected, the most symmetrical copolymer, $PS_{230}PAA_{165}$, is the only copolymer with intense PS and PAA peaks.

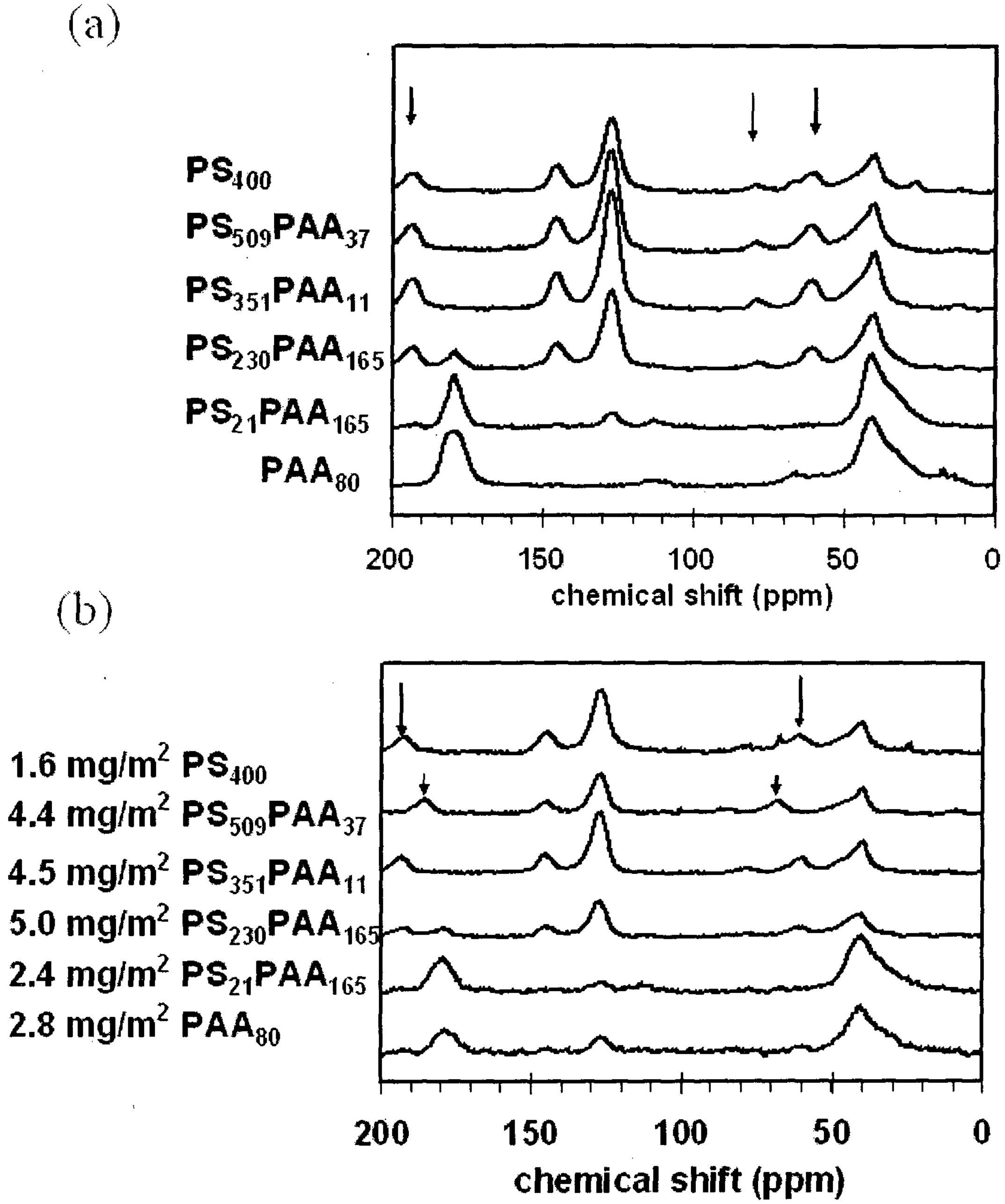

Figure 3.2: ^{13}C CP-MAS NMR spectra for (a) bulk polymers, and (b) polymers adsorbed on zirconia. The initial concentration for all of the adsorbed copolymers was 20 mg/ml. (spinning frequency = 4500 Hz, except for adsorbed $PS_{509}PAA_{37}$ spinning frequency = 4000Hz. Contact time = 1 ms, number of acquisitions = 1200 for bulk, and 2400 for adsorbed, pulse delay = 3 s, probe = 9.5 mm rotor). The arrows indicate the position of spinning sidebands.

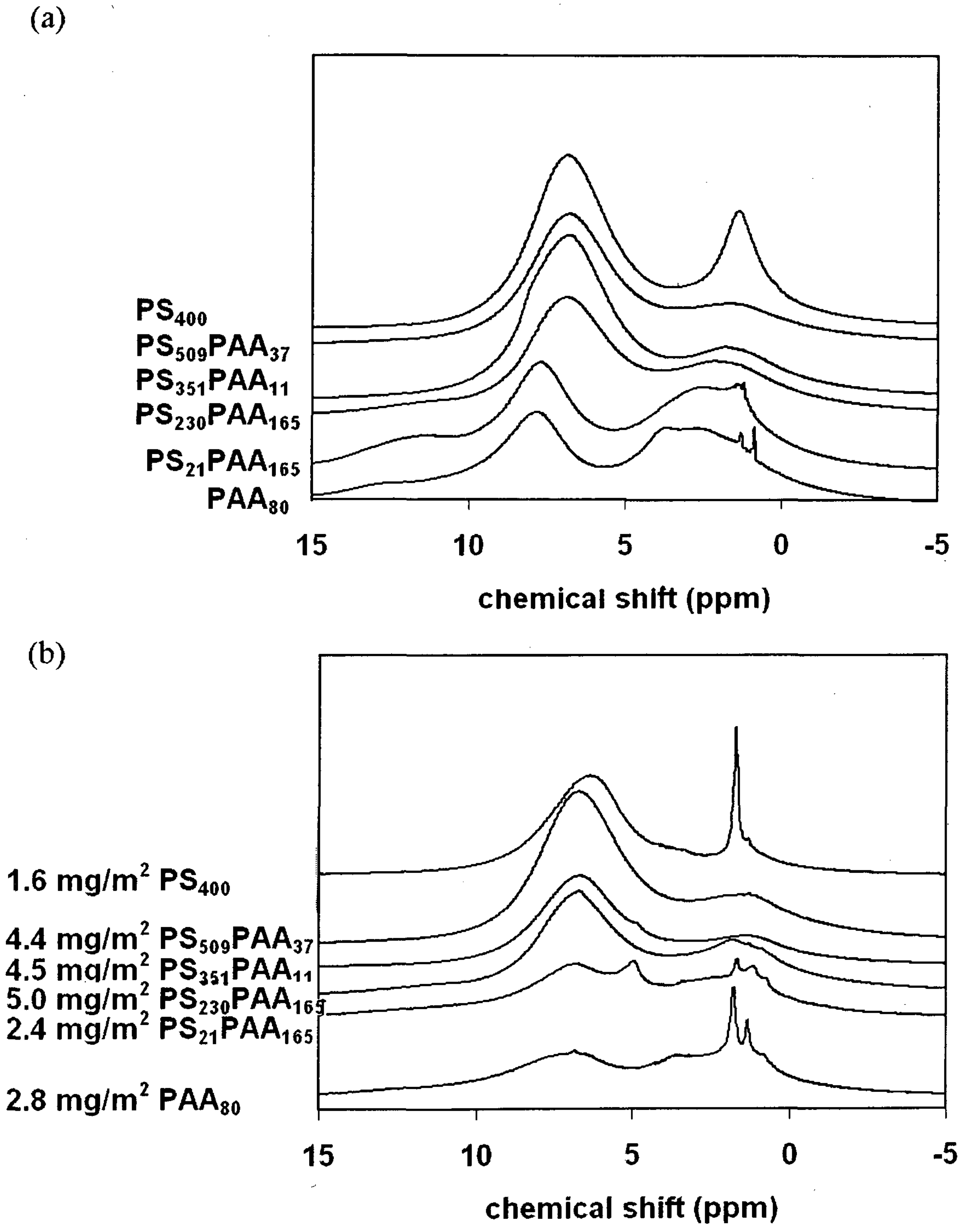

Figure 3.3: ^{1}H NMR spectra for (a) bulk polymers, and (b) polymers adsorbed on zirconia. The initial concentration for all of the adsorbed copolymers was 20 mg/ml. (spinning frequency = 25 kHz, number of acquisitions = 16 for bulk and 32 for adsorbed, pulse delay = 10 sec for bulk, and 5 sec for adsorbed, pulse width = 1.7 μsec).

The ^1H NMR spectrum for polystyrene, shown in Figure 3.3a, has two distinct regions: the styrene protons have a relatively broad chemical shift centered at 6.7 ppm, and a slightly narrower peak centered at 1.2 ppm due to the backbone methine and methylene protons. The ^1H NMR spectrum for poly (acrylic acid) consists of broad peaks at ~12.0, ~7.7 and ~2.5 ppm. Recently Li et al.[11] attributed the 12 ppm peak to hydrogen bonded acid protons of cyclic and open COOH dimers. An intense peak at 7.1 ppm was assigned to the protons of large clusters of water molecules that are mutually hydrogen bonded and/or also interact with the COOH side groups, as well as the COOH protons undergoing fast chemical exchange with water. ^1H CRAMPS experiments revealed four types of protons in hydrated PAA assigned to protons from (1) the mutually H-bonded COOH groups (12.9 ppm), (2) free COOH groups (10.7 ppm), (3) COOH groups bounded with water or water bounded with COOH groups which are undergoing mutual fast chemical exchange (8.5 ppm), and (4) main chain groups (2.5 ppm).[11] The water signal at 7.1 ppm broadens and shifts to 8.5 ppm upon dehydration, which is evidence of chemical exchange between water and COOH groups. Free, unbound water should appear at approximately 4.8 ppm. Since the ^1H fast MAS experiments do not provide as much resolution as the CRAMPS experiment, no splitting of the peak at ~12 ppm is observed. According to the TGA results there is between 0.5 and 1.5 % bound water for the block copolymers, while the homopolymer PAA is slightly more hydrophilic with 2.5 % bound water resulting in the broad peak at 7.1 ppm. Although all adsorbed samples were dried under vacuum at 70°C overnight before the NMR measurements, some tightly bound water remains, giving rise to the 7.7 ppm peak.

The relaxation times of the bulk copolymers, along with the glass transition temperatures, are listed in Table 3.4. The presence of a small amount of PAA increases the glass transition by approximately 20 °C and as the PAA block becomes significantly larger than the PS block, the glass transition approaches that of PAA. The DSC traces of the bulk copolymers are similar to those reported in the literature. For the first heating scan, two glass transitions are reported at approximately 60 and 130 °C, and for the second scan only one glass temperature appears at approximately 120 °C. Two explanations for the two glass transitions have been proposed. One interpretation is that in the acrylic acid rich phase, the PS segments dilutes the H-bonds, lowering the Tg (60°C), whereas in the PS-rich phase, the presence of a few H-bonds among PAA gives rise to a higher Tg (139°C).[22] Another group attributed the two glass transitions to the departure of bound water such that the glass transition temperature in the second heating scan moves to 116 °C from 51 °C.[11] The diblock with the longer PAA block, $PS_{21}PAA_{165}$ has a much higher glass transition temperature than the other block copolymers, and higher even than PAA. This is most likely explained by the interpretation given by Yan et al.[22], in combination with the low molecular weight of the PAA homopolymer used in this study. The homopolymer is about half the block length of $PS_{21}PAA_{165}$ and the observed T_g is in agreement with the reported molecular weight dependence of the glass transition temperature of PAA.[23]

Spin lattice relaxation times in the rotating frame, $T_{1\rho}$, and laboratory frame, T_1, are sensitive to kHz and MHz motional frequencies respectively. Since the bulk copolymers are far below their glass transition temperatures, the chain mobilities are expected to be on the slow side of the motional correlation time versus temperature curve where T_1 decreases with increasing frequency of motion. This limit is confirmed by the shorter ^{13}C T_1 values measured at 60 °C (data not shown). The chain mobilities of the polymers constituting the minor blocks are enhanced relative to the homopolymers. For example, the ^{13}C T_1 value of the aromatic carbons decreases from 30 s in copolymers where PS is the major block ($PS_{501}PAA_{37}$ and $PS_{351}PAA_{11}$) to 20 s in copolymers with a larger PAA content ($PS_{230}PAA_{165}$ and $PS_{21}PAA_{165}$), indicating an increase in mobility of the PS segments. Likewise the ^{13}C T_1 of the COOH group shortens from 33 s ($PS_{21}PAA_{165}$) to 8 s ($PS_{230}PAA_{165}$); reflecting enhanced mobility of the PAA segments presumably due to a weakened H-bonding network.

The ^{13}C CP-MAS technique can be employed to measure individual T_1 and $T_{1\rho}$ values of protons attached to or close to various carbons. However, in solid polymers the proton relaxation is often affected by spin diffusion, i.e. the propagation of magnetization by energy-conserving transitions of proton pairs having antiparallel spins (proton spin "flip-flops"). Because of this process, all protons often share the same spin lattice relaxation time and the individual relaxation characteristics are lost.[24] Accordingly, the bulk copolymers, Table 3.4, display uniform T_1 and $T_{1\rho}$ values for the different protons. We note that the most symmetric copolymer, $PS_{230}PAA_{165}$ has a distinctly smaller ^1H T_1 value. This shorter value probably originates from the higher mobility of the PAA segments in the block copolymers with equal or longer PS blocks combined with spin diffusion. However, this cannot be verified by ^{13}C NMR for the asymmetric copolymers with short PAA blocks since the COOH signal is below the detection limit in these copolymers.

3.5.3 Adsorbed Diblock Copolymers: Effect of Block Length

The ^{13}C and ^{1}H NMR spectra for a series of block and homopolymers adsorbed on zirconia powder are presented in Figures 3.2b and 3.3b along with the adsorbed amounts in mg/m^2. The initial copolymer concentration in all the sample preparations was 20 mg/ml. The adsorbed amount for the copolymers with larger PS blocks, $PS_{509}PAA_{37}$, $PS_{351}PAA_{11}$, and $PS_{230}PAA_{165}$ were very similar with approximately 4.5 mg/m^2 of polymer being adsorbed on the surface. The adsorbed amounts for the two homopolymers polymers and the diblock with a large anchor and small buoy block, $PS_{21}PAA_{165}$, are lower, between 1 and 2.5 mg/m^2. The solvent used in this study was THF, which was a good solvent for PS allowing for the rapid dissolution of $PS_{509}PAA_{37}$, $PS_{351}PAA_{11}$, and PS_{400}. THF is not as good a solvent for $PS_{230}PAA_{165}$, $PS_{21}PAA_{165}$, and PAA_{80}. These polymers either take longer to dissolve or do not dissolve completely.

There is obviously a large reduction of signal-to-noise for the adsorbed samples when compared to the bulk polymers, and a slight narrowing of the peaks but no change in the ^{13}C chemical shifts. Note that the ^{13}C signals for the backbone carbons of the PAA and PS blocks overlap but the aromatic and COOH carbons are well separated. The ^{1}H NMR spectra for adsorbed polymers, shown in Figure 3.3b, have two distinct regions: the aromatic region at approximately 7.0 ppm, and the aliphatic region at about 2 ppm. For PS, the aromatic peak is slightly narrower, and shifted 0.5 ppm downfield compared to the bulk polymers. In the aliphatic region for PS, the broad bulk peak has been split into two sharp peaks. One is still at 1.2 ppm, the other at 1.7 ppm. This is a phenomenon that is seen throughout this study where a highly mobile component is detected at the lowest surface loadings. For $PS_{501}PAA_{37}$, $PS_{351}PAA_{11}$, and $PS_{230}PAA_{165}$ there is slight line narrowing and a downfield shift of 0.5 ppm for both peaks. For $PS_{21}PAA_{165}$, and PAA_{80}, there is the loss of the carbonyl peak at 12 ppm, a downfield shift of 0.8 ppm for the aromatic carbon/bound water signal that was at 7.7 ppm in the bulk, and increased resolution in the aliphatic region.

Table 3.4: Glass transition temperatures (T_g), ^{1}H T_1 (s), ^{13}C T_1(s) and $T_{1\rho}$ (ms) of the bulk and adsorbed (mg/m^2) copolymers at ambient temperature.

Copolymer	**Tg**	**^{13}C backbone**		**^{13}C styrene**		**^{13}C COOH**		**^{1}H**	
Units	**(°C)**	**T_1 (s)**	**$T_{1\rho}$ (ms)**	**T_1 (s)**	**$T_{1\rho}$ (ms)**	**T_1 (s)**	**$T_{1\rho}$ (ms)**	**T_1 (s)**	**$T_{1\rho}$ (ms)**
PS_{400} bulk	87.9	50.2	0.59	32.1	1.44			1.70	2.78
Adsorbed 1.6 mg/m^2		**43.8**	**0.50**	**25.6**	**1.6**			**0.37**	**5.80**
$PS_{509}PAA_{37}$ bulk	107.2	54.5	0.85	30.7	2.2			1.40	2.14
Adsorbed 4.4 mg/m^2		**37.0**	**0.59**	**26.8**	**1.5**			**0.31**	**3.90**
$PS_{351}PAA_{11}$ bulk	105.5	52.8	0.62	29.6	1.7			1.10	3.40
Adsorbed 4.5 mg/m^2		**40.8**	**0.61**	**21.8**	**1.64**			**0.44**	**3.20**
$PS_{230}PAA_{165}$ bulk	105.2	22.9	0.60	21.3	1.6	8.3	4.3	0.39	3.20
Adsorbed 5.0 mg/m^2		**42.0**	**0.68**	**21.7**	**2.0**	**36.4**	**7.8**	**0.35**	**3.70**
$PS_{21}PAA_{165}$ bulk	127.7	28.3	0.66	20.6	1.46	33.1	5.1	1.20	3.10
Adsorbed 2.4 mg/m^2		**26.0**	**0.70**	**19.3**	**1.4**	**30.2**	**5.3**	**0.20**	**3.00**
PAA_{80} bulk	119.7	7.3	0.59			8.6	3.4	1.60	1.36
Adsorbed 2.8 mg/m^2		**27.3**	**0.69**	-	-	**24.5**	**3.9**	**0.21**	**3.80**
PAA_{1250} bulk[25]		23				18			

*The error on the ^{13}C T_1 values is ± 0.1 s, ^{13}C $T_{1\rho}$ is ± 0.02 ms, ^{1}H $T_{1\rho}$ is ± 0.02 ms, and ^{1}H T_1 is ± 0.01 s.

When the ^{13}C spin lattice relaxation times in the laboratory frame (T_1) of the bulk and adsorbed copolymers are compared (Table 3.4), the mobility of the PS segments of the asymmetric diblocks with long PS blocks generally increases, as reflected by shorter T_1 values for the aromatic carbons. However, the PAA segments' relaxation times greatly increase due to the COOH surface interactions. The most symmetric diblock studied, $PS_{230}PAA_{165}$, is an exception in that the ^{13}C T_1 values for PS segments are quite close to the bulk copolymer values. In the case of the highly asymmetric copolymer with a short PS block, $PS_{21}PAA_{165}$, the T_1 values for both PS and PAA blocks are similar to the bulk values. In general, the proton T_1 values of the copolymers are shortened by an order of magnitude upon adsorption, indicating the presence of chain segments with mobilities enhanced relative to the bulk state. There is less variation observed for the ^{13}C and ^1H $T_{1\rho}$ values of the adsorbed copolymers that are similar or slightly larger relative to the bulk values, reflecting little change in the kHz frequency range. However the proton $T_{1\rho}$ values of the adsorbed PS and PAA homopolymers are markedly larger, indicating more restricted motion in the kHz range.

The above relaxation measurements were carried out on adsorbed copolymer samples lying in the plateau region of their adsorption isotherms. In the case of the asymmetric copolymers with short polar blocks, $PS_{509}PAA_{37}$ and $PS_{351}PAA_{11}$, an extended brush structure should be formed in the presence of THF, a good solvent for PS. Upon removal of the solvent, the extended brushes are expected to collapse into flattened conformations, forming a thin glassy layer, as indicated by surface force and XPS studies of adsorbed PS-PVP copolymers.[26] The NMR relaxation measurements support this interpretation of the structure of the adsorbed diblock copolymers in the dry state. There is only a moderate enhancement of the segmental mobility of the collapsed PS brushes relative to the bulk copolymers. One may expect different dynamics for the two adsorbed diblocks with much longer PAA anchor groups, $PS_{230}PAA_{165}$ and $PS_{21}PAA_{165}$. As the size and thus the spacing of the anchor blocks increases, a transition from an extended brush to a mushroom structure is expected.[27] Therefore, a greater PS segmental mobility could be expected. Instead the chain dynamics of the PS layer formed by the collapse of the mushroom and intermediate brush/mushroom structures are unchanged from the glassy bulk state. High molecular weight PS-PVP brushes with long PS blocks swollen with toluene display enhanced mobilities relative to the PS homopolymer in solution whereas low molecular weight copolymers have similar mobilities.[4] The M_n values of the PS-PAA copolymers used here, ~ 30-50 kg/mol, fall into the high molecular weight range. In the case of the low molecular weight PS-PVP where the styrene segments are not long enough to form extended brushes, the retardation in mobility was attributed to proximity to bound segments. A similar effect may account for the lower mobility of the short PS blocks of adsorbed $PS_{21}PAA_{165}$. However the finding that the collapsed intermediate brush/mushroom structure formed by the adsorption of $PS_{230}PAA_{165}$ has retarded mobility relative to the collapsed extended brushes is not necessarily intuitive.

3.5.4 Effect of Loading and Anchor Group: PS-PAA versus PS-PtBuA

The effect of surface loading and the anchor surface binding strength on the chain mobility was examined for the highly asymmetric diblocks with large PS blocks. The adsorption isotherms with loadings ranging from 0.5 to 6.0 mg/m^2 are presented in Figure 3.4. The adsorption isotherm was fitted to a Langmuir type isotherm [5],

$$\theta = \frac{ac}{(1+bc)} \tag{3.1}$$

where θ is the amount adsorbed (mg of polymer/m^2), a and b are constants, and c is the polymer concentration (mg/ml). The equilibrium concentration was obtained by subtracting the concentration of adsorbed polymer from the initial concentration. The ratio a/b represent the limiting monolayer coverage. The monolayer quantity of material for $PS_{384}PAA_{10}$ and $PS_{384}PtBuA_{30}$ were approximately the same, while $PS_{500}PtBuA_{10}$ had the lowest plateau value. Even though the $PS_{384}PtBuA_{30}$ has a much more rounded isotherm than does $PS_{384}PAA_{10}$, they both end up at approximately the same plateau value. From Zhan and Mattice [28] we see that initial rise in the adsorption curve, *b*, is a ratio of the rate of polymer adsorption to the rate of desorption, $b = k_a/k_d$, which is a measure of the intensity of adsorption. Therefore, a large *b* value means that the polymer binds strongly to the substrate, so $PS_{500}PAA_{30}$ is the most strongly bound block copolymer. The adsorption isotherms for the polymers, $PS_{384}PAA_{10}$ and $PS_{500}PAA_{30}$, were of higher affinity than $PS_{384}PtBuA_{30}$ and $PS_{500}PtBuA_{10}$ where a more rounded isotherm was found. This could be due to a stronger interaction between the acrylic acid and the zirconia. As expected, a Langmuir isotherm is observed with an initial sharp increase in adsorption followed by a plateau region. The isotherm fits are relatively good, but as can be seen in the inset of Figure 3.4, there is quite a bit of scatter at low concentration. The order of adsorption is $PS_{384}PAA_{10} > PS_{500}PAA_{30} > PS_{384}PtBuA_{30} > PS_{500}PtBuA_{10}$ in regards to the maximum amount adsorbed. This trend is likely due to steric hindrance of the adsorption of adjacent polymer molecules with increasing PS block size combined with a larger anchor block. Likewise, the block copolymers containing PAA anchors have a higher adsorption maximum than those containing the bulky *t*-butyl acrylate group.

Table 3.5: *a* and *b* values from fits of adsorption data to equation 3.1, along with the ratio *a/b* (the monolayer coverage).

	a	*b*	*a/b*
$PS_{384}PAA_{10}$	1.22	0.20	6.2
$PS_{500}PAA_{30}$	2.63	0.51	5.1
$PS_{384}PtBuA_{30}$	0.25	0.041	6.3
$PS_{500}PtBuA_{10}$	0.28	0.064	4.4

At low coverages, the adsorbed asymmetric diblocks with large PS blocks in contact with a good solvent are expected to form mushrooms that will gradually transform to an extended brush structure as the spacings between the PAA anchors decrease with increasing coverage.[29] After solvent removal, the PS segments should collapse into flattened conformations and for low coverages where the spacing between PAA or PtBuA anchors exceeds the radius of gyration of PS blocks, the PS blocks may spread out on the surface in the form of trains and loops.

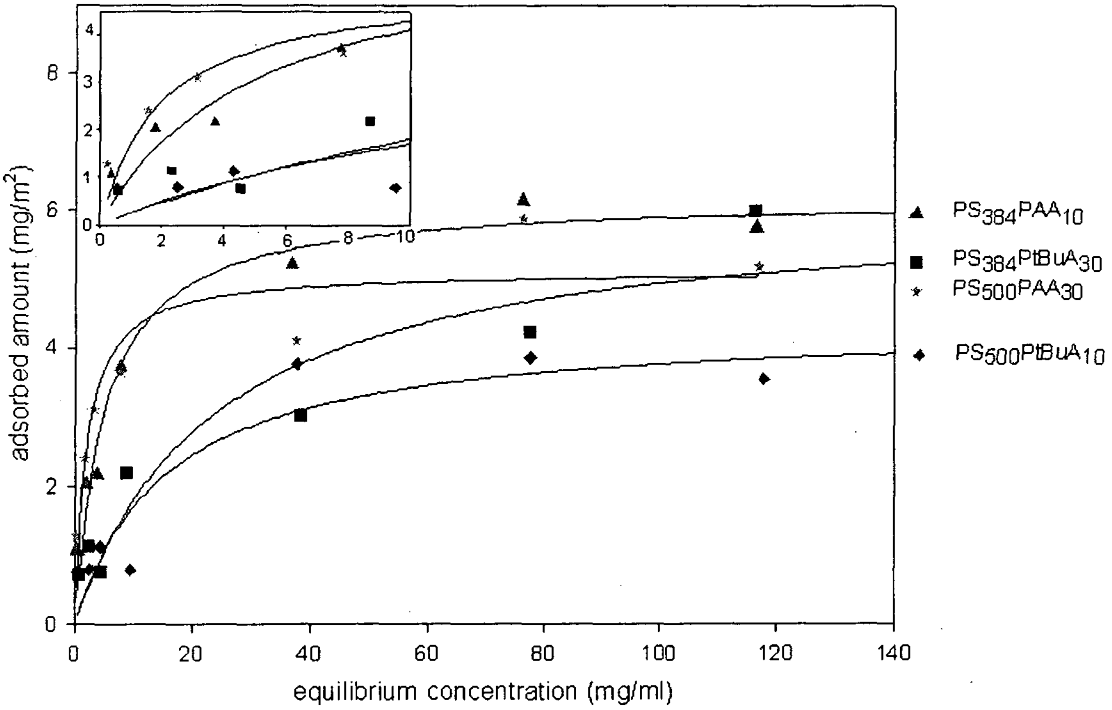

Figure 3.4: Adsorption isotherms for block copolymers adsorbed on zirconia. Inset shows the adsorbed amount at low concentrations. Lines are least squares fit to equation 3.1. The error on each adsorbed amount is ±0.2 mg/m^2.

Since ^{13}C CP-MAS NMR spectra with sufficient signal strength could not be acquired at the lowest loadings, higher sensitivity ^{1}H MAS NMR spectroscopy was used to probe the chain mobilities as a function of coverage. The ^{1}H MAS NMR spectra for the PS-PAA and PS-PtBuA copolymers absorbed on zirconia as a function of surface loading are given in Figure 3.5. At very low coverage, there is an increased resolution of the peaks in the aliphatic region. As the adsorbed amount is increased, the proton spectra become very similar, but the peaks do not reach the bulk copolymer line widths. The aromatic peak does not become resolved from the ZrO_2 surface hydroxyl proton signal until the higher loadings. The narrow resonances at low coverages are due to higher chain mobility as confirmed from the ^1H T_1 values (Table 3.6). Measurements were recorded for adsorbed amounts on the vertical part of the adsorption isotherm and for two values lying in the plateau regions.

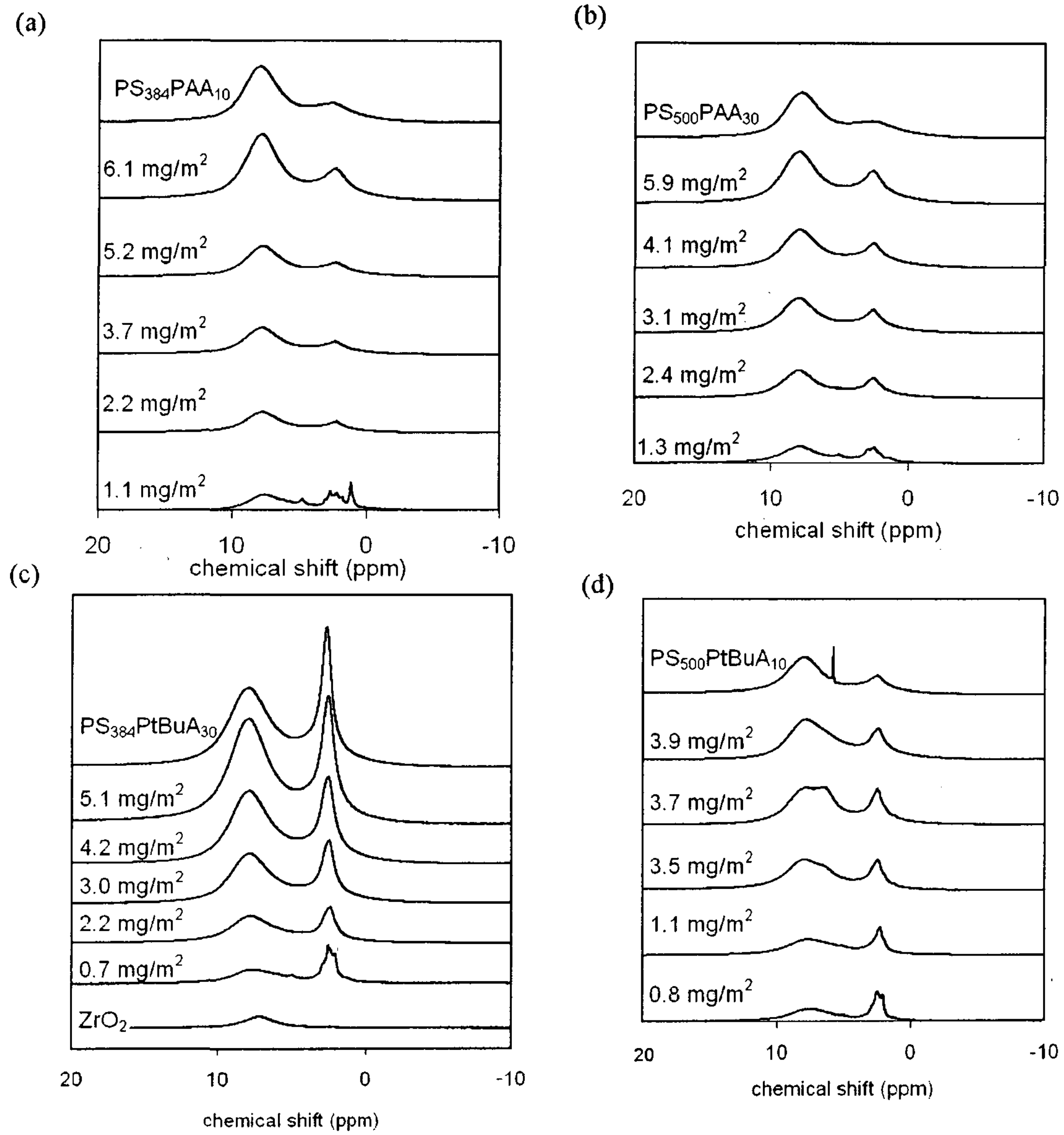

Figure 3.5: ^1H spectra for (a) $PS_{384}PAA_{10}$, (b) $PS_{500}PAA_{30}$, (c) $PS_{384}PtBuA_{30}$, and (d) $PS_{500}PtBuA_{10}$ adsorbed on zirconia. The initial concentrations of the adsorbed copolymers vary from 120 mg/ml to 1 mg/ml. (spinning frequency = 25 kHz, number of acquisitions = 16 for bulk and 32 for adsorbed, pulse delay = 10 sec for bulk, and 5 sec for adsorbed, pulse width = 1.7 μsec)

In the case of the PS-PAA copolymers, which interact more strongly with the metal oxide surface, only the very lowest coverages display T_1 values that are much smaller than those in the plateau region. The more weakly bound PS-PtBuA copolymers have markedly small ^1H T_1 values for both values measured in the initially increasing region of the adsorption isotherm. A small increase in the values is seen for higher loadings but the values never approach the bulk state values. For the lowest coverages, dynamics similar to the adsorbed PS homopolymer may be expected but instead the mobility is distinctly enhanced with ^{1}H T_1 values of 0.04 to 0.1 sec measured for the lowest adsorbed amounts as compared to the ^{1}H T_1 = 0.37 sec for the adsorbed PS homopolymer. The higher mobility is also evident from the narrow peaks superimposed on broader ones in the ^{1}H NMR spectra. This highly mobile component, combined with proton spin diffusion, is responsible for the short T_1 values relative to the bulk copolymers.

Table 3.6: ^{1}H T_1 (s) data for bulk and adsorbed block copolymers adsorbed on zirconia, the initial concentrations of the adsorbed copolymers being compared are 80 mg/ml, 10 mg/ml, and 1 mg/ml.

adsorbed amount (mg/m^2)	$PS_{384}PAA_{10}$ ^{1}H T_1 (s)	adsorbed amount (mg/m^2)	$PS_{500}PAA_{30}$ ^{1}H T_1 (s)
bulk	1.47	Bulk	0.99
5.8	0.65	5.2	0.67
3.7	0.38	3.6	0.41
1.1	0.09	1.3	0.14
adsorbed amount (mg/m^2)	$PS_{384}PtBuA_{30}$ ^{1}H T_1 (s)	adsorbed amount (mg/m^2)	$PS_{500}PtBuA_{10}$ ^{1}H T_1 (s)
bulk	1.10	bulk	1.27
6.0	0.42	3.5	0.33
2.2	0.14	0.84	0.13
0.7	0.05	0.77	0.04

*The error on the ^{1}H T_1 is ± 0.01 s.

Table 3.7 lists the adsorbed amounts for the adsorbed copolymers presented in Table 3.6. From the adsorbed amounts the surface density can be calculated, which can then be compared to the overlap density where the PS buoys overlap. The overlap density was calculated using the following equation [26]:

$$\sigma_{ol} = \frac{1}{\pi R_g^{\ 2}} \qquad (3.2),$$

where R_g is the radius of gyration previously calculated in Table 3.3. From Table 3.7 the surface density is greater than the overlap density even at the lowest coverages. This conforms with the picture of the adsorbed surface described in the previous section whereby the diblocks form two layers upon adsorption, a thin amorphous anchor layer and a glassy buoy layer.

Table 3.7: Adsorbed amount, surface density (σ), overlap density (σ_{ol}), and reduced surface density (σ*) for the adsorbed copolymers presented in Table 3.6.

adsorbed amount (mg/m^2)	surface density, σ (molecules/m^2)	overlap density, σ_{ol} (molecules/m^2)	ratio, σ^*
$PS_{384}PAA_{10}$			
5.8	8.6 x 10^{16}	4.0 x 10^{15}	21.5
3.7	5.5 x 10^{16}		13.7
1.1	1.6 x 10^{16}		4.1
$PS_{500}PAA_{30}$			
5.2	5.8 x 10^{16}	2.9 x 10^{15}	19.7
3.6	4.0 x 10^{16}		13.6
1.3	1.4 x 10^{16}		4.9
$PS_{384}PtBuA_{30}$			
6	8.4 x 10^{16}	4.0 x 10^{15}	28.6
2.2	3.1 x 10^{16}		10.5
0.7	9.8 x 10^{15}		3.3
$PS_{500}PtBuA_{10}$			
3.5	4.0 x 10^{16}	2.9 x 10^{15}	9.9
0.84	9.5 x 10^{15}		2.4
0.77	8.7 x 10^{15}		2.2

Belder et al.[30] have defined the reduced surface density to assist in expressing the surface density of polymer chains:

$$\sigma^* = \frac{\sigma}{\sigma_{ol}} \qquad (3.3)$$

where σ is the actual surface density and σ_{ol} the overlap density, the density above which the PS blocks are forced to overlap. Kent et al.[31] concluded that there are three regimes of stretching. Roughly speaking $\sigma^*<2$ corresponds to the *mushroom regime* (no stretching), $2 < \sigma^* < 20$ to the *intermediate (crossover) regime* (weak stretching), and $\sigma^* > 20$ to the "*true*" *brush regime*, where the chains are highly stretched. Thus the adsorbed block copolymers fall into the intermediate regime, except at the highest adsorbed amounts for $PS_{500}PAA_{30}$, $PS_{384}PAA_{10}$, and $PS_{384}PtBuA_{30}$ that are in the "true" brush regime.

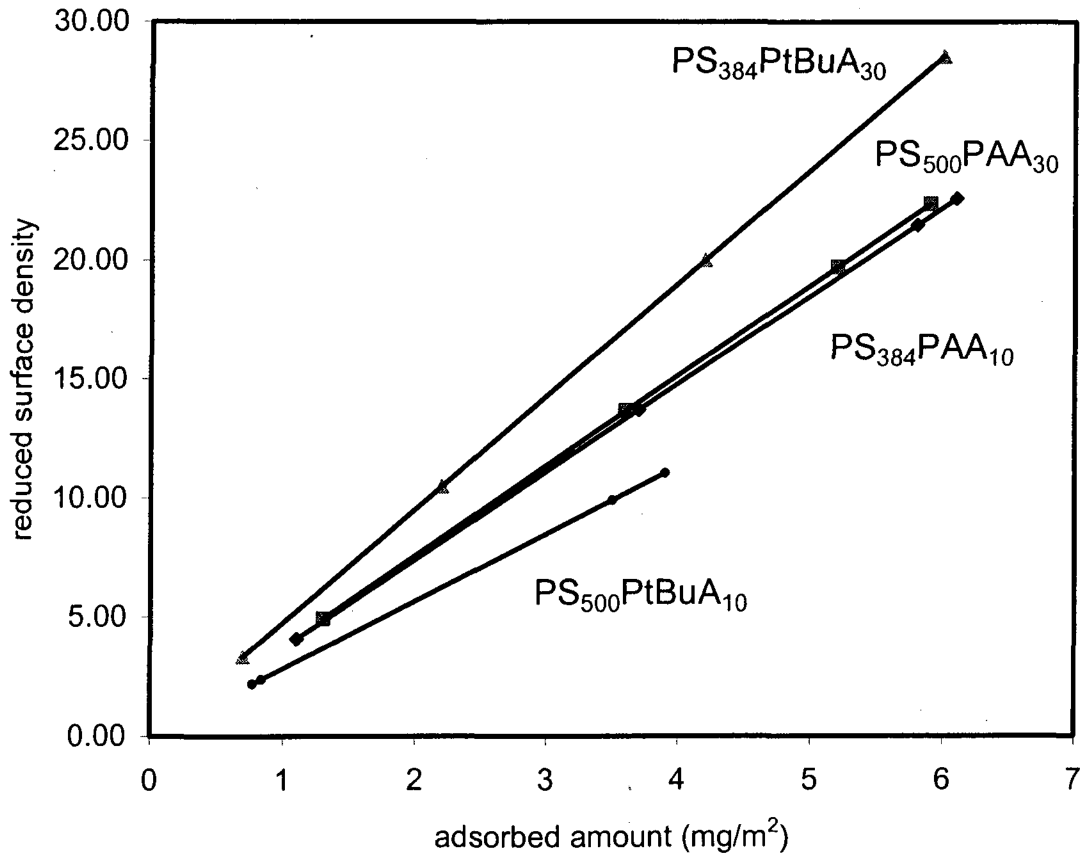

Figure 3.6: Reduced surface density from Table 3.6 plotted against the adsorbed amount (mg/m^2) for the asymmetric PSPAA and PSPtBuA block copolymers.

In Figure 3.6 reduced surface density is plotted against the adsorbed amount with the result that the two PSPAA block copolymers show the same increase in surface density with an increase in adsorbed amount. This means that the surface density is independent of the nature of the polymer for these two block copolymers. Also, the two PSPtBuA block copolymers had different slopes when compared to the PSPAA copolymers. The steeper slope associated with $PS_{384}PtBuA_{30}$ means that the adsorbed polymer is denser at a lesser adsorbed amount, suggesting that $PS_{384}PtBuA_{30}$ packs better than any of the other block copolymers.

3.6 Conclusions

The chain dynamics of adsorbed diblock copolymers in the dry state are reported for the first time. A series of PS-PAA diblock copolymers were studied as a function of block size, surface binding strength, and surface coverage. In the case of the bulk copolymers and constituent homopolymers, the variations in the chain mobilities of the PAA and PS components with block size could be rationalized in terms of the degree of interchain hydrogen bonding among the carboxylic acid groups as well as the lowering of the glass transition with molecular weight for the short blocks. The bulk state chain dynamics were then compared to the same copolymers and homopolymers adsorbed on a metal oxide surface at coverages close to or within the plateau region of the adsorption isotherm.

For all adsorbed copolymers, the segmental mobility of the PAA is highly restricted relative to the bulk state, reflecting the immobilization of these anchor blocks through strong ionic surface linkages. In the case of asymmetric copolymers with short anchor and long buoy blocks the PS segmental mobility is moderately enhanced relative to the bulk state, despite the fact that they are expected to form extended brushes in solution. However, the collapsed PS brushes of the dry state can still be characterized as forming a glassy layer, in agreement with the interpretation of surface force studies of similar adsorbed PVP-PS diblocks in the dry state.[26] In contrast, the PS chain mobility of adsorbed diblocks with a large anchor block is unchanged relative to the bulk state despite the larger spacings between the buoy blocks that should produce a lower density PS layer. In the case of the highly asymmetric diblock with short PS buoys, expected to form mushrooms, the restricted mobility of the PS segments may be due to their proximity to the surface bound segments, in agreement with an argument advanced to explain the mobility trends observed by NMR for analogous PVP-PS adsorbed copolymers in contact with solvent. However, it was observed that the mobility of the longer PS buoys was retarded for the most symmetric diblock that should have produced an intermediate mushroom/brush structure.

The highly asymmetric diblocks with short anchor blocks were studied as a function of coverage and surface binding strength by adsorbing the ester form of the precursor copolymer, PS-PtBuA. Both types of copolymers display the same NMR relaxation trends, indicating that the surface binding strength is not a determining factor. At low coverages where calculations predict mushroom/brush structures, the chain mobility of the long PS buoys is highly enhanced, in contrast to the restricted mobility of the intermediate structures formed through the adsorption of the symmetric diblock. As expected, the PS chain mobility decreases with increasing surface density but remains enhanced relative to the bulk state even at the highest coverages where extended brush structures are predicted.

3.7 Acknowledgements

The Natural Sciences and Engineering Research Council (NSERC) and the Centre for Self-Assembled Chemical Structures (CSACS/CRMAA) provided support for this research. The authors thank Dr. Cedric Malveau of the Université de Montreal and Dr. Frederick Morin of McGill for assistance with the solid-state NMR measurements.

3.8 References

1. McAlduff, M. and Reven, L., *Chain Conformation of Adsorbed Ethylene Random Copolymers.* Macromolecules, 2005. **38**: p. 3745-3753.
2. Nasreddine, V., *Solid state nuclear magnetic resonance spectroscopy of polymer thin films: Chain conformation, dynamics, and morphology.*, in *Chemistry.* 2003, McGill: Montreal.
3. Blum, F.D., Sinhat, B.R., and Schwab, F.C., *Density Profile of Terminally Adsorbed Polymers.* Macromolecules, 1990. **23**: p. 3592-3598.
4. Sinhat, B.R., Blum, F.D., and Schwab, F.C., *Dynamics of Adsorbed, Swollen Block Copolymers.* Macromolecules, 1993. **26**: p. 7053-7057.
5. Xie, M. and Blum, F.D., *Adsorption and Dynamics of Low Molecular Weight Poly(styrene-b-2-vinylpyridine) on Silica and Alumina in Toluene.* Langmuir, 1996. **12**: p. 5669-5673.
6. Bendejacq, D., et al., *Well-Ordered Microdomain Structures in Polydisperse Poly(styrene)-Poly(acrylic acid) Diblock Copolymers from Controlled Radical Polymerization.* Macromolecules, 2002. **35**: p. 6645-6649.
7. Terreau, O., Bartels, C., and Eisenberg, A., *Effect of Poly(acrylic acid) Block Length Distribution on Polystyrene-b-poly(acrylic acid) Block Copolymer Aggregates in Solution. 2. A Partial Phase Diagram.* Langmuir, 2004. **20**: p. 637-645.
8. Kang, N., et al., *The correlation between crystalline behavior of polyethylene segments and hydrogen bonds among carboxyl groups in ethylene-acrylic acid copolymers.* . Physical Chemistry Chemical Physics, 2000. **2**: p. 3627-3630.
9. La, Y.-H., et al., *Directed Assembly of Cylinder-Forming Block Copolymer Films and Thermochemically Induced Cylinder to Sphere Transition: A Hierarchical Route to Linear Arrays of Nanodots.* Nano Letters, 2005. **5**: p. 1379-1384.
10. Miao, S., *Investigation on NIR, coating mechanism of PS-b-PAA coated calcium carbonate particulate.* Applied Surface Science, 2003. **220**: p. 298-303.
11. Perelstein, O.E., et al., Macromolecules Rapid Communication, 2007. **28**: p. 977.
12. Sohma, J., et al., *Solid-state high resolution ^{13}C-NMR study of crosslinks in heavily gamma-irradiated polyethylene.* Radiation Physical Chemistry, 1991. **37**: p. 47-51.
13. Dewalt, L.E., Ouyang, H.D., and Dimonie, V.L., *Competition Between Micellization and Adsorption of Diblock Copolymers in a Colloidal System.* Journal of Applied Polymer Science, 1995. **58**: p. 265-269.
14. Kurganov, A., et al., *Characterization of covalently bonded and adsorbed polymer coatings on silica, alumina, and zirconia by means of physico-chemical and chromatographic methods.* Journal of Chromatography A, 1994. **660**: p. 97-111.

15. Pokrovski, K., Jung, K.T., and Bell, A.T., *Investigation of CO and CO_2 Adsorption on Tetragonal and Monoclinic Zirconia.* Langmuir, 2001. **17**: p. 4297-4303.
16. Davis, K.A. and Matyjaszewski, K., *Atom Transfer Radical Polymerization of tert-Butyl Acrylate and Preparation of Block Copolymers.* Macromolecules, 2000. **33**: p. 4039-4047.
17. Zhang, L. and Eisenberg, A., *Morphogenic Effect of Added Ions on Crew-Cut Aggregates of Polystyrene-b-poly(acrylic acid) Block Copolymers in Solutions.* Macromolecules, 1996. **29**: p. 8805-8815.
18. Bhutto, A.A., Vesely, D., and Gabrys, B.J., *Miscibility and interactions in polystyrene and sodium sulfonated polystyrene with poly(vinyl methyl ether) PVME blends. Part II. FTIR.* Polymer, 2003. **44**: p. 6627-6631.
19. Khougaz, K., Zhong, X.F., and Eisenberg, A., *Aggregation and Critical Micelle Concentrations of Polystyrene-b-poly(sodium acrylate) and Polystyrene-b-poly(acrylic acid) Micelles in Organic Media.* Macromolecules, 1996. **29**: p. 3937-3949.
20. Johner, A. and Joanny, J.F., *Block Copolymer Adsorption in a Selective Solvent: A Kinetic Study.* Macromolecules, 1990. **23**: p. 5299-5311.
21. Tao, Y.-T., *Structural Comparison of Self-Assembled Monolayers of n-Alkanoic Acids on the Surfaces of Silver, Copper, and Aluminum.* Journal of the American Chemical Society, 1993. **115**: p. 4350-4358.
22. Yan, L., et al., *Emulsifier-Free Synthesis and Self-Assembly of an Amphiphilic Poly(styrene-co-acrylic acid) Copolymer.* Journal of Applied Polymer Science, 2006. **100**: p. 3718-3726.
23. Cowie, J.M.G., McEwen, I.J., and Garay, M.T., *Molecular Weight and Tacticity Effects on the Glass Transition of Poly(acrylic acid)* European Polymer Journal, 1987. **23**: p. 917-920.
24. Schantz, S. and Ljungqvist, N., *Structure and Dynamics in Polymer Blends: A ^{13}C CPMAS NMR Study of Poly(3-octylthiophene)/Poly(phenylene oxide).* Macromolecules, 1993. **26**: p. 6517-6524.
25. Garces, F.O., et al., *Interpolymer Complexation of Poly(acrylic acid) and Poly(acrylamide): Structural and Dynamic Studies by Solution- and Solid-State NMR.* Macromolecules, 1994. **27**: p. 272-278.
26. Parsonage, E., et al., *Adsorption of Poly(2-vinylpyridine)-Poly(styrene) Block Copolymers from Toluene Solutions.* Macromolecules, 1991. **24**: p. 1987-1995.
27. Field, J.B., et al., *Neutron reflectivity study of end-adsorbed diblock copolymers: cross-over from mushrooms to brushes.* Journal de Physique II France, 1992: p. 2221-2235.
28. Zhan, Y. and Mattice, W.L., *Self-Assembly and Adsorption of Diblock Copolymers from Selective Solvents. 2. Surface Adsorption.* Macromolecules, 1994. **27**: p. 683-688.
29. Costa, A.C., et al., *Block Copolymer Adsorption from a Homopolymer Melt to Silicon Oxide: Effects of Nonadsorbing Block Length and Anchoring Block-Substrate Interaction.* Macromolecules, 2003. **36**: p. 9897-9904.

30. Belder, G.F., ten Brinke, G., and Hadziioannou, G., *Influence of Anchor Block Size on the Thickness of Adsorbed Block Copolymer Layers.* Langmuir, 1997. **13**: p. 4102-4105.
31. Kent, M., et al., *Characterization of Diblock Copolymer Monolayers at the Liquid-Air Interface by Neutron Reflectivity and Surface Tension Measurements.* Macromolecules, 1992. **25**: p. 6240-6247.

Chapter 4: A solid-state NMR study of poly (isoprene)-*b*-poly (vinylpyridine) copolymer adsorption on a metal oxide surface

4.1 Preface

Chapter 4 reports on the structures formed by the adsorption of commercially available polyisoprene (PI) and poly (vinylpyridine) (PVP) block copolymers on zirconia powder. In contrast to the PS-PAA block copolymers studied in the preceding chapter, the parent homopolymers have widely different glass transition temperatures, providing a large contrast in the chain dynamics of the separate blocks. As in the previous chapter, the effect of the block size, the polar group of the anchor block and surface coverage on the chain dynamics of the adsorbed PI-PVP block copolymers in the dry state was probed through spin lattice relaxation measurements and related to the predicted surface structures.

4.2 Abstract

The effect of the block length and binding strengths of adsorbed diblock copolymers on the chain dynamics was examined. Initially, the homopolymer poly (2-vinylpyridine), P2VP, was studied. This was followed by a series of poly (isoprene)-*b*-poly (2-vinylpyridine), PI-P2VP, diblock copolymers, and poly (isoprene)-*b*-poly (4-vinylpyridine) diblock copolymers, PI-P4VP. PI-P2VP was used to study the effect of block length, while PI-P4VP, was used to vary the surface binding strength. The segmental mobility of the anchor block, PVP, is moderately enhanced relative to the bulk or adsorbed homopolymer of comparable molecular weight, indicating a population of loops and tails rather than only flat trains. The PI buoys display higher mobilities than the bulk copolymers, even at the highest coverages, confirming the rubbery nature of the adsorbed copolymers in the dry state.

4.3 Introduction

The surface modifying ability of copolymers is potentially more versatile than that of homopolymers as distinct interactions can be incorporated into different parts of a single polymer chain. The structure of the adsorbed copolymer will depend on the particular chain architecture along with the surface and solvent interactions. In the case of block copolymers, the interfacial activity can be controlled by using blocks tailored to interact in specific ways with the surface and by the use of selective solvents.[1] The amphiphilic character of block copolymers can be exploited such that one block adsorbs strongly on a solid surface and avoids the solvent, while the other block, nonadsorptive on its own, swells into the good solvent surrounding medium, but remains tethered to the surface via the anchor block.

Whereas adsorbed diblock copolymer structures in the presence of good and bad solvents have been extensively studied both theoretically and experimentally and are relatively well understood, much less work has been reported for these same systems in the dry state. The conformation and chain dynamics of collapsed brushes and mushroom structures of adsorbed diblock copolymers in the dry state has been indirectly examined through AFM, ellipsometry and surface force measurements.[1-3] The previous chapter was a study of block copolymer adsorption where poly (styrene)-*b*-poly (acrylic acid), PS-PAA, and poly (styrene)-*b*-poly (*t*-butyl acrylate), PS-PtBuA, were characterized by solid-state NMR. It was shown that PS brushes collapsed displaying mobilities moderately enhanced over bulk state chain dynamics. The chain mobilities of mushrooms or intermediate brush/mushroom structures formed by highly asymmetric diblocks with long PS buoys at low coverages were also greatly enhanced, but the same structures formed at high coverages by increasing the PAA anchor block length show PS chain dynamics are restricted as in the glassy state bulk PS homopolymer.

Poly (isoprene)-*b*-poly (vinylpyridine), PI-PVP, another block copolymer that is a combination of hydrophilic/hydrophobic blocks is commercially available in a wide range of block lengths, and it was selected as an interesting contrast to the previously studied PS-PAA copolymers. The PVP acts as the anchor block, binding strongly to both metallic and polar surfaces. The pyridyl group has a strong affinity for metals and will undergo hydrogen bonding and/or electrostatic interactions whose strengths depend on the nitrogen position. As such, PVP has been demonstrated to be an effective universal surface modifier for immobilizing metal and semiconductor nanoparticles,[4] and it has demonstrated usefulness in many other applications.[3-6] PI-PVP copolymers are an attractive combination for dynamic ^{1}H and ^{13}C NMR studies due to the sufficient chemical shift separation of the two blocks as well as a large difference in the glass transition temperatures of the homopolymers (T_g(PI) ~-70 °C and T_g(PVP) ~100 °C) [5] which provides a contrast in the segmental mobilities of the blocks.

Initial work concerning the surface adsorption of PI-P2VP, carried out by Tirrell [3], showed that polymer brushes were formed by using a solvent selective for PI. The effect of anchor block size on chain packing for the adsorption of PS-P2VP on mica was examined by Hadziioannou.[7] The adhesive interactions of adsorbed block copolymers of PVP-PS and PVP-PI in the dry state have also been compared.[3] In contrast to the stretched brush conformation in toluene, the PS and PI blocks take on entropically unfavorable, flattened conformations in the dry layers. Whereas the adhesion of the thin glassy PS block layers is dominated by van der Waals interactions, similar to homopolymer PS surfaces, the adhesion energy of a PVP-PI sample is considerably larger than the surface energy of the bulk homopolymer PI films. The enhancement of adhesion for the PI blocks is attributed to the flattened conformation and rubbery state. When two PI surfaces are brought into contact, the PI blocks belonging to each layer can interpenetrate and gain a space twice as large, which results in a larger conformational freedom. This type of enhancement cannot occur for the adsorbed PVP-PS diblocks where the chain motion is frozen and no interpenetration takes place.[3]

Initially, our solid-state NMR study examines the anchor block homopolymer poly (2-vinylpyridine), P2VP, in the bulk and adsorbed state, followed by a series of adsorbed poly (isoprene)-*b*-poly (2-vinylpyridine) block copolymers, PI-P2VP, to study the effect of block length, and poly (isoprene)-*b*-poly (4-vinylpyridine), PI-P4VP, to vary the binding strength. ^{13}C and ^{1}H spin lattice relaxation measurements were carried out on adsorbed PI-P2VP and PI-P4VP in the plateau region and ^{1}H NMR alone was used to study the adsorbed copolymers at low coverages for sensitivity reasons. Due to the large differences in chain mobilities, the ^{13}C cross relaxation parameters could be adjusted to selectively observe the PI versus the PVP blocks.

4.4 Experimental Section

4.4.1 Materials

Block copolymers of poly (isoprene)-*b*-poly (2-vinylpyridine) (PIP2VP) and poly (isoprene)-*b*-poly (4-vinylpyridine) (PIP4VP) as well as the homopolymer poly (2-vinylpyridine) were obtained from Polymer Source, Inc. (Dorval, Canada) and were used as received. M_n, polydispersity and approximate block lengths for the copolymers are listed in Table 4.1. The metal oxide surface, zirconia (ZrO_2), was supplied by Degussa.

Zirconia had a reported average particle size of 30 nm and a BET surface area of 40 ± 10 m^2/g. Before sample preparation, the zirconia was heated at 400 °C for 5 h. The DSC of the block copolymers show two Tg's, one sharp transition at -62 °C due to the polyisoprene block, and one very broad transition at ~85 °C due to the poly(vinylpyridine) block. These two transitions are similar to those previously reported by Kosonen et al.[8] Unlike the previous study where samples were prepared below the Tg of the block copolymer, all samples in this study were prepared at a temperature between that of the two Tg's.

Table 4.1: M_n, polydispersity, asymmetry parameter (β), radius of gyration of polyisoprene block (R_g), and block length of copolymers used.

Block Copolymer	M_n	polydispersity	Asymmetry parameter (β)	R_g of PI blocks (nm)	Block lengths
$PI_{440}P2VP_{25}$	I=30000 2VP=2800	1.06	174	9.6	(I)≈440, (2VP)≈25
$PI_{300}P2VP_{200}$	I=20200 2VP=20500	1.03	27	7.7	(I)≈300, (2VP)≈200
$PI_{440}P4VP_{90}$	I=30000 4VP=9200	1.06	74	9.6	(I)≈440, (4VP)≈90
$P2VP_{30}$	2VP=3500	1.08			(2VP)≈30
$PI_{440}P4VP_{100}$	I=30000 4VP=10220	1.05	69	9.6	(I)≈440, (4VP)≈100
$PI_{280}P2VP_{115}$	I=19200 2VP=12200	1.03	37	7.4	(I)≈280, (2VP)≈115

The PIPVP block copolymers were all rather sticky and viscous, which made them difficult to handle. Therefore, MAS NMR experiments could not be carried out because the bulk copolymers did not pack well enough in the rotor to allow stable magic angle spinning. As can be seen in Table 4.1, the block copolymers were chosen to have comparatively large hydrophobic blocks and short hydrophilic blocks. The dimensionless asymmetry parameter, β, is calculated using equation 4.1 [7]

$$\beta = \frac{R_{G,PI}^2}{R_{G,P2VP}^2} = \frac{N_{PI}^{6/5}}{N_{P2VP}^{2/3}}. \qquad (4.1)$$

The radius of gyration is calculated in a manner similar to that found in Zhang and Eisenberg [9]. The radius of gyration, R_g, is calculated for the PI buoy block only. In a good solvent the radius of gyration is given by $R_g \approx aN_{PI}^{3/5}$, where "a" is the length of the repeat unit.

4.4.2 Sample Preparation

For each block copolymer, 5 ml solutions were prepared by dissolving the block copolymer in THF at initial concentrations of 1, 3, 5, 10, 20, and 40 mg/ml. A second solution was prepared by dispersing 150 mg of zirconia in 5 ml of THF with 15 min of sonication. The zirconia and copolymer solutions were added and allowed to stir at room temperature for 24 h. The resultant solution was centrifuged at 4000 rpm for one hour, the supernatant was discarded, and the adsorbed block copolymer was dried under vacuum at 70°C overnight. Thermal gravimetric analysis (TGA) was used to determine the weight percent of copolymer adsorbed on zirconia.

4.4.3 Solid-State ^{13}C CP-MAS NMR and ^{1}H fast MAS NMR

All solid-state ^{13}C NMR spectra (67.03 MHz) were recorded on a Chemagnetics CMX-270 NMR spectrometer with a 9.5 mm HX MAS solids probe with low ^{13}C background. Samples were spun at a rate of 4 kHz. The NMR parameters used in the collection of ^{13}C CP-MAS spectra are listed in the appropriate figure captions. The inversion recovery pulse sequence was used to determine the various T_1 values, with spectra obtained under the following conditions: a pulse delay of 3 s, 2000 scans, and a pulse width of 7.25 μs.

All solid-state ^{1}H NMR spectra were recorded on a Bruker Avance 600MHz wide bore NMR spectrometer with a Bruker bl2.5 probe. The NMR parameters used in the collection of ^{1}H spectra are listed in the appropriate figure captions. The inversion recovery pulse sequence was used to determine the various T_1 values.

4.4.4. FTIR-PAS

A Fourier Transform IR spectrometer (Mattson Research Series 1 spectrometer) equipped with a photoacoustic cell (MTEC model 300) was used to collect all IR spectra. The spectra were collected with a 4.0 cm^{-1} nominal resolution.

4.4.5. Thermal Gravimetric Analysis (TGA)

All samples were heated to 600 °C in a nitrogen environment at a rate of 10 °C/min, and then they were held at 600 °C in an oxygen environment for 10 min. This process allowed the amount of organic material attached to the metal oxide surface to be determined. All samples were run on the TGA Q500 from TA Instruments.

4.4.7 Differential Scanning Calorimetry (DSC)

DSC experiments were performed on a TA instruments Q1000 differential scanning calorimeter in dry nitrogen atmosphere. Samples of ~8 mg were placed in an aluminum pan. All samples were first heated from -80 to 100 °C at a rate of 10 °C/min (first heating scan) and kept at that temperature for 5 min; subsequently, they were cooled to -80 °C at a rate of -10 °C/min and kept at that temperature for 5 min. Following the cooling scan, a second heating scan was conducted with the same heating rate as the first one. The midpoint of the slope change of the heat capacity plot was taken as the glass transition temperature (*T*g).

4.5 Results and Discussion

4.5.1 Adsorption isotherms

The adsorption properties of the PVP homopolymer and PI-PVP copolymers on zirconium oxide powder were first investigated. Adsorption isotherms are prepared for some of the polymer systems so that samples could be prepared in a specific region of the isotherm. Figure 4.1 shows the adsorption isotherm for the homopolymer P2VP and PI-PVP copolymers where the adsorbed amounts ranged from 0.5 to 6.0 mg/m^2. The adsorption isotherm was fitted to a Langmuir type isotherm [10],

$$\theta = \frac{ac}{(1+bc)} \tag{4.2}$$

where θ is the amount adsorbed (mg of polymer/m^2), a and b are constants, and c is the equilibrium polymer concentration (mg/ml). The equilibrium concentration was obtained by subtracting the concentration of adsorbed polymer from the initial concentration. The ratios *a/b* represent the limiting monolayer coverage. The monolayer quantity of material for $PI_{440}P4VP_{90}$ was 5.5 mg of polymer/m^2, $PI_{440}P2VP_{25}$ was similar at approximately 5.1 mg of polymer/m^2, $PI_{300}P2VP_{200}$ was 3.0 mg of polymer/m^2, and $P2VP_{30}$ was approximately 2.2 mg of polymer/m^2. The adsorption isotherms for the polymers, $PI_{440}P4VP_{90}$ and $PI_{440}P2VP_{25}$, were of higher affinity than $PI_{300}P2VP_{200}$ and $P2VP_{30}$ where a more rounded isotherm was found. This could be due to a stronger interaction between the 4-vinylpyridine and the zirconia, as well as a better packing of the $PI_{440}P2VP_{25}$ compared to the two other polymers. As expected, a Langmuir isotherm is observed with an initial sharp increase in adsorption followed by a plateau region. The isotherms fits are relatively good, but as can be seen in the inset of Figure 4.1, there is quite a bit of scatter at low concentration. The adsorption isotherms could be improved if after the determination of the general shape more samples were prepared in the intermediate region between the initial sharp rise and the plateau region. As well a few more points in the plateau region would help smooth out the isotherms.

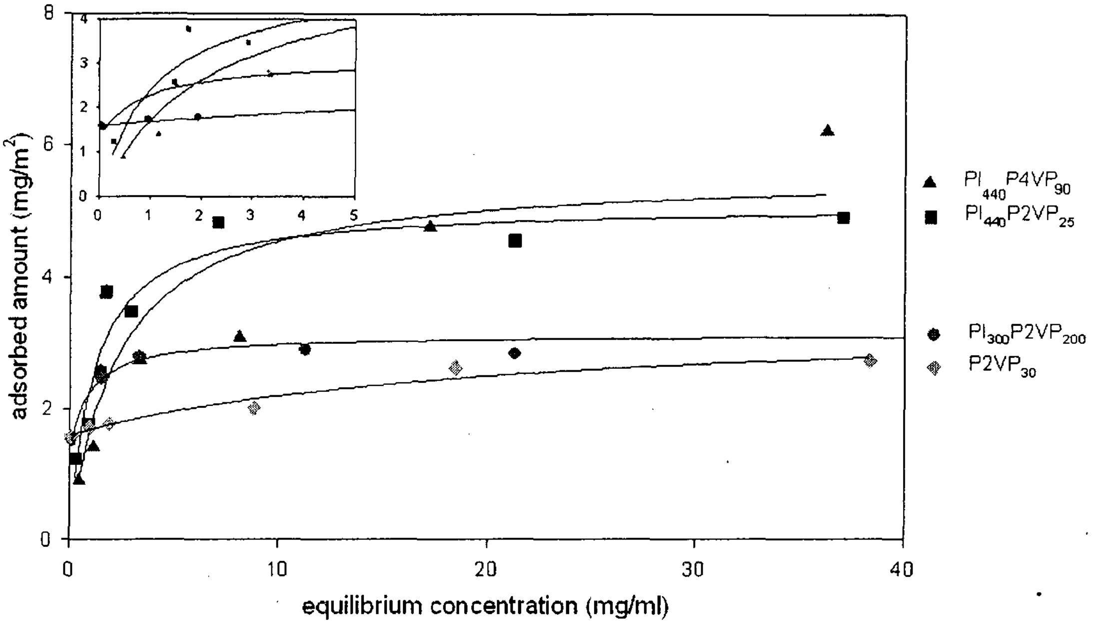

Figure 4.2: Adsorption isotherms for various block copolymers adsorbed on zirconia. The inset shows the adsorbed amounts at low concentrations. Lines are least squares fit to equation 4.2. The error on each adsorbed amount is ±0.2 mg/m^2.

The general trend in maximum adsorbed amount for the four polymers chosen is $PI_{440}P4VP_{90} > PI_{440}P2VP_{25} > PI_{300}PI2VP_{200} > P2VP_{30}$. The observed trend is what would be expected since the nitrogen in the 4 position is more easily accessible to the surface, making binding easier. In addition, as the size of the anchor block is increased, the adsorbed amount decreases. For comparison purposes, adsorbed samples equivalent to the plateau quantity were prepared since the surface structure might vary during the initial sharp increase. For the most part, the same initial concentration of 40 mg/ml was used in sample preparations because according to Figure 4.1 this concentration would be well within the plateau region for all samples.

4.5.2 Homopolymer adsorption: P2VP

The NMR and vibrational spectra of the P2VP homopolymer were examined first. Figure 4.2a shows the FTIR-PAS spectra for P2VP adsorbed on zirconia. The FTIR ethylene crystalline bands (i.e., CH_2 rocking modes) at 710-730 cm^{-1}, which are sensitive to chain conformation, were not detected because the metal oxide fingerprint region below 1100 cm^{-1} masks any polymer signal in this region. Likewise, the very broad OH stretching modes of zirconia at ~3500 cm^{-1}, did not show any significant changes in the presence of adsorbed polymer. However, the band at 3100 cm^{-1}, assigned to hydrogen bonding of the nitrogen with the backbone CH_2 protons in the bulk homopolymer [11], does not appear in the spectrum of adsorbed P2VP. The bands at 1589 and 1471 cm^{-1} arise from dipole transition moments along the para-direction of the pyridine ring [12] whereas those at 1568 and 1433 cm^{-1} are due to dipole transition moments that lie in the phenyl ring plane, perpendicular to the vibrations at 1589 and 1471 cm^{-1}.[13] Other than the disappearance of the 3100 cm^{-1} band, no significant changes in the peak positions or relative intensities of the IR bands of the adsorbed P2VP relative to the bulk state are observed. The FTIR-PAS spectra for the block copolymers adsorbed on zirconia are not shown here because there is no significant change in the peak position of the IR bands, and the relative intensities of the IR bands stay constant when comparing bulk to adsorbed.

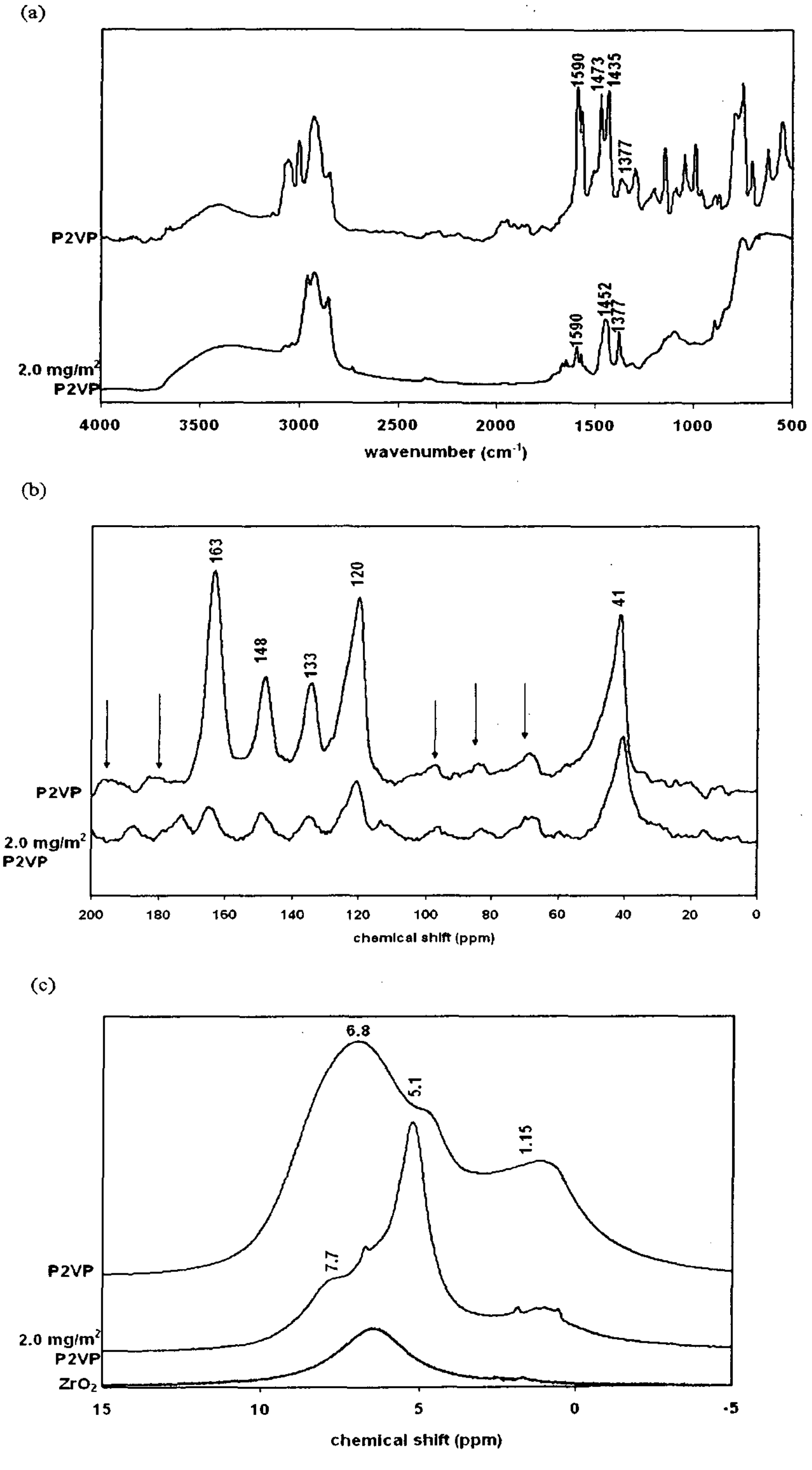

Figure 4.3: Spectra for bulk and adsorbed P2VP, (a) FTIR-PAS (number of scans = 32 for bulk, and 64 for adsorbed, resolution = 4 cm^{-1}), (b) ^{13}C CP-MAS NMR (spinning frequency = 3500 Hz, contact time = 1 ms, number of acquisitions = 2000, pulse delay = 3 s). The arrows indicate the position of spinning sidebands. (c) ^{1}H NMR (spinning frequency = 25 kHz, number of acquisitions = 16 for bulk and 32 for adsorbed, pulse delay = 10 sec for bulk, and 5 sec for adsorbed, pulse width = 1.7 μsec).

The ^{13}C CP-MAS NMR spectra for bulk P2VP, shown in Figure 4.2b, has five peaks: the peak at 41 ppm is due to the backbone carbon attached to the vinyl pyridine, the peak at 120 ppm is due to the protonated vinyl pyridine carbons in the 4 and 6 positions, the peak at 133 ppm is due to the protonated vinyl pyridine carbon in the 5 position, the peak at 148 ppm is due to the protonated vinyl pyridine carbon in the 3 position, and the peak at 163 ppm is due to the non-protonated vinyl pyridine carbon.[11] The ring carbons give rise to arrays of spinning sidebands, as indicated in the figure, due to the chemical shift anisotropy which is large relative to the spinning frequency. The small amount of polymer present in the adsorbed polymer samples requires the use of large volume 9.5 mm diameter rotors that have low spinning frequencies. The adsorbed P2VP shown in Figure 4.2b is similar to that of the bulk with regards to peak position, and number of peaks. The relative intensities of the peaks have changed, due to the changes in motion associated with adsorption that influence the degree of cross polarization enhancement.

As typical for a glassy polymer, the ^{13}C resonances of the bulk P2VP are all quite broad with long T_1 values, ranging from 25 s to 55 s (Table 4.2). Upon heating the bulk homopolymer to 60°C, the T_1 values for all of the peaks decreased, as characteristic for the slow limit side of the correlation time curve. Variations in the ^{13}C T_1 values arise from the number of attached protons and the degree of mobility of the polymer backbone versus the side groups. The backbone of the homopolymer is more rigid than the ring group, and the non-protonated carbon at 165 ppm has the largest T_1 value.

Table 4.2: ^{13}C and ^{1}H T_1 (s) for bulk and adsorbed P2VP

Peak (ppm)	P2VP 25 °C ± 0.1°C	P2VP 60 °C	2.0 mg/m^2 P2VP 25 °C
165	52.6	31.4	33
149	30.3	15.7	21.5
135	28.5	14.7	21.9
121	26.5	16.8	26.0
42	37.6	22.5	28.1
^{1}H T_1 (s)	2.23		0.22

The ^{1}H NMR spectra for bulk and adsorbed P2VP, shown in Figure 4.2c, have two distinct regions: aromatic protons appear at approximately 7.0 ppm, and aliphatic protons appear between 1.0 and 2.0 ppm.[13] Bulk P2VP has a broad peak with a peak maximum at 7 ppm, and a broad aliphatic peak at 1.25 ppm attributed to the backbone protons. Bare zirconia also gives a proton signal at 6.0 ppm, but this peak is almost always enveloped by the P2VP aromatic signal. There is a very strong signal at approximately 5.0 ppm due to associated water. For the adsorbed homopolymer, there is still a broad peak in the region of 1.5 ppm due to backbone CH_2 protons, but there is also the appearance of a sharp peak at 2.1 ppm due to backbone CH protons. Peaks in the region from 6-8 ppm are due to the protons on the pyridine molecule, but unlike the bulk homopolymer, there is a shift in peak maxima to between 6 and 5.25 ppm depending on the adsorbed amount. There is also a sharp peak at 6.7 ppm, which could suggest an increase in motion of the pyridine group upon adsorption. At very low loadings, there is a small, highly mobile component, as indicated by higher resolution of the peaks in the aliphatic region, which is not necessarily anticipated for a strongly adsorbing polymer.

Whether the mobility of the adsorbed homopolymer increases or decreases relative to the bulk state depends on the surface binding strength as compared to the intra and inter chain interactions as well as the surface conformation, i.e., loops and tails versus flat trains. The ^{1}H T_1 values in Table 4.2, show the same trend as the ^{13}C values, decreasing after adsorption. The proton spin lattice relaxation is in the slow limit as indicated by the field dependence. Thus, the P2VP polymer has increased mobility upon adsorption. Whereas the polymer signals all have a common proton T_1 as expected, the water signal has a distinct value indicating that its association with the polymer is not strong enough to effect the relaxation times through spin diffusion. Most studies of the adsorption of PVP homopolymers concern aqueous solutions at low pH where it behaves as a weak polyelectrolyte and assumes a flat surface conformation.[14] In the case of neutral PVP adsorption from THF, the moderate increase in mobility that is seen in the relaxation measurements suggests that the surface conformation contains a population of loops and tails. In contrast, the previously studied anchor homopolymer, PAA, also adsorbed from THF, displayed a large increase in the relaxation times relative to its bulk state and presumably assumes a flat, rigid surface conformation due to the stronger zirconium carboxylate linkages.

4.5.3. Block Copolymer Adsorption

The chemical shift assignments of the ^{13}C CP-MAS NMR spectra for the bulk copolymers are made in reference to $PI_{300}P2VP_{200}$, since it is the only block copolymer that shows peaks for both blocks. As discussed later, the PI and P2VP blocks of the other block copolymers have sufficiently different cross polarization time constants such that the PI signals are greatly attenuated at the CP parameters where the P2VP signals are enhanced and vice versa.

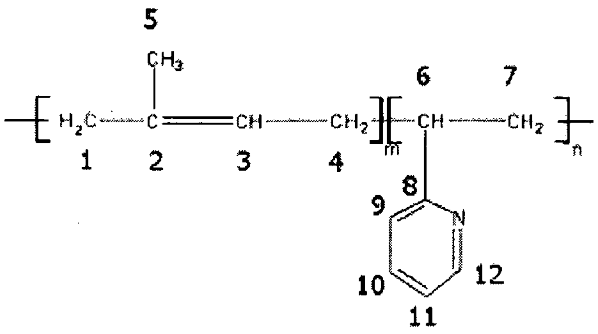

Figure 4.3: structure and carbon assignments for PI_mP2VP_n

The peaks corresponding to single carbons are C5 (16 ppm, terminal CH_3), C7 (23 ppm, CH_2), C4 (27 ppm, CH_2), C1 (32 ppm, CH_2), C6 (41 ppm, CH), C12 (148 ppm, CH) and C8 (165 ppm, C_q) and the peaks corresponding to overlapping carbons C9, C11 (125 ppm, CH) which overlap with C2 of the isoprene molecule, and C10, C3 (135 ppm, CH).[11, 15]

Figure 4.4 shows the bulk and adsorbed ^{13}C CP-MAS NMR spectra for all of the PI-PVP block copolymers. As discussed below, the cross polarization intensity depends on molecular mobility and the particular contact time of 1 ms for the spectra of the adsorbed copolymer shown in Figure 4.4 favors the detection of the less mobile P2VP blocks.

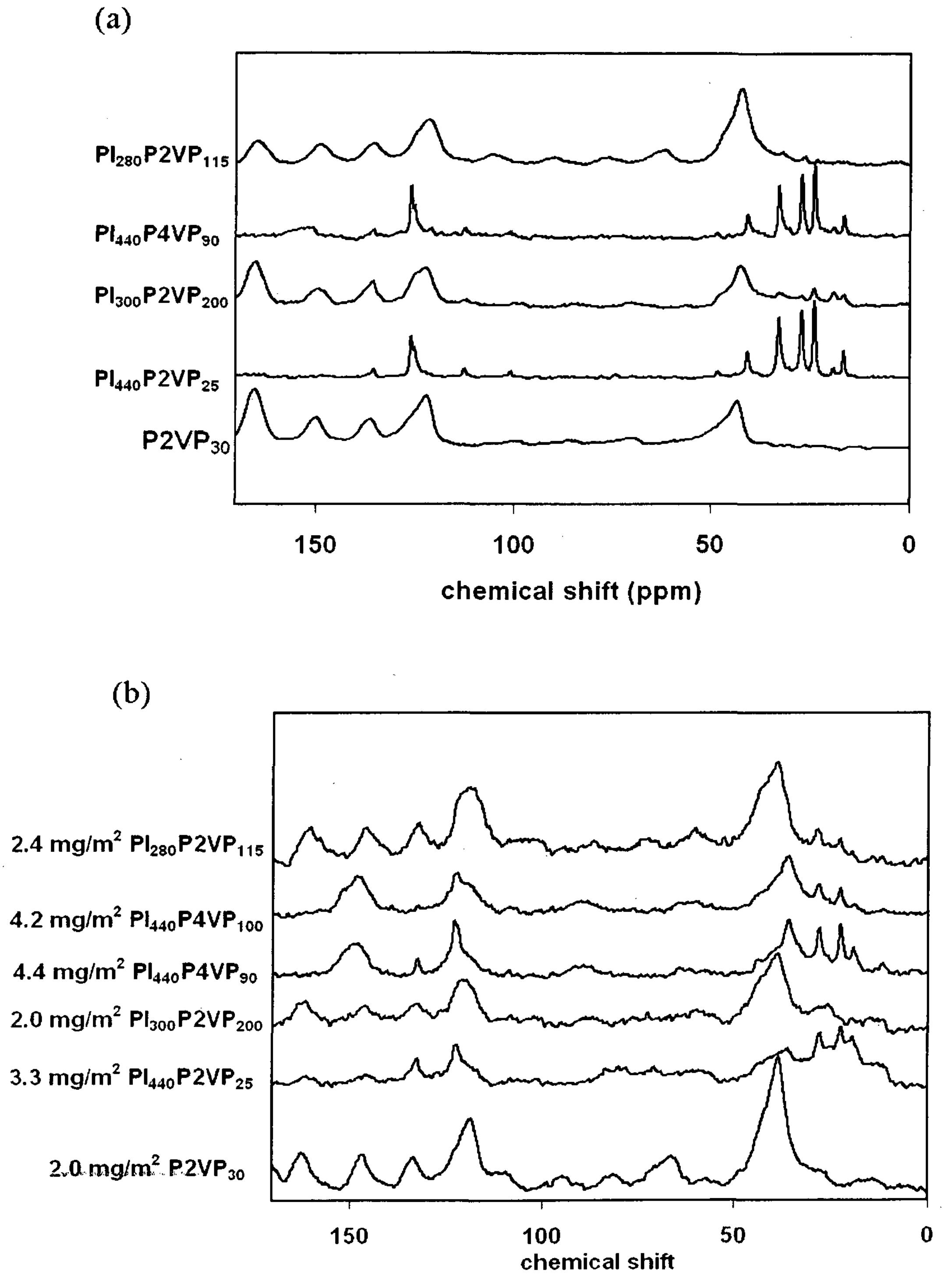

Figure 4.4: ^{13}C CP-MAS NMR spectra for (a) bulk copolymers, and (b) adsorbed block copolymers at an initial concentration of 40 mg/ml. (spinning frequency = 3500 Hz, contact time = 1 ms, number of acquisitions is between 2000 and 6000 depending on signal strength, pulse delay = 3 s)

4.5.3.1 Variable Contact Time Measurements

Although there is overlap of the isoprene and vinylpyridine signals for the peaks at 125 and 135 ppm, these ^{13}C signals obtained by ^{1}H-^{13}C cross polarization could be separated by variable contact time measurements. A plot of the ^{13}C signal intensity as a function of the contact time displays a maximum value that depends on the strength of the heteronuclear dipolar coupling. The ^{13}C signal intensity builds up with increasing contact time, CT, depending on the efficiency of the polarization transfer, characterized by the time constant T_{CH}. This build up in ^{1}H-^{13}C cross polarization signal intensity is followed by a decrease due to the decay of the proton spin locked magnetization, characterized by the time constant $T_{1\rho}$. More mobile carbons with weakened heteronuclear dipolar couplings require longer contact times for magnetization transfer whereas the signals of more motionally restricted carbons will be attenuated due to rapid decay of the spin locked magnetization (short proton $T_{1\rho}$ values). Whereas the signal intensities of the adsorbed P2VP homopolymer and P2VP block of the copolymer are mostly decayed at CT = 5 ms, the PI signals are still on the increasing side of the cross polarization intensity curve (Figure 4.5). As is typical for a glassy polymer, the P2VP ^{1}H $T_{1\rho}$ values are relatively small, < 1 ms, whereas the ^{1}H $T_{1\rho}$ value for the rubbery polyisoprene block (Figure 4.5b) is much longer, > 5 ms. These differences in the optimal cross polarization contact times can be used for spectral editing to select the P2VP versus the PI blocks by using short versus long contact times respectively.

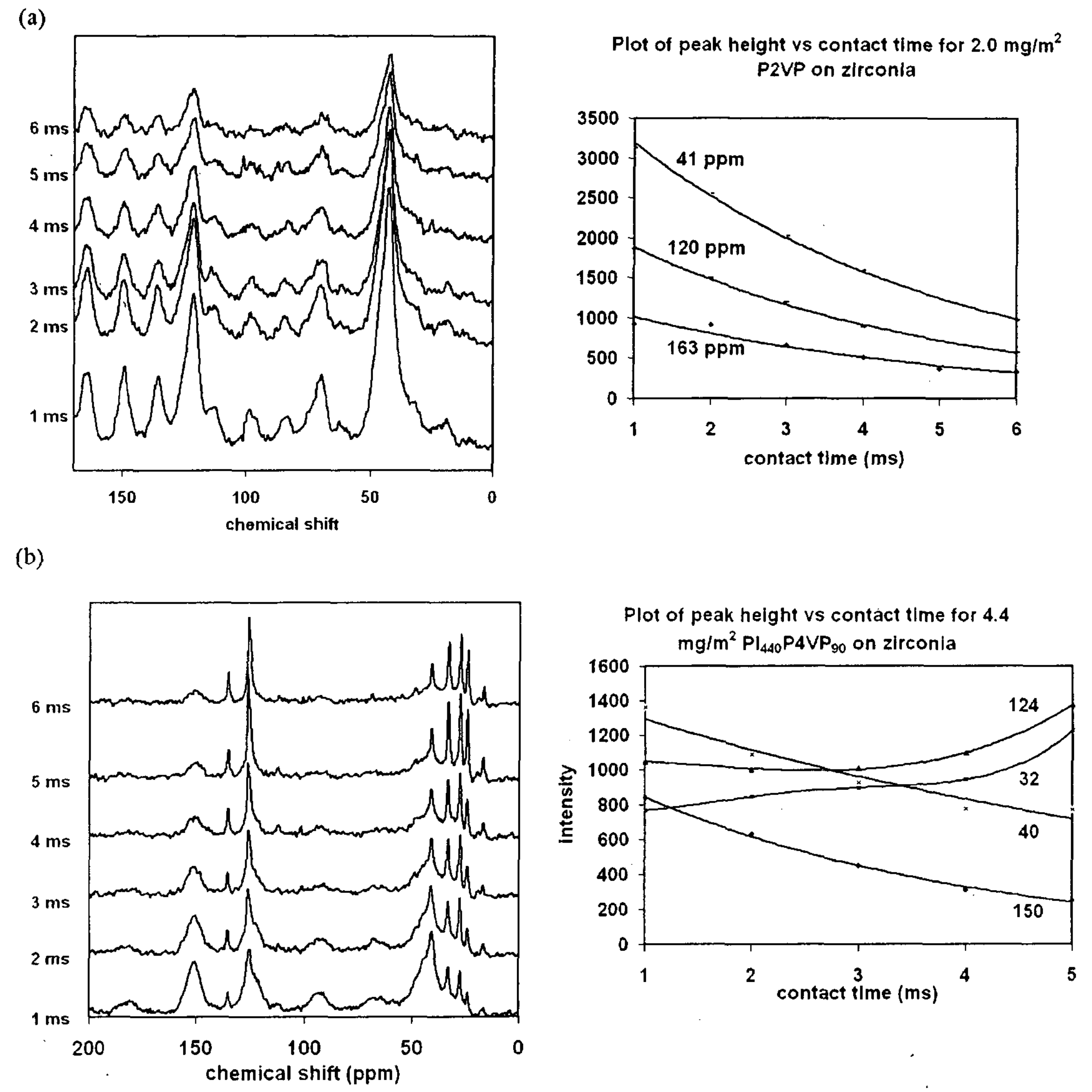

Figure 4.5: Variable contact time study of polymers adsorbed on zirconia at an initial concentration of 40 mg/ml. (a) P2VP, and (b) PI$_{440}$P4VP$_{90}$. (spinning frequency = 3500 Hz, contact time = variable, number of acquisitions = 2400, pulse delay = 3 s)

4.5.3.2 Effect of block size: ^{13}C Relaxation data

^{13}C T$_1$ measurements of the bulk PI-PVP block copolymers, which require long acquisition periods with stable sample spinning, were not feasible because the bulk copolymers did not pack well in the rotor due to their viscous, sticky state. Table 4.3 compares the carbon T$_1$ relaxation values for all the adsorbed copolymers along with the adsorbed and bulk state P2VP homopolymer. The ^{13}C spin lattice relaxation times were measured selectively for the P2VP and PI blocks by using contact times of 1 and 5 ms respectively in the inversion-recovery pulse sequence.

Table 4.3: ^{13}C T_1 (s) for adsorbed copolymer samples at two different contact times

CT = 1 ms					
PVP carbons	adsorbed amount (mg/m^2)	C12, P2VP 148 ppm	C9, C11, P2VP ~ 120 ppm	C6, P2VP 41 ppm	
$PI_{440}P4VP_{90}$	4.4		14.3	15.2	
$PI_{300}P2VP_{200}$	2.0	36.2	15.1	21.1	
$PI_{280}P2VP_{115}$	2.4	12.2	17.8	17.1	
$PI_{440}P2VP_{25}$	3.3		10.5	7.9	
$P2VP_{30}$	2.0	21.5	26.0	28.1	
Bulk $P2VP_{30}$		30.3	26.5	37.6	
CT = 5 ms					
PI carbons			C2, PI ~ 120 ppm		C1, PI 31 ppm
$PI_{280}P2VP_{115}$	2.4		0.5		0.2
$PI_{440}P2VP_{25}$	3.3		0.4		0.6
$PI_{440}P4VP_{90}$	4.4		0.3		0.1

*The error on the ^{13}C T_1 values is ± 0.1 s

First focusing on the trends for the P2VP block (C6, C9, C11, C12), it is seen that with the possible exception of the most symmetric diblock, $PI_{300}P2VP_{200}$, the shorter T_1 values indicate that anchor block chain mobility is enhanced relative to the adsorbed or bulk P2VP homopolymer. The P2VP anchor blocks strongly associate with the surface but their density is influenced by the packing of the PI buoys. For adsorption from non-selective solvents two regimes are differentiated, the buoy regime occurs when $\beta > N_{anchor}$, and the anchor regime when $1 < \beta < N_{anchor}$.[3] From Table 4.1, all of the copolymers except $PI_{440}P2VP_{25}$, which has the shortest P2VP T_1 values, are estimated to be in the anchor regime. The P2VP anchors are swollen by the nonselective solvent, THF, and thus may form a looser network of loops and trains than in the case of a selective solvent.

The short T_1 values of < 1 s for the PI blocks (C1, C2) reflect their rubbery state. In the case of the most symmetric diblock $PI_{300}P2VP_{200}$, the ^{13}C T_1 values for the PI block are not reported since the signal-to-noise ratio was insufficient for the 5 ms contact time, indicating a higher mobility which may be expected due to the larger anchor block size and wider spacing of the PI buoys. Although the position of the nitrogen group leads to higher adsorbed amounts for P4VP relative to P2VP, this does not lead to significant differences in the chain mobilities of either the PVP anchor blocks or PI buoy blocks.

4.5.3.3 Effect of loading: Solid-state ^1H MAS NMR

Due to higher sensitivity and much shorter acquisition times as compared to ^{13}C NMR, ^1H MAS NMR allowed measurements of the chain mobilities at low coverages and for some of the bulk copolymers respectively. The bulk $PI_{440}P4VP_{90}$ however was still too viscous for stable spinning even for the short times required to acquire a ^1H NMR spectrum.

The ^1H MAS NMR spectra for $PI_{440}P2VP_{25}$, on zirconia, presented in Figure 4.6b, have two distinct regions: the signal at 5.1 ppm (-CH= of 1,4-unit) and the signals at 4.68 and 4.75 ppm (=CH_2 of 3,4-unit and =CH_2 of 1,2-unit), and aliphatic protons appear between 1.5 and 2.0 ppm.[13] The broad aromatic signal at 7 ppm that was observed for bulk P2VP is not visible in the bulk $PI_{440}P2VP_{25}$ spectrum. For the adsorbed block copolymer, there are three broad peaks, when compared to the relatively sharp peaks in the bulk spectra: a broad peak in the region of 1.5 ppm due to backbone CH_2 protons, which was split in the bulk but is broadened into one upon adsorption, a broad peak at 2.1 ppm due to backbone CH protons, and a broad beak at 5.2 ppm due to the –CH= protons.

Despite the significantly broadened signals at low coverages, the ^{1}H T_1 values, listed in Table 4.4, show a continual increase in T_1 with the adsorbed amount, indicating an enhanced mobility at low coverages. Variable temperature data (not shown) confirm that the PI chains are still on the slow side of the spin lattice relaxation time versus correlation time curve. The residual line broadening at the lowest coverages that is not removed by MAS may be due to interactions of the PI chain segments with the metal oxide surface, similar to what is typically observed for filled rubbers. Early studies of carbon black filled polyisoprene found that the filler affected the line widths but not the T_1 values.[16] Chemical shift effects rather than relaxation provide the major contribution to the residual linewidths of filled rubber.[17] Since the T_1 values of the adsorbed copolymers with surface loading in the plateau region of the adsorption isotherm are shorter than the bulk values, the overall mobility of the adsorbed copolymer is more mobile than in the bulk state even at the highest coverages. It is possible that the enhanced mobility is due to the possibility that in a non-specific solvent, no phase separation occurred during the mixing and evaporation processes, so one has an intimate mixture of PVP and PI segments in the solid state. The mobile PI segments might act as a plasticizer for the PVP chain segments. The PVP alone shows higher mobility on adsorption, which was attributed to a rather loopy structure.

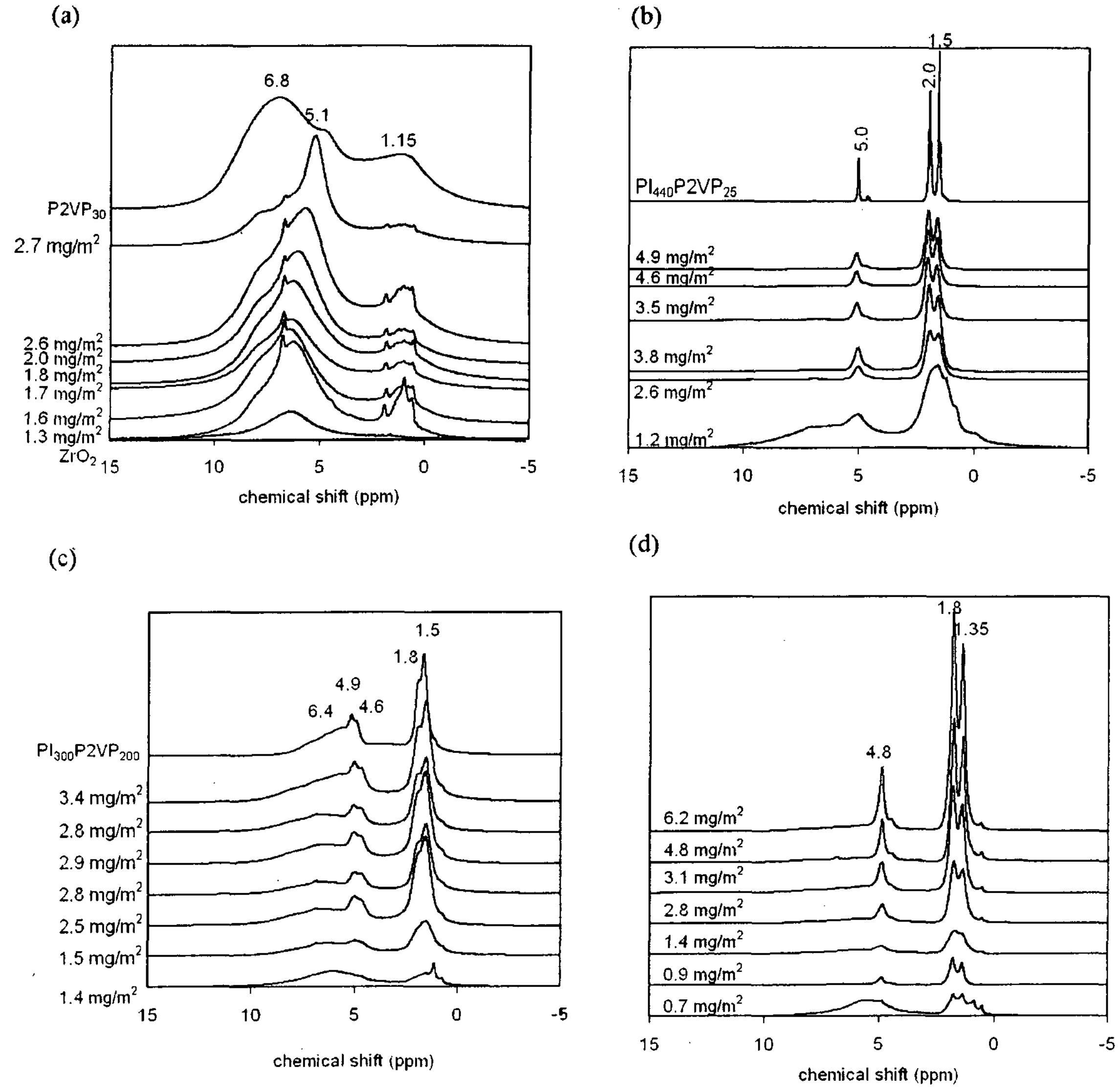

Figure 4.6: ^{1}H NMR spectra for (a) P2VP, (b) PI$_{440}$P2VP$_{25}$, (c) PI$_{300}$P2VP$_{200}$, and (d) PI$_{440}$P4VP$_{90}$ adsorbed on zirconia. The initial concentrations of the adsorbed copolymers vary from 120 mg/ml to 1 mg/ml. (spinning frequency = 25 kHz, number of acquisitions = 16 for bulk and 32 for adsorbed, pulse delay = 10 sec for bulk, and 5 sec for adsorbed, pulse width = 1.7 μsec).

From the adsorbed amounts the surface density (σ) can be calculated. The surface density was then compared to the overlap density (σ_{ol}). The overlap density is the value of the surface density above which the PI buoys will overlap in the adsorbed layer. The calculations were performed as described previously in Chapter 3 (pages 98) of this thesis.

Table 4.4: ^{1}H T_1 (sec) data for bulk and adsorbed block copolymers as a function of surface loading.

*The error on the ^{1}H T_1 values is ± 0.01 s

adsorbed amount (mg/m^2)	$PI_{440}P2VP_{25}$ ^{1}H T_1 (sec)	adsorbed amount (mg/m^2)	P2VP ^{1}H T_1 (sec)
bulk	0.88	Bulk	2.23
4.9	0.59	2.7	0.22
4.8	0.57	2.0	0.15
1.2	0.24	1.6	0.12
1.2	0.1	1.3	0.11
adsorbed amount (mg/m^2)	$PI_{300}P2VP_{200}$ ^{1}H T_1 (sec)	adsorbed amount (mg/m^2)	$PI_{440}P4VP_{90}$ ^{1}H T_1 (sec)
bulk	0.67	bulk	
3.4	0.34	6.2	0.51
2.9	0.29	3.1	0.44
1.5	0.14	0.9	0.23
1.4	0.12	0.7	0.29

Table 4.5: adsorbed amount, surface density, overlap density, and reduced surface density for the adsorbed copolymers presented in Table 4.4.

adsorbed amount (mg/m^2)	σ (molecules/m^2)	σ_{ol} (molecules/m^2)	$\sigma^* = \sigma/\sigma_{ol}$
$PI_{440}P2VP_{25}$			
4.9	9.0×10^{16}	3.5×10^{15}	26
4.8	8.8×10^{16}		25
1.2	2.2×10^{16}		6.4
1.2	2.2×10^{16}		6.4
$PI_{300}P2VP_{200}$			
3.4	5.0×10^{16}	5.4×10^{15}	9.3
2.9	4.3×10^{16}		8.0
1.5	2.2×10^{16}		4.1
1.4	2.1×10^{16}		3.9
$P2VP_{30}$			
2.7	4.6×10^{17}		
2.0	3.4×10^{17}		
1.6	2.8×10^{17}		
1.3	2.2×10^{17}		
$PI_{440}P4VP_{90}$			
6.2	9.5×10^{16}	3.5×10^{15}	28
3.1	4.8×10^{16}		14
0.9	1.4×10^{16}		4.0
0.7	1.1×10^{16}		3.1

From Table 4.5 the surface density (σ), is greater than the overlap density (σ_{ol}), even at the lowest coverages. The adsorbed block copolymers are therefore in the intermediate or weak stretching regime, where the reduced surface density as given in equation 3.3 is in the range $2 < \sigma^* < 20$. Adsorbed $PI_{440}P2VP_{25}$ and $PI_{440}P4VP_{90}$ are predicted to be in the extended brush regime, where $\sigma^* > 20$, only at the very highest adsorbed amounts listed in Table 4.5. Upon removal of the solvent, the collapsed brushes of the most densely packed PI chains are still more mobile than in the bulk state. As expected, the relative mobilities of the PI buoys for the adsorbed copolymers in the plateau region of their adsorption isotherm, follows the trend $PI_{440}P2VP_{25} \geq PI_{440}P4VP_{90} > PI_{300}P2VP_{200}$ in order of increasing mobility since increasing the anchor block changes the structure from the extended brushes to the intermediate mushroom/brush regime.

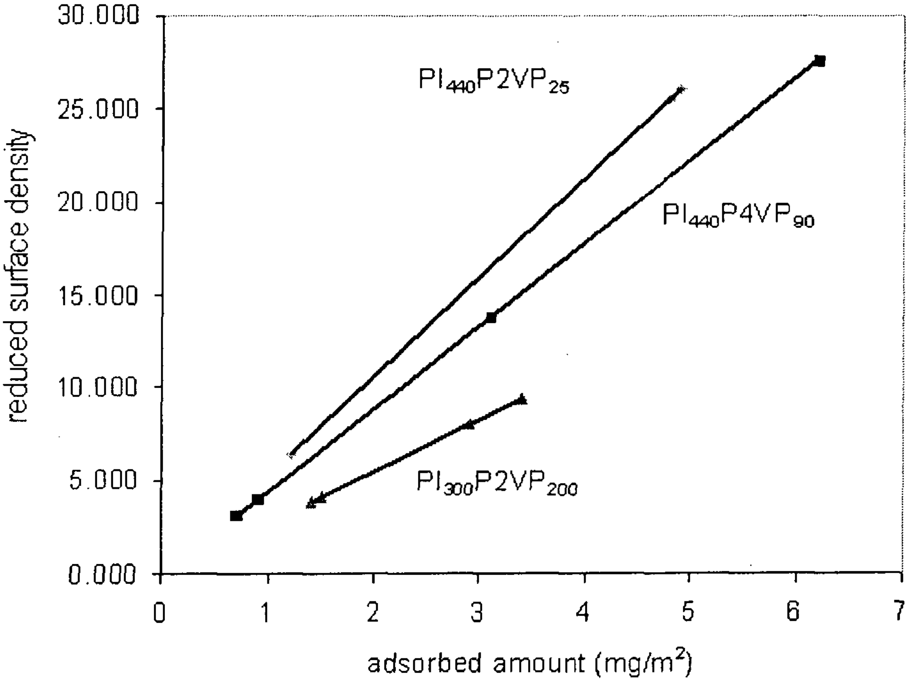

Figure 4.7: Reduced surface density from Table 4.5 plotted against the adsorbed amount (mg/m^2) for the asymmetric PIPVP block copolymers.

What is seen in Figure 4.7 where the reduced surface density is plotted against the adsorbed amount is that the three PIPVP block copolymers show different slopes in surface density with an increase in adsorbed amount. The steepest slope, which was associated with $PI_{440}P2VP_{25}$, means that the adsorbed polymer is denser at a lesser adsorbed amount suggesting that $PI_{440}P2VP_{25}$ packs better than any of the other PIPVP block copolymers.

4.6 Conclusions

The observed trends in the chain mobility of the adsorbed PVP-PI diblock copolymers in the dry state can be rationalized in terms of the predicted surface structures which depend on the block size, surface interactions and solvent. This system differed from the previously studied PS-PAA diblocks in that there is a large difference in the intrinsic chain mobilities of the constituent homopolymers and a nonselective solvent was used. In contrast to the PS-PAA system, the chain mobility of the PVP anchor block was moderately enhanced relative to the bulk state. This may be attributed to the nonselective solvent that plasticizes the PVP layer, resulting in a surface conformation with more loops and tail as compared to the PAA anchor blocks whose motion is highly restricted by the strong carboxylate surface linkages. Secondly, the most symmetric PVP-PI diblocks behave as predicted with the PI buoys displaying higher mobilities than the more densely packed buoys of the highly asymmetric diblocks. The opposite trend with block size was found for the PS-PAA system since the PS buoys of most symmetric adsorbed diblocks displayed a more restricted mobility. However the chain mobilities of both systems followed the expected trends with coverage. The rubbery state of the PI layer as inferred from surface force studies is directly confirmed by the NMR measurements presented here since the chain mobility of the most densely packed collapsed brushes exceeds that of the bulk state.

4.7 Acknowledgements

The Natural Sciences and Engineering Research Council (NSERC) and the Centre for Self-Assembled Chemical Structures (CSACS) provided support for this research. The authors thank Professor Thomas Ellis and Mr. Craig Hyett of the Université de Montreal for access to the FTIR-PAS spectrometer. The authors thank Dr. Cedric Malveau of the Université de Montreal for assistance with the 600 MHz NMR. We also thank Dr. Fred Morin for valuable assistance.

4.8 References

1. Watanabe, H. and Tirrell, M., *Measurement of Forces in Symmetric and Asymmetric Interactions between Diblock Copolymer Layers Adsorbed on Mica.* Macromolecules, 1993. **26**: p. 6455-6466.
2. Field, J.B., et al., *Neutron reflectivity study of end-adsorbed diblock copolymers: cross-over from mushrooms to brushes.* Journal de Physique II France, 1992: p. 2221-2235.
3. Parsonage, E., et al., *Adsorption of Poly(2-vinylpyridine)-Poly(styrene) Block Copolymers from Toluene Solutions.* Macromolecules, 1991. **24**: p. 1987-1995.
4. Malynych, S., Luzinov, I., and Chumanov, G., *Poly(Vinyl Pyridine) as a Universal Surface Modifier for Immobilization of Nanoparticles.* Journal of Physical Chemistry B, 2002. **106**: p. 1280-1285.
5. Falsafi, A., Bates, F.S., and Tirrell, M., *Role of Chain Architecture in the Adhesion of Block Copolymers.* Macromolecules, 2001. **34**: p. 1323-1327.
6. Hong, P.P., et al., *An investigation of the adsorption of polystyrene/poly(2-vinylpyridine) diblock copolymers onto silver substrates using surface-enhanced Raman scattering.* Macromolecules, 1993. **26**: p. 3953-3959.
7. Belder, G.F., ten Brinke, G., and Hadziioannou, G., *Influence of Anchor Block Size on the Thickness of Adsorbed Block Copolymer Layers.* Langmuir, 1997. **13**: p. 4102-4105.
8. Kosonen, H., et al., *Self-organized cross-linked phenolic thermosets: thermal and dynamic mechanical properties of novolac/block copolymer blends.* Polymer, 2001. **42**: p. 9481-9486.
9. Zhang, L. and Eisenberg, A., *Morphogenic Effect of Added Ions on Crew-Cut Aggregates of Polystyrene-b-poly(acrylic acid) Block Copolymers in Solutions.* Macromolecules, 1996. **29**: p. 8805-8815.

10. Xie, M. and Blum, F.D., *Adsorption and Dynamics of Low Molecular Weight Poly(styrene-b-2-vinylpyridine) on Silica and Alumina in Toluene.* Langmuir, 1996. **12**: p. 5669-5673.
11. Afonin, A.V., et al., *^{1}H and ^{13}C NMR Study of Bifurcated Intramolecular Hydrogen Bonds in 2,6-Bis(2-pyrrolyl)pyridine and 2,6-Bis(1-vinyl-2-pyrrolyl)pyridine.* Russian Journal of Organic Chemistry, 2005. **41**(10): p. 1516-1521.
12. Lee, S.W., et al., *Rubbed films of isomeric poly(4-vinylpyridine) and poly(2-vinylpyridine): surface morphology, molecular orientation, and liquid crystal alignability.* Polymer, 2005. **46**: p. 4068-4076.
13. Shin, Y.-D., et al., *Synthesis of Poly(2-vinyl pyridine)-b-poly(n-hexylisocyanate) Amphiphilic Coil-Rod Block Copolymer by Anionic Polymerization.* Journal of Polymer Science: Part A: Polymer Chemistry, 2005. **434**: p. 607-615.
14. Burtovyy, R. and Luzinov, I., *Reversibility of pH-Induced Dewetting of Poly(vinyl pyridine) Thin Films on Silicon Oxide Substrate.* Langmuir, 2008. **24**: p. 5903-5910.
15. Mengezaz, H., et al., *Segmental mobility in poly(isoprene) rubber studied by deuterium-carbon NMR correlation spectroscopy.* Polymer Bulletin, 2001. **46**: p. 183-190.
16. Schaefer, J., *Comparisons of the Carbon-13 Nuclear Magnetic Resonance Spectra of Some Solid cis- and trans-Polyisoprenes.* Macromolecules, 1972. **5**: p. 427-440.
17. Dybowski, C.R. and Vaughan, R.W., *Motional Phenomena and Multiple Pulse Nuclear Magnetic Resonance. Nonisotropic Motion in Natural Rubber.* Macromolecules, 1975. **8**: p. 50-54.

Chapter 5: Conclusions, contributions, and future work

5.1 Conclusions and Contributions to Knowledge

5.1.1 Ethylene Based Random Copolymers

This work was motivated by the role that the chain conformation plays in the adhesion of polymer films to solid surfaces and the importance of ethylene random copolymers as adhesion promoters for polyethylene films. The influence of the particular polar functional group on ethylene random copolymer surface microstructure was examined. The chain conformation and mobility will vary with the chain length, the densities of binding groups on the polymer chain and surface receptor groups, and the strength of the polymer-substrate interactions. In this study, the surface receptor group density was constant and the fraction of sticker groups as well as the binding strength was varied.

In the case of poly (ethylene-co-acrylic acid) (PEA) on zirconia powder, the chain conformation was previously found to be strongly dictated by the polar group content rather than coverage. This behaviour persisted for PEA adsorbed on alumina, a more weakly binding substrate as compared to zirconia. The dependence of the conformation on sticker group density was found to decrease with binding strength. The chain conformation of adsorbed ethylene copolymers with functional groups with the relative binding strengths, $COOH > OH > -O(C{=}O)CH_3 >> CH_2$ were compared. The main conclusion is that there is more conformational order with weaker binding strength. The picture supported by these results is that of PEA binding so strongly that it sticks randomly and irreversibly to the surface during the adsorption process, so that until all the sites are occupied, the ethylene segments will be conformationally disordered. For the copolymer poly (ethylene-co-vinyl acetate), EVA, the binding is sufficiently weak that the sticker groups can more easily detach from the surface during the adsorption process and thus reach a more ordered chain conformation even at low loadings.

The ethylene segments of EVA copolymers that had high acetate content were observed to have a strong transoid component. Relaxation measurements, as well as the absence of an FTIR band for free acetate groups for low coverage samples, indicate that the trans component of EVA arises from chains lying flat on the surface, in contrast to adsorbed PEA where the ordered component is proposed to arise from folded loops.

5.1.2 Block Copolymers

Although the surface structures and associated chain dynamics of adsorbed diblock copolymers in the presence of solvent have been extensively studied both theoretically and experimentally, the dynamic properties of surfaces modified by diblock copolymers in the dry state has not been previously examined at the chain level. This is the main contribution to knowledge of Chapters 3 and 4 of this thesis.

A series of poly (styrene)-*b*-poly (acrylic acid), PS-PAA, and poly (styrene)-*b*-poly (*t*-butyl acrylate) diblock copolymers, PS-PtBuA, in the bulk and adsorbed states were studied by ^{13}C and ^{1}H solid-state NMR as a function of block size, surface binding strength and surface coverage. Variations in the chain mobilities of the bulk copolymers with block size was explained by the degree of interchain hydrogen bonding among the carboxylic acid groups of the PAA blocks combined with the effect of the molecular weight on the glass transition. The effect of the block size on the chain dynamics for the adsorbed copolymers in the plateau region of the adsorption isotherm was examined. For all adsorbed copolymers, the segmental mobility of the PAA is highly restricted relative to the bulk state, reflecting the immobilization of these anchor blocks through strong ionic surface linkages. In the case of highly asymmetric diblocks, the segmental mobility of the long PS buoys that form extended brushes in the presence of solvent is moderately enhanced relative to the bulk state. However, the motion is sufficiently restricted that the collapsed PS brushes of the dry state can still be characterized as forming a glassy layer, in agreement with the interpretation of surface force studies of similar PVP-PS diblocks. In contrast, the PS chain mobility of adsorbed diblocks with larger anchor blocks is unchanged relative to the bulk state despite the larger spacings between the buoy blocks that should produce a lower density PS layer upon removal of the solvent. In the case of the highly asymmetric diblock with short PS buoys, expected to form mushrooms, the restricted mobility of the PS segments can be rationalized by their proximity to the surface bound segments. However, restricted motion of the long PS buoys of the most symmetric diblock produces an intermediate mushroom/brush structure that cannot be explained by this argument. The dependence of the PS chain mobility with coverage for the highly asymmetric diblocks was correlated with the evolution of the surface structure from mushrooms to intermediate to true extended brushes.

The diblock copolymers poly (2-vinylpyridine), poly (isoprene)-*b*-poly (2-vinylpyridine), (PI-P2VP) and poly (isoprene)-*b*-poly (4-vinylpyridine) (PI-P4VP) were selected to complement the PS-PAA system as both systems have been studied by surface force microscopy. The large contrast in chain mobilities of the PI and PVP blocks allowed spectral editing of the ^{13}C CP-MAS NMR spectra to study the separate blocks through variation of the cross polarization parameters. In contrast to the PS-PAA system, the chain mobility of the PVP anchor block was moderately enhanced relative to the bulk state due to the nonselective solvent that plasticizes the PVP layer, resulting in a surface conformation with more loops and tails as compared to the PAA anchor blocks. Broadening of the PI signals in the ^{1}H MAS NMR spectra at low coverages was not due to restricted mobility but rather to interaction of the PI segments with the metal oxide surface as observed for filled rubbers. The trends in the chain mobility of the adsorbed PI-PVP copolymers with block size differ from that of PS-PAA in that the segmental mobility of the buoys increases with the anchor block size as expected. The rubbery state of the PI layer as inferred from surface force studies is directly confirmed by the NMR measurements since the chain mobility of the most densely packed collapsed brushes was found to exceed that of the bulk state.

5.2 Future Work

The interpretation of the NMR measurements on the adsorbed random copolymers would be strengthened by complementary variable temperature FTIR and mechanical studies such as peeling tests. The variable temperature FTIR studies would allow direct detection of any detachment of the more weakly bound polar sticker groups upon heating of adsorbed EVA. The detection of the detachment would account for the chain disordering observed for adsorbed EVA copolymers with heating and support the proposal that this random copolymer forms flat extended trains at the surface. Mechanical measurements of the cohesive versus adhesive failure of the same series of ethylene random copolymers on the same substrates (alumina and zirconia) would allow correlations between the surface conformation as determined by NMR and the adhesion properties. Multiblock ethylene copolymers, while difficult to synthesize, would provide an interesting variant to test the interpretation of the NMR data and correlations between the surface microstructure and adhesion properties.

The NMR studies of the adsorbed block copolymers would benefit from the application of more sophisticated solids ^{1}H MAS NMR experiments which have sufficient sensitivity to examine the systems at low coverages and provide additional information in regards to dynamics and local order. In particular, it would be interesting to apply the proton multiple quantum experiments that have been developed to study the chain dynamics and structural constraints in elastomers and polymer melts to the PI-PVP system in the dry state and the PS-PAA system in the swollen state.[1] Finally, the surface structures formed by triblock copolymers is another possible direction for solids NMR studies of the dynamic properties of adsorbed copolymers

5.3 Reference

1. Saalwachter, K., *Proton multiple-quantum NMR for the study of chain dynamics and structural constraints in polymeric soft materials.* Progress in Nuclear Magnetic Resonance Spectroscopy, 2007. **51**: p. 1-35.